NAVAL POSTGRADUATE SCHOOL
Monterey, California

AD-A264 951

THESIS

DTIC
ELECTE
MAY 2 8 1993
S E D

A NUMERICAL STUDY OF SEASONAL
WIND FORCING EFFECTS ON THE
CALIFORNIA CURRENT SYSTEM

by

Ross P. Mitchell

March, 1993

Thesis Advisor: Mary L. Batteen

93-12024

93 5 27 0 8

NAVAL POSTGRADUATE SCHOOL
Monterey, CA 93943

Rear Admiral Thomas A. Mercer   Harrison Shull
Superintendent   Provost

Reproduction of all or part of this report is authorized.
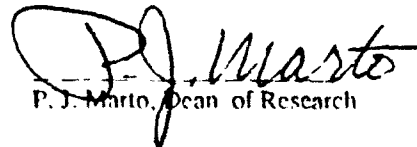
Principal author for this report was

R. P. Mitchell

R. P. Mitchell, LT, USN

Approved by:

C. A. Collins

C. A. Collins, Chairman
Department of Oceanography

Released by:

P. J. Marto

P. J. Marto, Dean of Research

REPORT DOCUMENTATION PAGE

1a. REPORT SECURITY CLASSIFICATION UNCLASSIFIED	1b. RESTRICTIVE MARKINGS
2a. SECURITY CLASSIFICATION AUTHORITY 2b. DECLASSIFICATION/DOWNGRADING SCHEDULE	3. DISTRIBUTION/AVAILABILITY OF REPORT Approved for public release; distribution is unlimited
4. PERFORMING ORGANIZATION REPORT NUMBER(S) NPS OC-93-001	5. MONITORING ORGANIZATION REPORT NUMBER(S)

6a. NAME OF PERFORMING ORGANIZATION Oceanography Dept. Naval Postgraduate School	6b. OFFICE SYMBOL (if applicable) OC	7a. NAME OF MONITORING ORGANIZATION Office of Naval Research
6c. ADDRESS (City, State, and ZIP Code) Monterey, CA 93943-5000		7b. ADDRESS (City, State, and ZIP Code) 800 N. Quincy St., Arlington, VA 2217-5000
8a. NAME OF FUNDING/SPONSORING ORGANIZATION Office of Naval Research	8b. OFFICE SYMBOL (if applicable)	9. PROCUREMENT INSTRUMENT IDENTIFICATION NUMBER O&MN, Direct Funding

8c. ADDRESS (City, State, and ZIP Code) 800 N. Quincy St., Arlington, VA 2217-5000	10. SOURCE OF FUNDING NUMBERS			
	PROGRAM ELEMENT NO.	PROJECT NO.	TASK NO.	WORK UNIT ACCESSION NO

11. TITLE (Include Security Classification)
A NUMERICAL STUDY OF SEASONAL WIND FORCING ON THE CALIFORNIA CURRENT SYSTEM (U)

12. PERSONAL AUTHOR(S)
Ross P. Mitchell in conjunction with M.L. Batteen

13a. TYPE OF REPORT Master's Thesis	13b. TIME COVERED FROM TO	14. DATE OF REPORT (Year, Month, Day) March 1993	15. PAGE COUNT 125

16. SUPPLEMENTARY NOTATION
The views expressed in this thesis are those of the author and do not reflect the official policy or position of the Department of Defense or the United States Government.

17.	COSATI CODES		18. SUBJECT TERMS (Continue on reverse if necessary and identify by block number) Primitive equation model, eddies, filaments, wind forcing, coastal jet and undercurrent, California Current System
FIELD	GROUP	SUB-GROUP	

19. ABSTRACT (Continue on reverse if necessary and identify by block number)
A high resolution, multi-level, primitive equation ocean model is used to examine the response of an idealized, flat-bottomed, eastern boundary oceanic regime on a beta-plane to both steady and seasonally-varying climatological wind forcing. The focus of this study is the California Current System along the coastal region, from 35° N to 45° N, off the Western United States. With steady equatorward wind forcing, a surface equatorward current and poleward undercurrent develop. Eddies form around days 60 and 70 with initial development in the northern region of the domain. The strong meandering current continues to grow throughout the 360 days of model time and can produce eddies that have wavelengths up to ~200 km and can propagate at least ~200 km offshore. When the alongshore component of the temporally averaged seasonally-varying climatological wind forcing is used, there is a weak poleward undercurrent and equatorward surface current. There is weak upwelling and very little eddy activity with the eddies only propagating to ~100 km offshore. When alongshore component of the time-dependent wind forcing with spatial variability in latitude is used, a surface equatorward jet, poleward undercurrent and eddies are generated. The eddies form throughout the domain in this experiment due to competition between the β-plane effect and the continuous and

20. DISTRIBUTION/AVAILABILITY OF ABSTRACT [X] UNCLASSIFIED/UNLIMITED [ ] SAME AS RPT. [ ] DTIC USERS	21. ABSTRACT SECURITY CLASSIFICATION UNCLASSIFIED
22a. NAME OF RESPONSIBLE INDIVIDUAL Mary L. Batteen	22b. TELEPHONE (Include Area Code) (408) 656-3265	22c. OFFICE SYMBOL OC/BV

DD FORM 1473, 84 MAR	83 APR edition may be used until exhausted All other editions are obsolete	SECURITY CLASSIFICATION OF THIS PAGE UNCLASSIFIED

stronger equatorward wind forcing in the southern portion of the domain. The eddies in this experiment propagate at least ~150 km from shore. When the full climatological winds are used, there is again a surface equatorward jet and poleward undercurrent generated. The surface currents and eddies reach speeds of ~65-85 cm s^{-1}. The wavelengths of the eddies are ~300 km and can propagate to ~350 km offshore. These results are closest to the observed structure of the California Current System. Therefore, I conclude that both temporal and spatial variability in wind forcing are critical elements in the formation and maintenance of currents and eddies in the California Current System.

A NUMERICAL STUDY OF SEASONAL WIND FORCING EFFECTS ON THE CALIFORNIA CURRENT SYSTEM

by

Ross P. Mitchell
Lieutenant, United States Navy
Bachelor of Science in Physical Science, U.S. Naval Academy, 1987

Submitted in partial fulfillment of the
requirements for the degree of

MASTER OF SCIENCE IN PHYSICAL OCEANOGRAPHY

from the

NAVAL POSTGRADUATE SCHOOL
March, 1993

Accesion For		
NTIS CRA&I		X
DTIC TAB		☐
Unannounced		☐
Justification		
By		
Distribution /		
Availability Codes		
Dist	Avail and / or Special	
A-1		

Author: _Ross P. Mitchell_

Ross P. Mitchell

Approved By: _Mary L. Batteen_
Mary L. Batteen , Thesis Advisor

Curtis A. Collins
Curtis A. Collins, Second Reader

Curtis A. Collins
Curtis A. Collins, Chairman,
Department of Oceanography

iii

ABSTRACT

A high-resolution, multi-level, primitive equation ocean model is used to examine the response of an idealized, flat-bottomed, eastern boundary oceanic regime on a beta-plane to both steady and seasonally-varying climatological wind forcing. The focus of the study is the California Current System along the coastal region, from 35° N to 45° N, off the Western United States. With steady equatorward wind forcing, a surface equatorward current and poleward undercurrent develop. Eddies form around days 60 and 70 with initial development in the northern region of the domain. The strong meandering current continues to grow throughout the 360 days of model time and can produce eddies that have wavelengths up to ~ 200 km and can propagate at least ~200 km offshore. When the alongshore component of the temporally averaged seasonally-varying climatological wind forcing is used, there is a weak poleward undercurrent and equatorward surface current. There is weak upwelling and very little eddy activity with the eddies only propagating to ~100 km offshore. When alongshore component of the time-dependent wind forcing with spatial variability in latitude is used, a surface equatorward jet, poleward undercurrent and eddies are generated. The eddies form throughout the domain in this experiment due to a competition between the β-plane effect and the continuous and stronger equatorward wind forcing in the southern portion of the domain. The eddies in this experiment propagate at least ~150 km from shore. When the full climatological winds are used, there is again a surface equatorward jet and poleward undercurrent generated. The surface currents and eddies reach speeds of ~65-85 cm s^{-1}. The wavelengths of the eddies are ~300 km and can propagate to ~350 km offshore. These results are closest to the observed structure of the California Current System. Therefore, I conclude that both temporal and spatial variability in wind forcing are critical elements in the formation and maintenance of currents and eddies in the California Current System.

TABLE OF CONTENTS

LIST OF TABLES

LIST OF FIGURES

ACKNOWLEDGMENTS

The author wishes to thank Dr. Mary Battcen for her patience and guidance. Her expertise in both oceanography and writing scientific papers made this learning experience possible. Thanks also to Dr. Collins for his encouragement and assistance in finalizing this report. The many hours of help and assistance in computer programming and problem solving by Pedro Tsai was invaluable to the completion of this thesis and is gratefully acknowledged. Finally, I would like to thank my wife, Jennifer, and my two daughters, Casey and Samantha, for their support and understanding through these two years of academic trial.

I. INTRODUCTION

The California Current System is a complex system of eddies and meandering jets superimposed on a mean equatorward flow extending to ~1000 km from the coast. There have been several major experiments including Coastal Upwelling Experiments (CUE-I and CUE-II), Coastal Ocean Dynamics Experiment (CODE), Ocean Prediction through Observations, Modeling and Analysis (OPTOMA), and Coastal Transition Zone (CTZ), designed to better understand this eastern boundary current. The purpose of this study is to explain the generation of the eddies and filaments found in the above experiments. Batteen *et al.* (1989) demonstrated how a steady equatorward wind is able to generate a reasonable current, undercurrent and eddy field with a full primitive equation (PE) model. The process-oriented study described here extends the work of Batteen *et al.* (1989) by using seasonal rather than steady winds to force the same PE model. These winds are then averaged into different components to understand the role these components play in the generation of mesoscale features.

This thesis is organized as follows. Chapter II describes the region being modeled as well as the type of winds used to force the model. A brief look at some numerical models used in the past is at the end of this chapter. In Chapter III there is a description of the model and the design of the experiments. The results of the model experiments are presented in Chapter IV. A summary is provided in Chapter V.

II. BACKGROUND

A. REGIONAL DESCRIPTION

Oceanic flow off California is classified as an eastern boundary current. It was described as a broad, weak, equatorward flow extending to ~1000 km from the coast (Sverdrup et al., 1942). Source water is carried eastward in the West Wind Drift of the North Pacific Gyre (Lynn and Simpson, 1987). This water forms a relatively cold, low salinity current along the west coast of North America. The principal equatorward flow is above 1000 meter depth with the bulk of the average 11.9 Sv transported equatorward occurring within 1000 km of the coast (Wooster and Reid, 1963). Numerous eddies and irregularities in the flow as well as the existence of coastal countercurrents have been observed (Wooster and Reid, 1963). Equatorward winds in the summer can cause equatorward currents and strong upwelling while a coastal, poleward countercurrent with no upwelling can be present in the winter (Reid et al., 1958). Non-seasonal variations in upwelling appear to be related to wind changes (Reid, 1960).

The California Current System (CCS) can be broken into four general currents: the California Current (CC), the California Countercurrent (CCC), the California Undercurrent (CUC), and the Southern California Countercurrent (SCC). Since only the first three are included in the area of this modeling study, the SCC will not be further discussed.

The equatorward CC has a core that is within 100-200 km of the coast and reaches a depth of nearly 300 m (Chelton, 1984). The average current speeds are less than 25 cm s^{-1} (Reid and Schwartzlose, 1962). Core speeds often in excess of 75 cm s^{-1} have been observed (Brink et al., 1991).

2

The poleward CCC is observed inshore of the CC and is characterized by its seasonal variability (Chelton, 1984; Hickey, 1979) The flow of the CCC is equatorward from February through September and poleward from November through February (Hickey, 1979). When flowing poleward on the surface, it is called the Davidson Current (Chelton, 1984). Observations north of Cape Mendocino show that the flow can be either poleward or equatorward during the same month (Chelton *et al.*, 1988).

The CUC flows poleward over the continental shelf (Hickey, 1979; Reid, 1962). Its core has a mean velocity greater than 15 cm s^{-1} with instantaneous speeds of up to 40 cm s^{-1} (Hickey, 1979; Reid, 1962). The CUC is 20 - 70 km wide and vertically extends ~ 300 meters with its center 200 - 250 meters below the surface (Hickey, 1979; Reid, 1962).

The colder temperatures found near the coast and observations of the CCC below 200 m depth were originally attributed to a classical two-dimensional upwelling system closely related to the winds (Smith, R. L., 1968). This simple one-celled circulation of upwelling was later disputed by observations during CUE-1 and CUE-2, where the vertical distributions of temperature, chlorophyll and optical parameters contradicted the simple two-dimensional theory (Huyer, 1983).

The CODE program in 1981-1982 was designed to study and identify those dynamical processes which govern the wind-driven motion of water over the continental shelf (Beardsley and Lentz, 1987). Kosro (1987) used the shipboard Doppler acoustic log (DAL) to show that near-surface currents often deviated substantially from classical two-dimensional wind-driven upwelling. DAL results indicated a close association between the complex temperature structures in satellite imagery and the presence of vigorous current structures including squirts, eddies, and countercurrents (Kosro, 1987). The OPTOMA program further showed the persistence of the eddy field and its potential for drawing the cold waters offshore (Mooers and Robinson, 1984) The CTZ program was the next

major experiment designed to help understand the complex CCS. A major portion of this program was dedicated to resolving what caused the filaments (cold surface features) found during CODE and OPTOMA (Brink and Cowles, 1991). Drifters showed core speeds often in excess of 75 cm s^{-1} in the generally southward meandering jet during July to December 1988 (Brink *et al.*, 1991). When the winds were poleward and the Davidson Current was present, there was little eddy activity and no coherent flow or filaments were observed (Kosro *et al.*, 1991).

CTZ was designed to study filaments. Yet in the EBC region many large-scale eddies were present. The newest program, "Weakly Nonlinear Accelerated Research Initiative", sponsored by the Office of Naval Research (ONR), is designed to try to understand more about the eddies in the CCS. Of particular interest is the question of the role of wind forcing in generating eddies in the CCS.

B.   CLIMATOLOGICAL WINDS

The atmospheric circulation off the west coast of North America is dominated by the North Pacific High, which varies seasonally in position and strength (Huyer, 1983). In February the High is centered near 28°N, 130°W, while in August it migrates to its most northward location of 38°N, 150°W (Huyer, 1983). Nelson (1977) showed that the strongest equatorward wind stress migrates from ~25°N in the winter to ~38°N in the summer. This shifting of the High causes the winds to split at ~40°N near Cape Mendocino during the winter. The northward winds blow around the eastern side of the Aleutian Low, north of the cape, while southward winds blow around the North Pacific High, south of the cape. In the summer, the winds are predominately southward on both sides of the cape (Nelson, 1977).

4

Smith (1968) showed that open ocean upwelling can occur if there is positive wind stress curl away from the boundary of the coast. Bakun and Nelson (1991) found that the large-scale wind stress curl in the CCS is predominately cyclonic near the coast and anticyclonic offshore. As a result, Ekman convergence dominates near the coast, while Ekman divergence dominates offshore. There is a transition zone located approximately 200 - 300 km off the coast between the cyclonic and anticyclonic curl which is associated with the offshore maximum of alongshore wind stress (Bakun and Nelson, 1991).

There are two local maximums in the wind stress curl. The first is yearlong and associated with the Southern California Bight. The second extends south from Cape Mendocino to past Monterey Bay and occurs during the fall and winter (Bakun and Nelson, 1991).

C.   NUMERICAL MODEL STUDIES

Numerical models have been used to help unravel some of the mysteries concerning the causes and behavior of the phenomena observed in the CCS. They can give the solution to complicated, non-linear problems that are intractable with standard analytical methods (Allen, 1980).

Two-dimensional models, which ignored alongshore variability, were a first attempt at using the computer to generate results that were reasonable when compared to available observations. For example, the two-layered stratified models discussed by Allen (1980) with a flat bottom produced a coastal jet in the upper layer and a countercurrent in the lower layer. When a shelf and slope topography were added to the same model, results showed that the countercurrent strength would be significantly reduced, consistent with available observations.

5

As computers have advanced in speed and power, three-dimensional models have replaced the two-dimensional models and can be run with results obtained in a reasonable amount of time. For example, for eastern boundary current regions, two-layer and continuously stratified three-dimensional models have been used by Suginohara (1977) to study the effects of alongshore variations in wind stress. The results have been shown to be consistent with forced coastal trapped wave theories. The results also show a pycnocline upwelling near the coast and the formation of fronts, consistent with available upwelling observations (e.g., Curtin, 1979).

None of the models mentioned above simulated eddies, jets or filaments. Haidvogel *et al.* (1991) was able to produce these results but used no wind forcing. Batteen *et al.* (1989) had the first eastern boundary current model to simulate eddies and jets with steady wind forcing, followed by McCreary *et al.* (1991), who used the same type of wind forcing.

In this study, the model used by Batteen *et al.* (1989) is extended to include seasonal rather than steady wind forcing. The seasonal winds are then averaged into different components to understand the role each component plays in the generation of eddies, jets and filaments.

III. MODEL DESCRIPTION

The numerical model used in this research was developed by Haney (1974,1985) for a closed basin, and modified by Batteen (1989) and Batteen et al. (1989) for use in limited area eastern boundary current (EBC) regions with open borders on the northern, western and southern borders. It is explained in detail in Batteen et al. (1989) and will be summarized below.

A. MODEL EQUATIONS

The model is a multi-level, primitive equation (PE) model, and uses the hydrostatic, rigid lid, β-plane and Boussinesq approximations. The governing equations are the following:

a. Momentum Equations:

$$\frac{du}{dt} = \frac{-1}{\rho_o}\frac{\partial p'}{\partial x} + fv - A_m\nabla^4 u + K_m\frac{\partial^2 u}{\partial z^2} + \delta_d(u) \tag{3.1}$$

$$\frac{dv}{dt} = \frac{-1}{\rho_o}\frac{\partial p'}{\partial y} + fu - A_m\nabla^4 v + K_m\frac{\partial^2 v}{\partial z^2} + \delta_d(v) \tag{3.2}$$

b. Continuity Equation:

$$w = \int_{-H}^{z} (\frac{\partial u}{\partial x} + \frac{\partial v}{\partial y})d\xi \tag{3.3}$$

c. Vertically Integrated Hydrostatic Equation:

$$p' = \int_{z}^{0} \rho g d\xi - \frac{1}{H}\int_{-H}^{0}\left[\int_{z}^{0}\rho g d\xi\right]dz \tag{3.4}$$

d. Equation of State:

$$\rho = \rho_o(1 - \alpha(T - T_o)) \tag{3.5}$$

7

e.   Thermodynamic Equation:

$$\frac{dT}{dt} = -A_H \nabla^4 T + K_H \frac{\partial^2 T}{\partial z^2} + Q_s + \delta_d(T).$$ (3.6)

In the above equations, t is time, (x,y,z) is a right-handed Cartesian coordinate system with x pointing eastward toward shore, y pointing northward alongshore, and z upward. The velocity components are (u,v,w), respectively. T is temperature, ρ is density and p' is the departure from the vertically averaged pressure. ξ is a dummy variable in equations (3.3) and (3.4). The density function is assumed to be a function of temperature only in equation (3.5). This is consistent with the region being modeled (Lynn *et al.*, 1982). Salinity may be a good tracer for water masses in the CCS (Huyer and Kosro, 1987); however it is not essential for a zero-order description since there are no major sources or sinks of salinity in this region of the CCS. In equation (3.6), $Q_s = \partial S / \rho_o C \partial z$ is the heating due to solar radiation, where

$$S = S_o (\mathrm{Re}^{-dz_1} + (1-R)e^{-dz_2}).$$ (3.7)

S_o is the downward flux of the solar radiation at the surface, $R = .62$ is the fraction of solar radiation absorbed in the upper few meters ($z_1 = 1.5$ m) and $(1-R) = .38$ is the fraction that penetrates to somewhat deeper levels ($z_2 = 20$ m) as given by Paulson and Simpson (1977). The vertical turbulent mixing of heat and momentum by a dynamic adjustment mechanism is represented by the terms $\delta_d(u)$, $\delta_d(v)$ and $\delta_d(T)$. This adjustment, a generalization of the convective adjustment mechanism, is based on the assumption of a critical Richardson number, and it serves to maintain dynamic stability in the water column (Adamec *et al.*, 1981).

8

The boundary conditions at the top $(z = 0)$ of the model are:

$$K_m \frac{\partial u}{\partial z} = \tau^x / \rho_o \qquad (3.8a)$$

$$K_m \frac{\partial v}{\partial z} = \tau^y / \rho_o \qquad (3.8b)$$

$$K_H \frac{\partial T}{\partial z} = -Q_B \qquad (3.8c)$$

$$w = 0 \qquad (3.8d)$$

and at the bottom $(z = -H)$ they are

$$K_m \frac{\partial u}{\partial z} = C_D (u^2 + v^2)^{1/2} (u \cos \gamma - v \sin \gamma) \qquad (3.9a)$$

$$K_m \frac{\partial v}{\partial z} = C_D (u^2 + v^2)^{1/2} (v \cos \gamma - u \sin \gamma) \qquad (3.9b)$$

$$K_H \frac{\partial T}{\partial z} = 0 \qquad (3.9c)$$

$$w = 0 . \qquad (3.9d)$$

τ^x and τ^y are the cross-shore and alongshore components of the surface stress in equations (3.8a) and (3.8b). In (3.8c), Q_B is the net upward flux of longwave radiation, sensible and latent heat across the sea surface. $\gamma = 10^o$ is a geostrophic inflow angle in equations (2.9a) and (2.9b) (Weatherly, G. L., 1972). Table 1 provides constants used in this study as well as other symbols in the model equations.

B. DOMAIN SIZE AND RESOLUTION

The domain of the model is a rectangular region extending from 35°N to 45°N and 6° longitude off the west coast of the United States. This region extends approximately 500 km offshore and it spans over 1000 km in the alongshore direction. Point Conception marks the southern boundary of the study while Cape Mendocino is located in the middle of the study area. The horizontal resolution of the model is 8 km in the cross-shore direction and 17.5 km in the alongshore direction. This resolution should allow realistic spatial resolution of mesoscale features in the CCS, which have typical wavelengths of the order of 100 km (Breaker and Mooers, 1986). Variations in the coastline and ocean depth are omitted in this process-oriented study to focus on the role of wind forcing in the generation of eddies and filaments.

C. FINITE DIFFERENCE SCHEME AND TIME STEPPING

A space staggered B-scheme which has u and v defined at one set of grid-points and T, ρ, and p at another (Arakawa and Lamb, 1977; Batteen and Han, 1981) is used in the horizontal. There are 10 layers in the vertical, separated by constant z-levels at depths of 13, 46, 98, 182, 316, 529, 870, 1416, 2283 and 3656 m. The time stepping used consists of a Matsuno time step followed by 10 leapfrog time steps and is continuously repeated throughout the model run.

D. HEAT AND MOMENTUM DIFFUSION

Biharmonic lateral momentum and heat diffusion with the coefficients listed in Table 1 are used in the model to allow the generation of mesoscale eddies. Laplacian

lateral heat diffusion is not used since it can diminish the baroclinic signal associated with mesoscale processes (Holland and Batteen, 1986).

E. SURFACE THERMAL FORCING

The surface thermal forcing was highly simplified in this model in order to focus on wind's role in generating thermal variability. The solar radiation at the sea surface, S_o, was specified to be the mean summer CCS value from Nelson and Husby (1983). The mean summer CCS value was used even though the study used climatological winds for all seasons because during the summer upwelling season there will be a net heat gain due to the cold upwelled water. Q_B, the net longwave radiation was computed during model experiments from standard bulk formulas using the summer CCS mean value of alongshore wind, cloud cover, air temperature, relative humidity, and model-predicted sea surface temperature (Haney et al, 1978). The initial sea-surface temperature was chosen so that the total heat flux across the sea surface, S_o - Q_B, equals zero. The only surface heat flux forcing was developed in Q_B as a result of wind-forced fluctuations in the sea surface temperature. A more detailed discussion of this formulation can be found in Batteen et al. (1989) and Haney (1985).

F. HORIZONTAL BOUNDARY CONDITIONS

The California coastline, the eastern boundary, is modeled as a straight vertical wall. A no-slip condition is imposed on the tangential velocity.

The other three boundaries are open using a modified version of the radiation boundary conditions of Camerlengo and O'Brien (1980). Forcing to the boundaries caused unrealistic surface currents with no undercurrent in cases where the wind does not have an alongshore component. To remedy this problem, we impose a band where there

11

is no wind forcing (McCreary, 1981; Batteen *et al.*, 1989; McCreary *et al.*, 1987). The bands of no wind forcing are located approximately 100 km from the northern and southern boundaries. This allows for the propagation of coastal Kelvin waves. A surface-trapped coastal jet and a relatively realistic undercurrent are established by the alongshore pressure gradient field generated by the Kelvin waves (Batteen *et al.*, 1989).

G. INITIAL CONDITIONS

An exponential temperature profile with a vertical length scale of $h = 450$ m was the initial mean stratification. The form was:

$$T_z = T_B + \nabla T e^{z/h},\qquad\qquad(3.10)$$

where $T_B = 2^{o}C$ is the temperature at the bottom layer and $\Delta T = 13^{o}C$ is the increase in temperature between the bottom and surface layer. This profile is considered to be climatologically representative of the CCS (Blumberg and Mellor, 1987).

H. WIND DATA DESCRIPTION

The winds used to force the model are from the European Centre for Medium Range Weather Forecasts (ECMWF) (Trenberth *et al.*, 1990) and were provided by the National Center for Atmospheric Research (NCAR). World-wide mean monthly wind velocities were provided at 2.5 degree spacing for the years 1980 to 1989. Two climatologies derived from 80 months and 120 months of data were also provided. Since a comparison of the two climatologies showed no apparent contrast in our area of interest, the 120-month climotology was chosen to be the representative winds for this study. The data was linearly interpolated in both time and space to provide daily forcing at the required grid points. The interpolated values are separated by approximately 8 km in the

cross-shore direction and 17.5 km in the along-shore direction, consistent with the model horizontal grid resolution. All the seasonal experiments used this 120-month climatolgical wind as the base for which the averaging (explained below) was done.

I.   EXPERIMENTAL DESIGN

The first experiment is forced with a steady -830 cm s^{-1} southward wind. The subsequent three time-varying cases broke the wind fields into different components to identify the importance each of these components played in the development of eddies and filaments. For the second and third experiments, the cross-shore component of the wind field is set to zero. The alongshore component in the second and third experiment is then averaged and applied to the model grid in the following manner:

- varying in time but averaged spatially over the entire domain (second experiment); and

- varying in time and in the alongshore direction but averaged in the cross-shore direction (third experiment).

In the final experiment, the full climatological wind field is used. All four experiments are run for 360 days.

J.   ENERGY ANALYSIS TECHNIQUE

The energy technique used in Batteen and Rutherford (1990) and Batteen *et al.* (1992) will be used to analyze the generation and stability of the California Current System, eddies and filaments. The following is a summary of the Batteen *et al.* (1992) description of this technique.

To gain an understanding of the energy transfers in the unstable flow, an energy analysis based on that of Han (1975) and Semtner and Mintz (1977) is made. The energy calculations with Semtner and Mintz (1977) notation is used in the energy calculations:

$\overline{(\ )}$ time average

$(\ )'$ time deviation

$(\ )^-$ horizontal space average

$(\ )^*$ horizontal space deviation

The kinetic energy is calculated by:

$$K = \frac{u^2 + v^2}{2}. \tag{3.11}$$

The time mean and time eddy kinetic energy are calculated, after reaching a quasi-steady state, by:

$$\overline{K} = \frac{\overline{u}^2 + \overline{v}^2}{2} \tag{3.12}$$

$$K' = \frac{\overline{u'}^2 + \overline{v'}^2}{2}. \tag{3.13}$$

Available potential energy (P) is:

$$P = \alpha g \left[\frac{1}{2} (T^*)^2 (\frac{\partial \tilde{T}}{\partial z})^{-1} \right] \tag{3.14}$$

This determines when a quasi-steady state is reached in order to collect statistics. The temporal mean and eddy available potential energy are then calculated by:

$$\overline{P} = \alpha g \left[\frac{1}{2} (\overline{T^*})^2 (\overline{\frac{\partial \tilde{T}}{\partial z}})^{-1} \right] \tag{3.15}$$

14

$$P' = \alpha g \left[\frac{1}{2} \overline{(T^*)^2} \left(\frac{\overline{\partial \tilde{T}}}{\partial z} \right)^{-1} \right] \qquad (3.16)$$

Following Semtner and Mintz (1977), transfers between energy types are defined as:

$$\left\{ \overline{K} \rightarrow \overline{P} \right\} = -\alpha g \left[\overline{Tw} \right] \qquad (3.17)$$

$$\left\{ P' \rightarrow K' \right\} = \alpha g \left[\overline{T'w'} \right] \qquad (3.18)$$

$$\left\{ \overline{K} \rightarrow K' \right\} = \bar{v} \left(\nabla \bullet \overline{v'v'} + \frac{\partial}{\partial z} \overline{w'v'} \right) \qquad (3.19)$$

$$\left\{ \overline{P} \rightarrow P' \right\} = \alpha g \left(\overline{T^* \nabla \bullet v'T^*} + \left(\frac{\overline{\partial \tilde{T}}}{\partial z} \right)^{-1} \right) \qquad (3.20)$$

Vertical velocity and advection terms calculated by the model are not stored. Vertical velocity and advection terms are recalculated in the same manner as in the model using stored values of u, v and T as the input data. The recalculated energy transfers are consistent with the initial calculations of vertical velocity and advection terms in the model.

The energy transfer analysis is used to argue for the instability mechanism which leads to the initial eddy generation by studying the quasi-steady energetic state prior to eddy generation.

Table 3.1. VALUES OF CONSTANTS USED IN THE MODEL

	VALUE	DEFINITION
c	$0.958 \text{ cal gm}^{-1} (^{\circ}\text{K})^{-1}$	specific heat of sea water
c_D	1.225×10^{-3}	bottom drag coefficient
T_o	278.2°K	constant reference temperature
ρ_a	$1.23 \times 10^{-3} \text{ gm cm}^{-3}$	density of air
ρ_o	$1.0276 \text{ gm cm}^{-3}$	density of sea water at T_o
α	$2.01 \times 10^{-4} (^{\circ}\text{K})^{-1}$	thermal expansion coefficient
K	10	number of levels in vertical
Δx	$7.6 \times 10^{5} \text{ cm}$	cross-shore grid spacing
Δy	$1.75 \times 10^{6} \text{ cm}$	alongshore grid spacing
D	$4.5 \times 10^{5} \text{ cm}$	total ocean depth
Δt	800 s	time step
f_o	$0.93 \times 10^{-4} \text{ s}^{-1}$	mean Coriolis parameter
g	980 cm s^{-1}	acceleration of gravity
A_M	$2 \times 10^{17} \text{ cm}^4 \text{ s}^{-1}$	biharmonic momentum diffusion coefficient
A_H	$2 \times 10^{17} \text{ cm}^4 \text{ s}^{-1}$	biharmonic heat diffusion coefficient
K_M	$0.5 \text{ cm}^2 \text{ s}^{-1}$	vertical eddy viscosity
K_H	$0.5 \text{ cm}^2 \text{ s}^{-1}$	vertical eddy conductivity

IV. RESULTS OF WIND FORCING EXPERIMENTS

Experiment 1 studies the effects of steady, equatorward (upwelling-favorable) winds in the CCS. Experiments 2 through 4 investigate the effects of seasonally varying winds in the same region, using climatological monthly values that have been interpolated to daily values. Experiment 2 uses temporally varying, spatially averaged winds, while Experiment 3 uses winds with temporal variation and alongshore variability. In Experiment 4 the full climatological, seasonally varying wind field is used.

A. EXPERIMENT 1

In Experiment 1 the model was forced with a steady -830 cm s^{-1} equatorward wind. This wind forcing of 1 dyne cm^{-2} is the summer (June-August) average for the modeled area (Batteen et $al.$, 1989). Inertial oscillations of near-surface ocean currents developed initially, as in Batteen et $al.$ (1991). After a few days the oscillations were damped, leaving quasi-steady offshore Ekman transport (not shown). By day 20 an equatorward coastal jet developed with speeds of ~15 cm s^{-1} (Fig. 4.1a,c). Colder surface temperatures also appeared near the coast (Fig. 4.1b). A poleward undercurrent is also discernible at 182 m depth (Fig. 4.1d). The surface current flowed at ~25 cm s^{-1}, and extended ~35 km offshore (Fig. 4.1c), while the undercurrent, centered along the coast, had weaker velocities of ~5 cm s^{-1} (Fig. 4.1d).

Plots of the zonal velocity (Figs. 4.2a, b) show that eddies begin to form around days 60 and 70 as evidenced by perturbations in the zonal velocity fields. (Since meridional velocity plots tend to be dominated by the predominately meridional currents, perturbations are more clearly seen in zonal rather than meridional velocity plots.) The isotherms also show meanderings in the same region where the eddies are generated

17

(Figs. 4.2c, d). As expected, eddies first formed in the poleward end of the region, as in the β-plane experiment of Batteen et al. (1989). The vertical cross-section of meridional velocity at day 90 (Fig. 4.3) shows that the surface equatorward current has its core at ~80 m depth with a speed of ~25 cm s^{-1}, while the undercurrent develops below a depth of ~240 m within ~25 km of the coast.

Both baroclinic and barotropic transfers (equations 3.18 and 3.19, respectively) can contribute to the formation of eddies. Baroclinic instability draws its energy from the vertical shear in the mean flow while barotropic instability receives energy from the horizontal shear (Haltiner and Williams, 1980; Batteen et al. 1989). Figure 4.4 shows that although both baroclinic (Fig. 4.4a) and barotropic (Fig. 4.4b) instabilities play a key role in the generation of eddies, barotropic instability is the dominant generation mechanism. Plots of the surface velocity vectors superimposed on the isotherms (Fig. 4.5a-d)and the meridional velocity contours (Fig. 4.6a-d) at 90 day intervals show how the meandering current continues to grow in strength and to spin off isolated eddies. This strong meandering current can produce eddies that have wavelengths up to ~ 200 km and that can propagate at least ~ 200 km offshore (Figs. 4.5 and 4.6).

Although these results show a meandering current and eddies, it is very unlikely that there will be steady strong equatorward (upwelling favorable) winds for 360 days, since there are many periods of poleward winds and also wind relaxations in the CCS region. Therefore, three more experiments with a time varying wind, were conducted in order to better understand what critical unsteady wind forcing elements are needed for the formation and maintenance of currents and eddies.

B. EXPERIMENT 2

The second experiment utilized the alongshore-component of the temporally averaged ECMWF winds. The seasonal cycle of this wind field is plotted in Figs. 4.7 and 4.8. At the beginning of the year, the wind forcing was very weak, and the winds remained weak until day 135. From days 135 to 225, the wind was equatorward and continued to grow in strength. The wind then decreased in strength until it was nearly zero again at day 360.

The model simulation results show an equatorward coastal jet and colder surface temperatures near the coast by day 180 (Fig. 4.9b). The surface current flowed at ~10 cm s^{-1}, and extended ~25 km offshore, while the undercurrent had weaker velocities of ~1.5 cm s^{-1} and was centered along the coast at ~120 m depth (Fig. 4.10).

The isotherms show meanderings in the same region where the eddies are generated (Figs. 4.9 and 4.10). Again the eddies first formed in the poleward end of the region, as expected. Fig. 4.12 shows that both baroclinic and barotropic instabilities contribute to the generation of eddies, with the barotropic instability being the dominant mechanism. The plots of the surface velocity vectors superimposed on the isotherms at selected days between 130 and 270 show how the meandering current continues to grow in strength and to spin off isolated eddies (Figs. 4.9 and 4.10). As expected, this meandering current weakens and dissipates as the seasonal cycle of the temporal wind weakens.

With this non-spatially varying seasonal cycle, currents and eddies are generated much later than with the ideal upwelling favorable winds of the first experiment. The major portion of activity happened between day 135 and day 290 and only showed very

19

weak upwelling and little eddy activity (Figs. 4.9-4.10). The eddies also only propagated to ~ 100 km offshore.

C. EXPERIMENT 3

The third experiment uses the alongshore component of the time-dependent wind forcing with spatial variability in latitude The wind forcing is divergent at the beginning of the year with poleward winds north of 40° N latitude and equatorward winds south of 40° N latitude. The wind stress shifts to being equatorward everywhere by day 135, intensifying from days 135 to 225, and then splits again by day 315 (Figs. 4.13 and 4.14).

The ocean response is evident by day 70 when an equatorward coastal jet forms (not shown). Eddies form by days 240 and 260 (Figs. 4.15a,b). Meanders in the isotherms in the areas of these eddies are also evident (Figs. 4.15c,d). The cross-section of the meridional velocity at day 260 (Fig. 4.16) shows an equatorward surface current with speeds of ~35 cm s^{-1} and a poleward undercurrent with its core located 40 km offshore and at a depth of 350 m.

In this experiment, there is a competition between the β-plane effect, which will cause eddies to form in the poleward end of the domain, and the continuous and stronger equatorward wind forcing in the southern portion of the domain. This causes eddies to form throughout the region so that by day 300 the eddies encompass the area from the northern boundary to the southern boundary of the domain (Figs. 4.17a,c). Day 360 shows the strong meandering current with large eddies imbedded in it (Figs. 4.17b,d).

Figures 4.18a,b show that while both baroclinic and barotropic instabilities are eddy generating mechanisms in the poleward portion of the domain, it is primarily the barotropic instability that contributes to the generation of eddies in the southern portion of the domain where the wind is predominately equatorward. The wind forcing in this

20

experiment produced larger eddies (that propagate at least ~ 150 km from shore) and eddy velocities than were seen in the previous experiment, which is more consistent with available observations.

D. EXPERIMENT 4

The final experiment uses full climatological wind forcing (Figs. 4.19 and 4.20). Again the divergence in the winds at 40° N is evident in the beginning of the year. By day 135, the winds over the entire domain have an equatorward component and by day 225 the winds are predominately equatorward everywhere and strongest in magnitude. After day 225 the winds become less intense and by day 360, north of 40° N the wind becomes poleward again.

As in the previous cases, inertial oscillations of near-surface ocean currents developed initially. After a few days these observations were damped, leaving quasi-steady offshore Ekman transport (not shown). By day 20 an equatorward coastal jet developed(not shown). At day 110 the surface current flowed at ~40 cm s^{-1}, and extended ~35 km offshore, while a weak undercurrent was evident (Fig. 4.21). The meridional velocity cross-section at day 180 (Fig. 4.22) shows a strong equatorward surface jet centered ~50 km offshore with speeds of ~60 cm s^{-1}. The poleward undercurrent is located at ~360 m depth and ~40 km offshore.

Plots of the zonal velocity (Fig. 4.23d) show that eddies begin to form around day 260 as evidenced by perturbations in the zonal velocity fields. As expected, the isotherms also show meanderings in the same region where the eddies are generated (Fig. 4.23c). The eddies again formed initially in the poleward end of the region.

Figure 4.24 shows that, although both baroclinic (Fig. 4.24a) and barotropic (Fig. 4.24b) instabilities play a key role in the generation of eddies, barotropic instability is the

dominant generation mechanism. Days 300 to 360 (Figs. 4.25-4.27) show the current becoming stronger with the eddies continuing to grow and to separate from the coast The speeds of the currents and eddies reach ~ 65-85 cm s^{-1} with wavelengths of ~ 300 km and can propagate to ~ 350 km offshore. This case gives results that are more consistent with available observations than was obtained in any of the previous cases. However, the speed and depth of the undercurrent are still not quite in agreement with observations
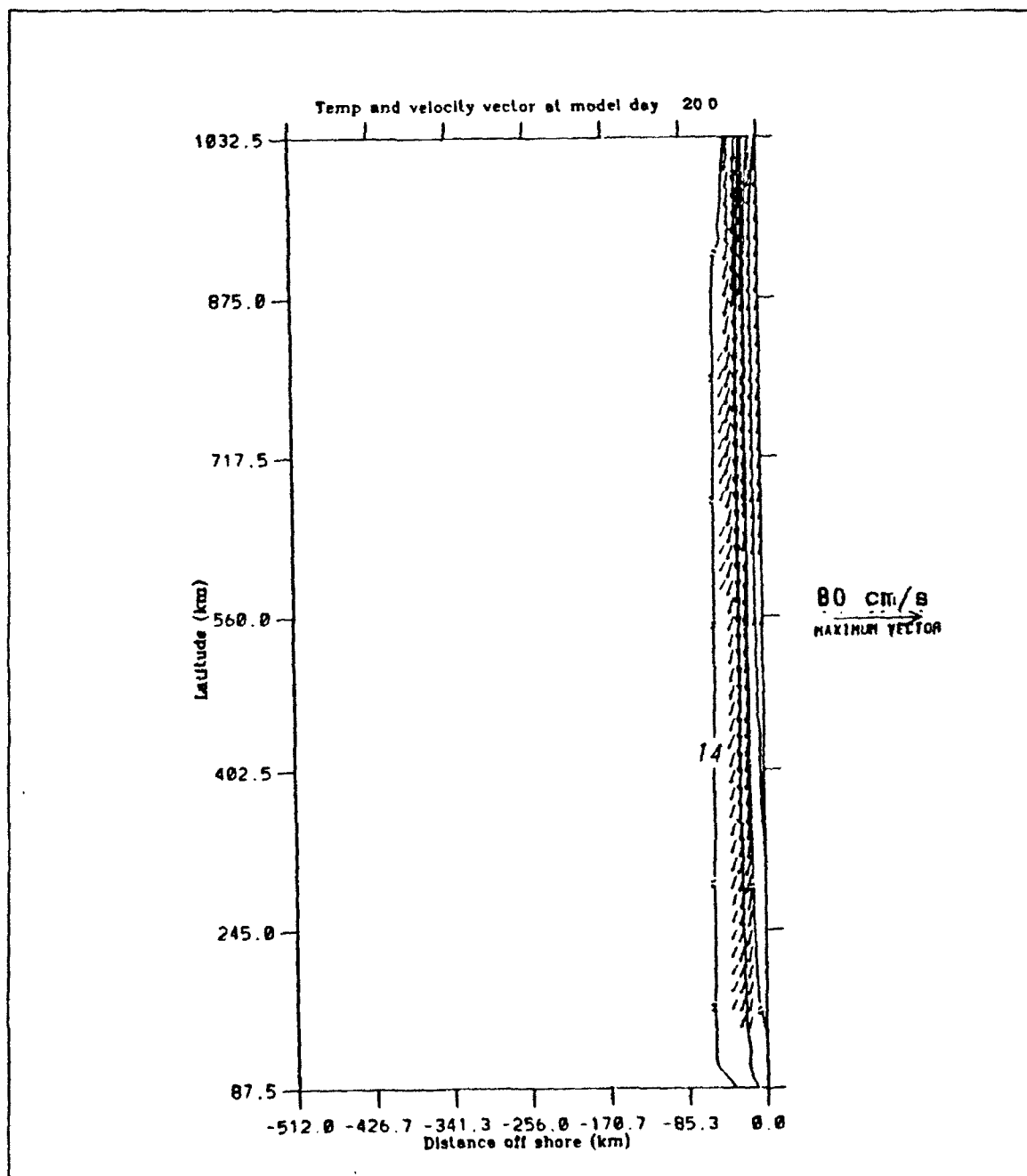
Figure 4.1a) Experiment 1 Day 20: Surface velocity vectors superimposed on isotherms. The contour interval for the isotherms is 0.5° C. The temperature decreases toward the coast.
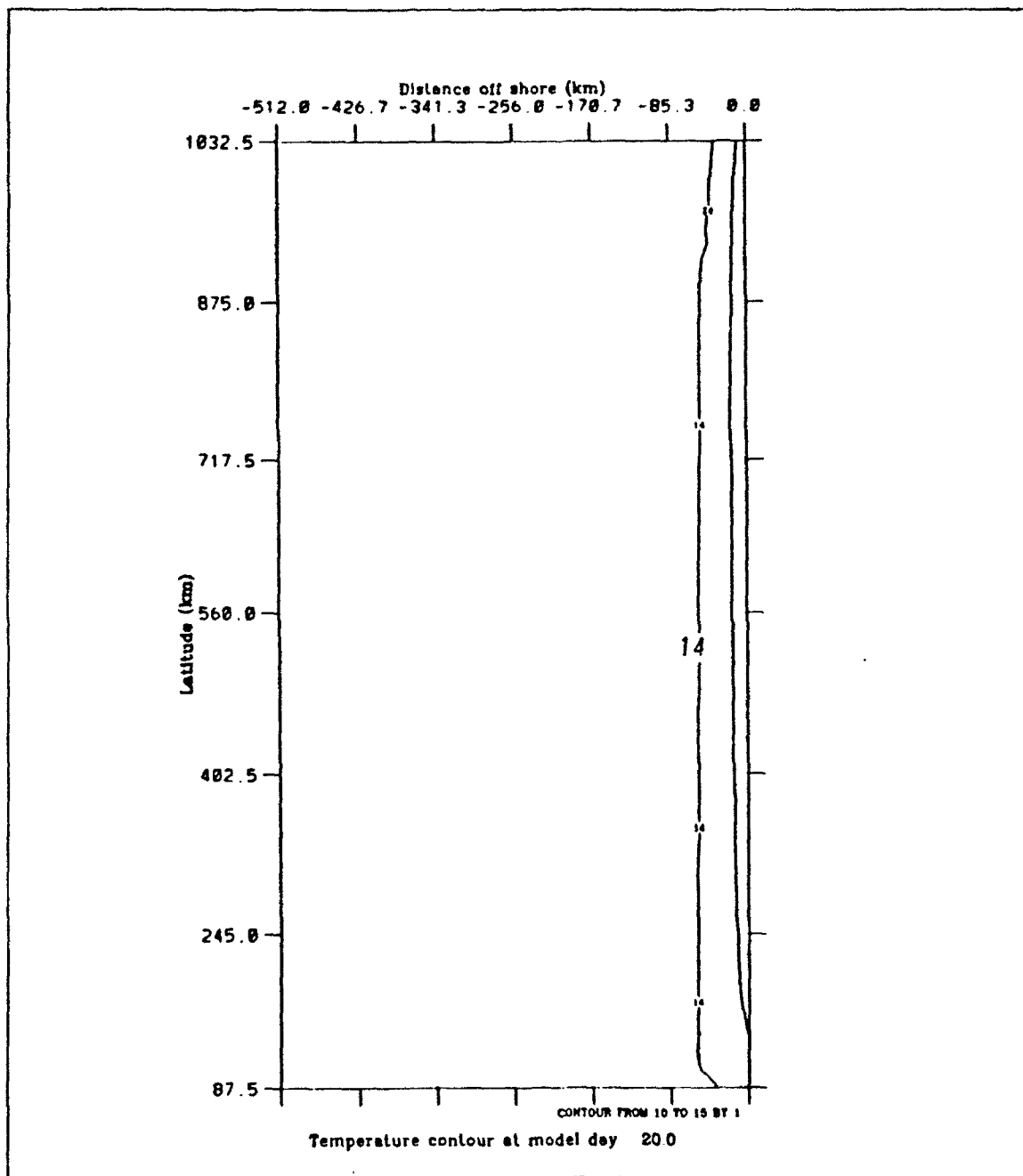
Figure 4.1 b) Experiment 1: Day 20 Temperatures. The contour interval for the isotherms is 1.0° C. The temperature decreases toward the coast.

Distance off shore (km)

North-South vel contour at model day 20.0
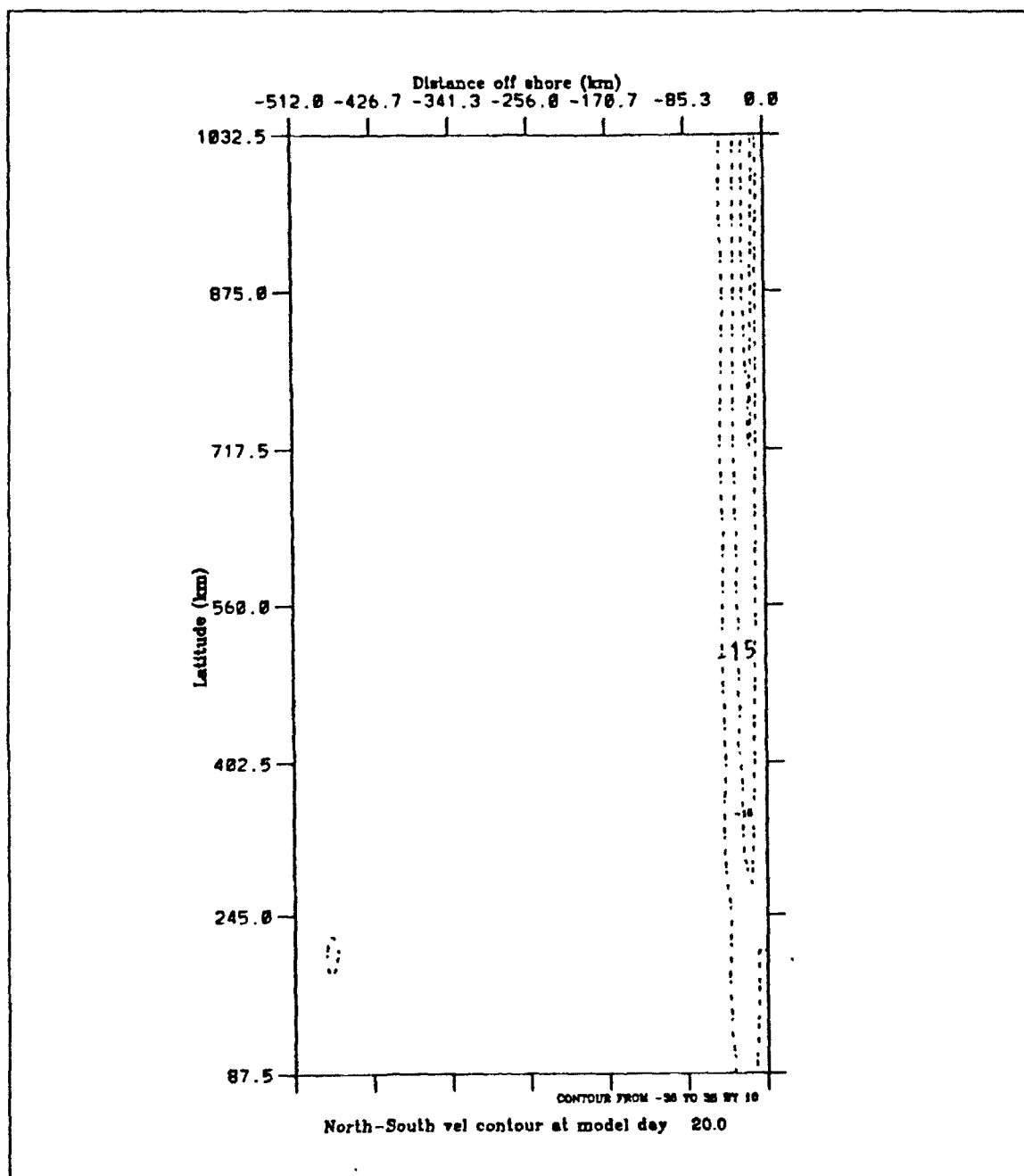
Figure 4.1 c) Experiment 1: Day 20 Meridional velocities. The contour interval is 10 cm s⁻¹. The dashed lines indicate southward velocities. The equatorward velocity increases to ~ 25 cm s⁻¹ near the coast.

25
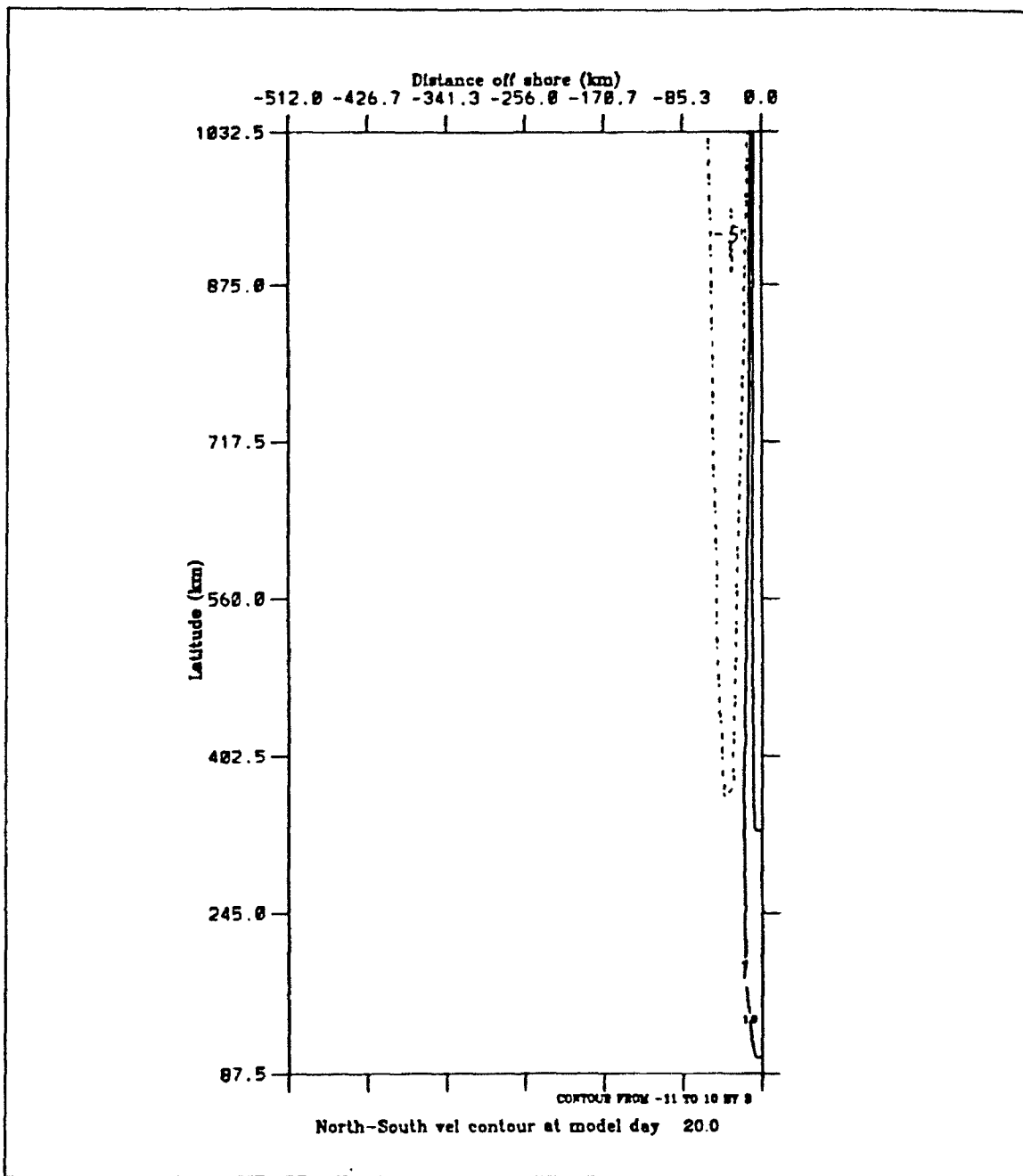
Figure 4.1 d) Experiment 1: Day 20 Meridional velocities at 182m.   The contour interval is 3 cm s^{-1}.
The dashed lines indicate southward velocities. The poleward undercurrent is seen at the coast.

Figure 4.2 a) Experiment 1: Surface Zonal velocities at day 60. The contour interval is 10 cm s⁻¹. The dashed lines indicate westward velocities. Closed contours show the locations of eddies.
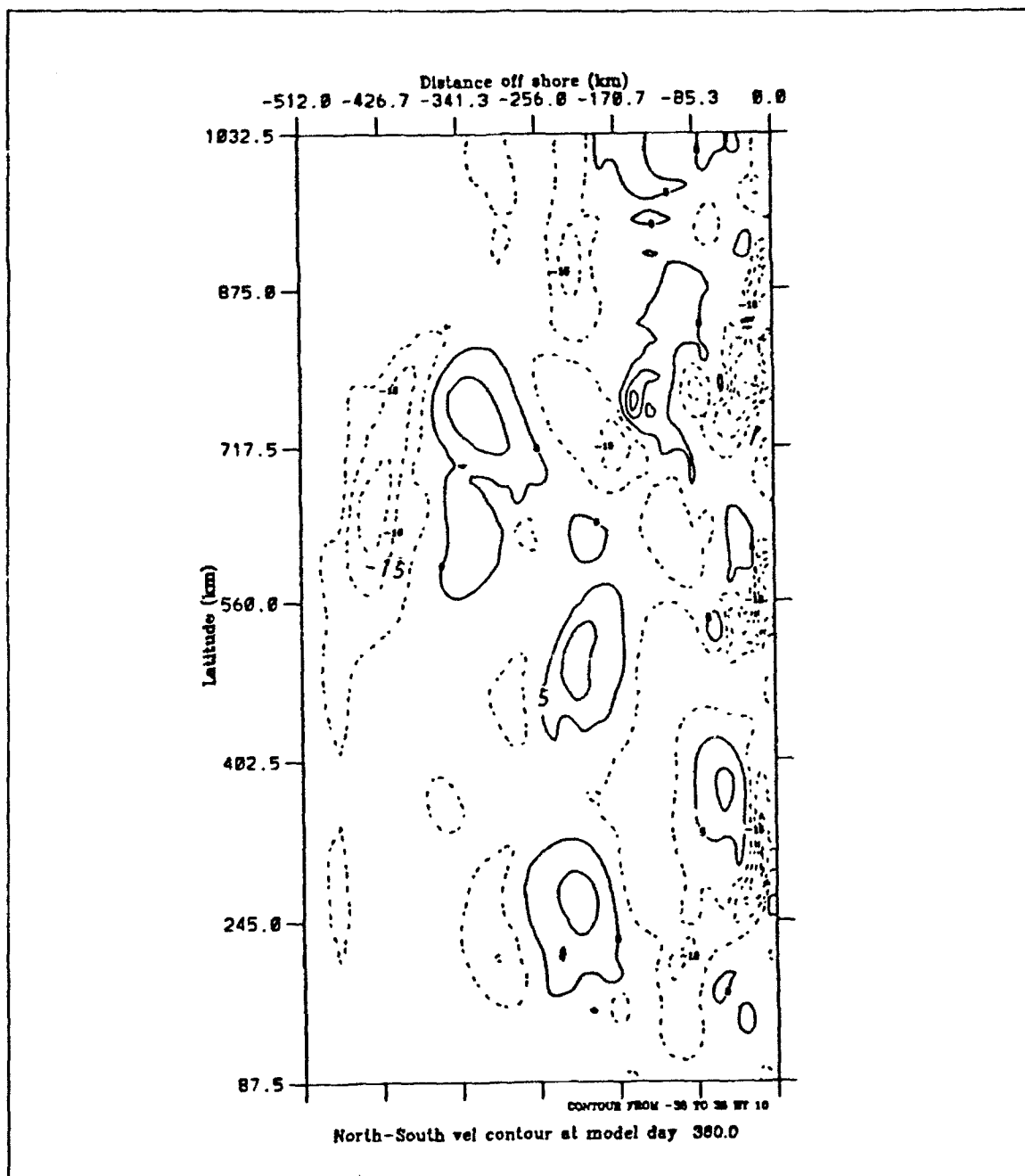
27

Figure 4.2 b) Experiment 1: Surface Zonal velocities at day 70. The contour interval is 10 cm s^{-1}. The dashed lines indicate westward velocities. Closed contours show the locations of eddies.

Figure 4.2 c) Experiment 1: Surface temperatures at day 60. The contour interval is 1° C. The temperature decreases toward the coast.
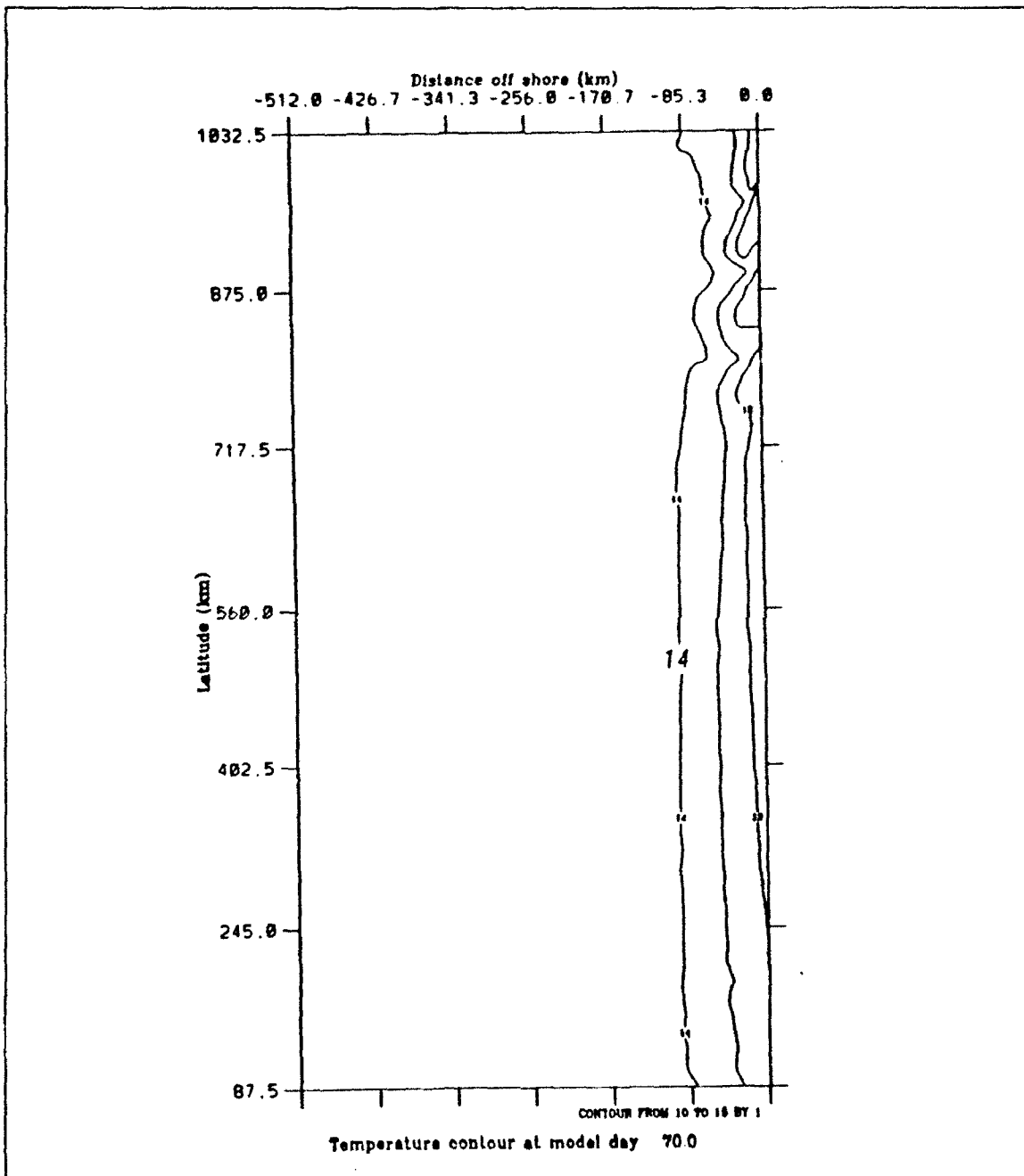
Figure 4.2 d) Experiment 1: Surface temperatures at day 70. The contour interval is 1° C. The temperature decreases toward the coast.

North–South velocity at model day   90.0

Depth (meter)

Distance off shore (km)

CONTOUR FROM −25 TO 2.8 BY 1.1
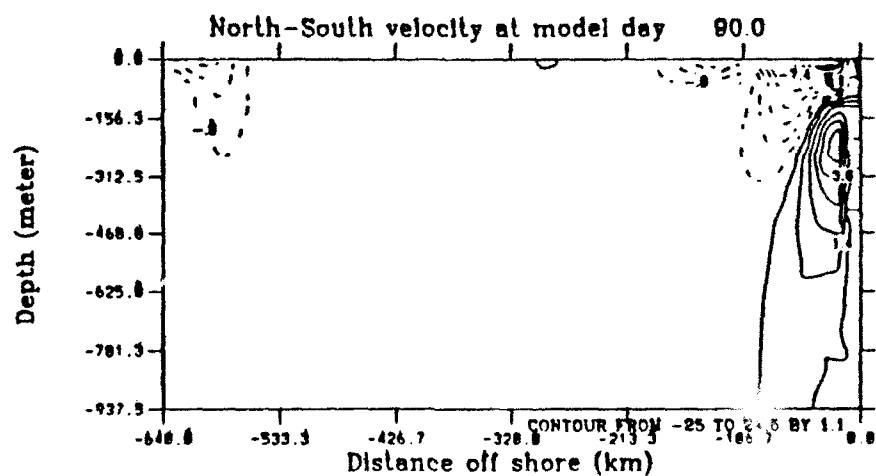
Figure 4.3 Experiment 1: Cross-section at 40° N latitude of meridional velocities at day 90. The contour interval is 1.1 cm s⁻¹. The dashed lines indicate southward velocities and show the surface equatorward current. The solid lines indicate northward flow and show the poleward undercurrent.

31
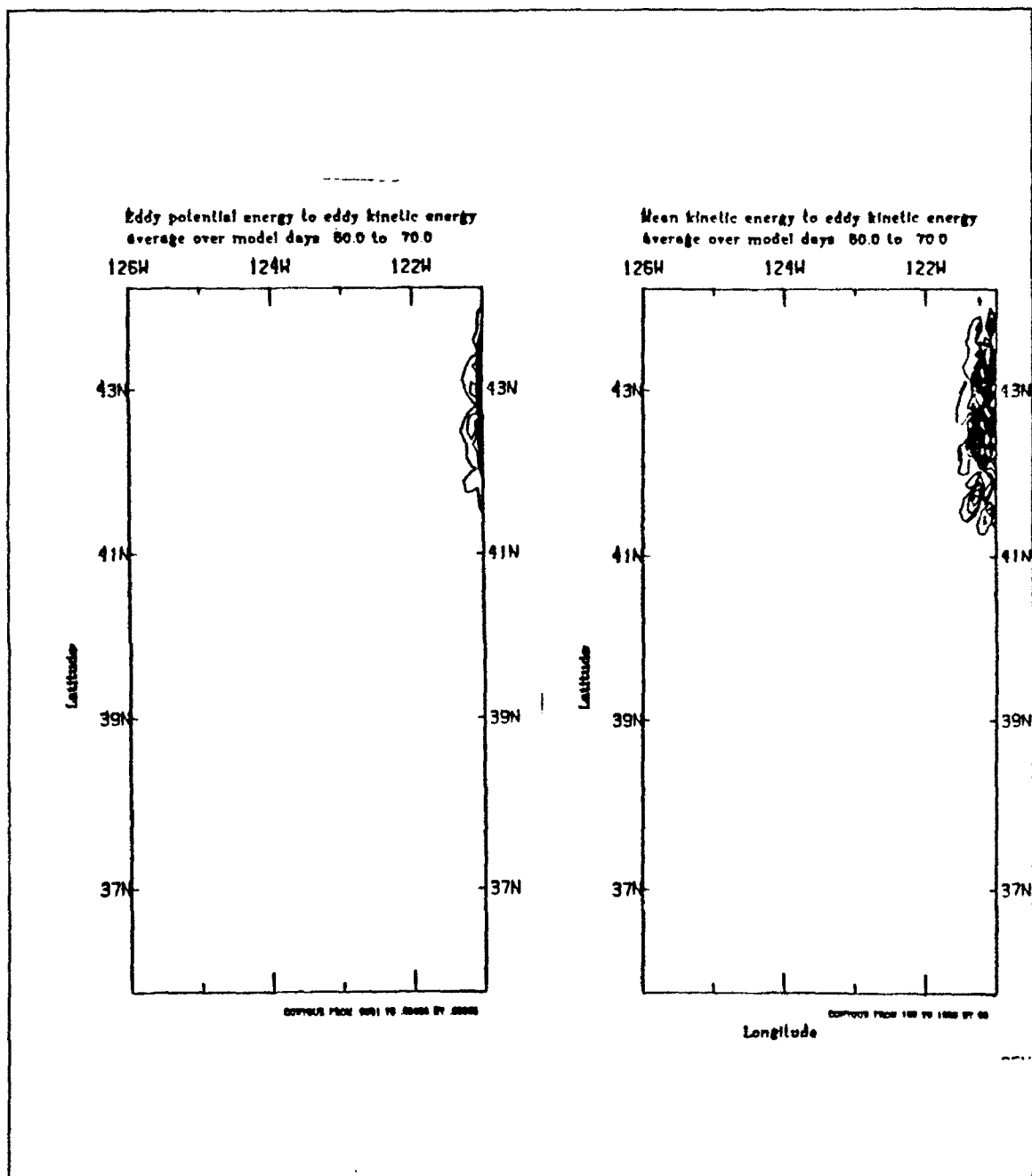
Figure 4.4 Experiment 1 Transfers of energy (as defined in equations 3.18 and 3.19) from: a) P' to K' (eddy available to eddy kinetic energy), and b) $\overline{K}$ to K' (mean to eddy kinetic energy). Transfers of energy are averaged over the days 50-70 and summed over the upper five layers. The contour intervals are 0.00005 ergs cm^{-3} s^{-1} in a) and 50 ergs cm^{-3} s^{-1} in b).

32
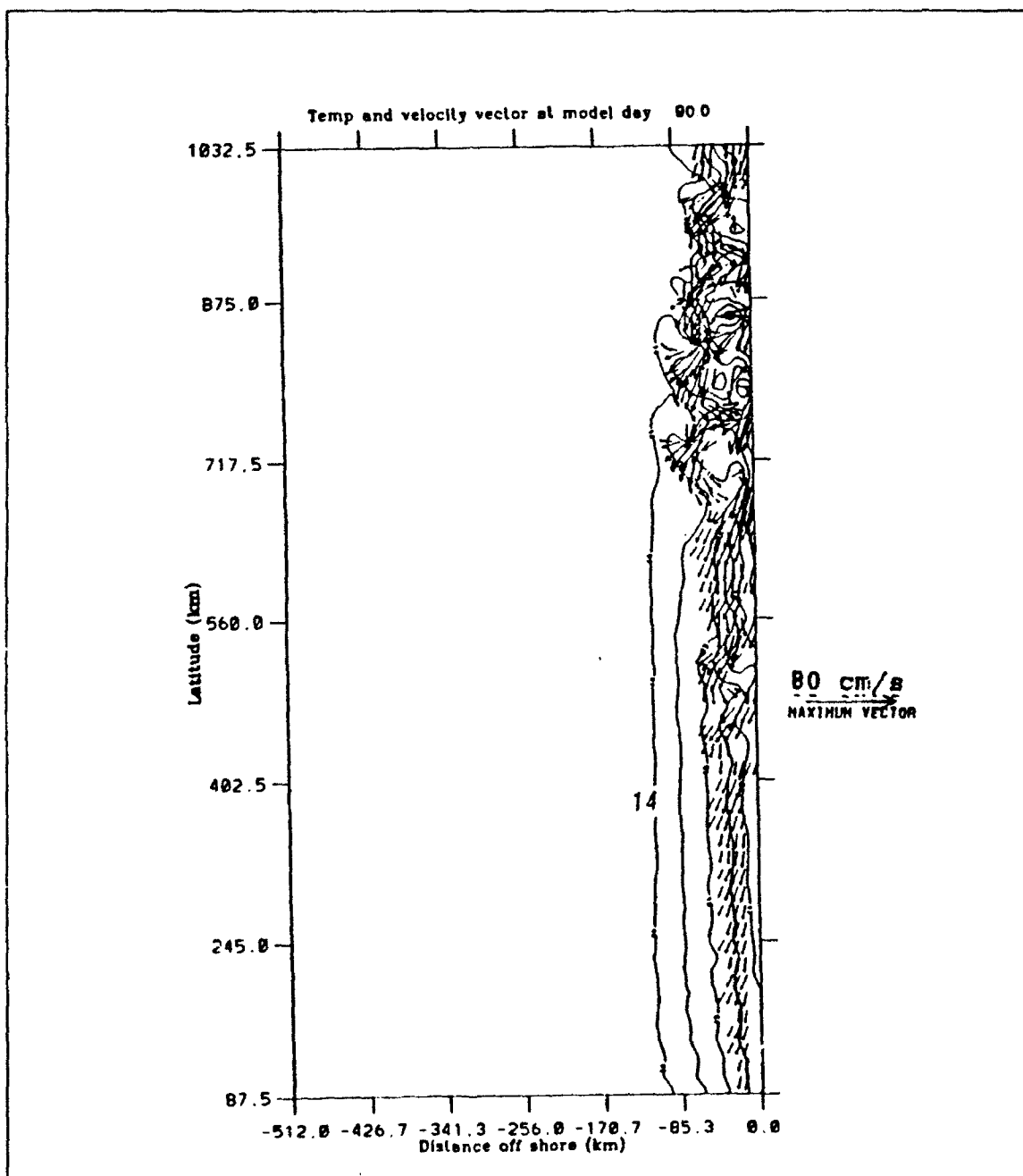
Figure 4.5a) Experiment 1: Surface velocity vectors superimposed on temperatures at day 90. The contour interval is 0.5° C. The temperature decreases toward the coast.
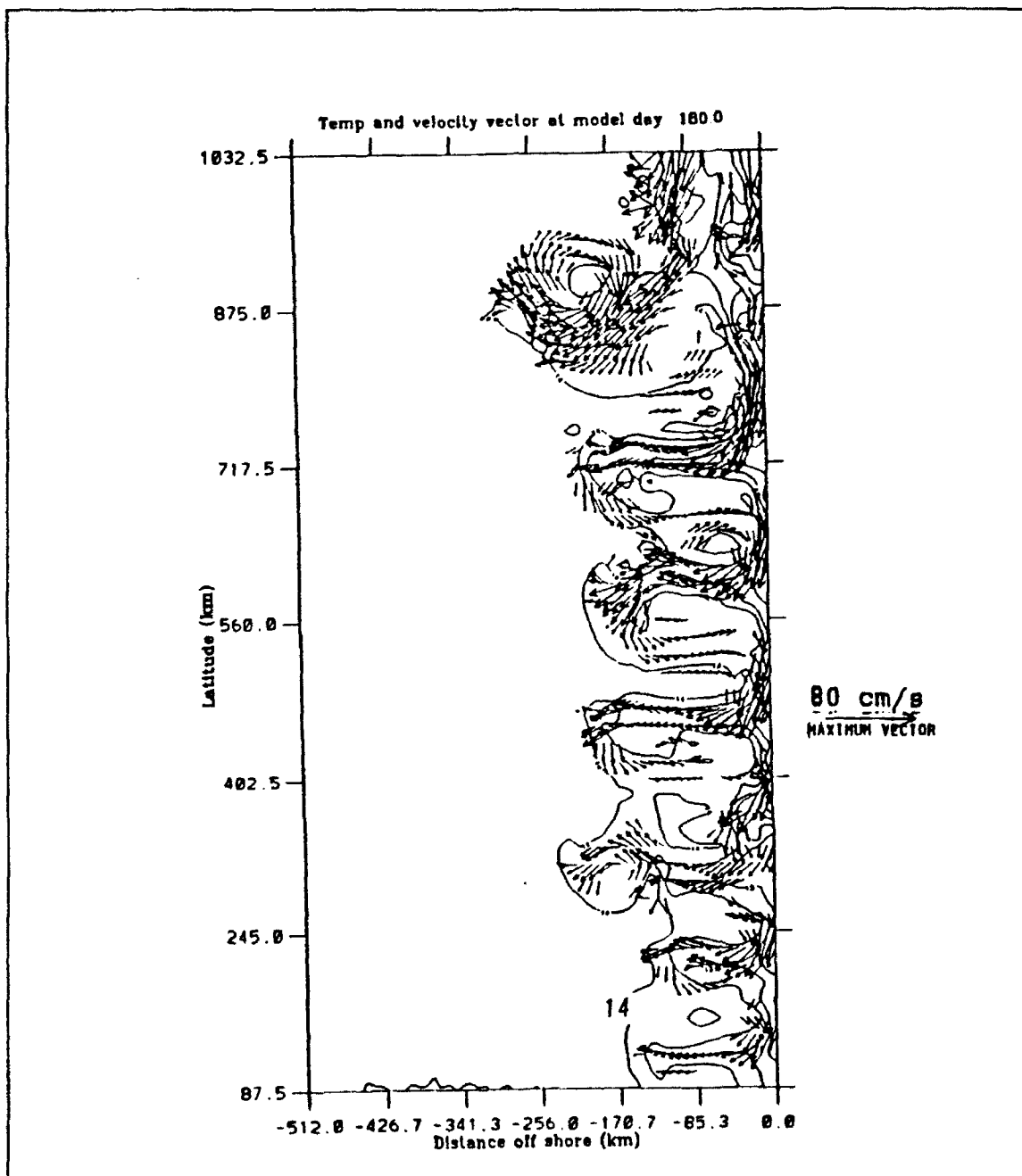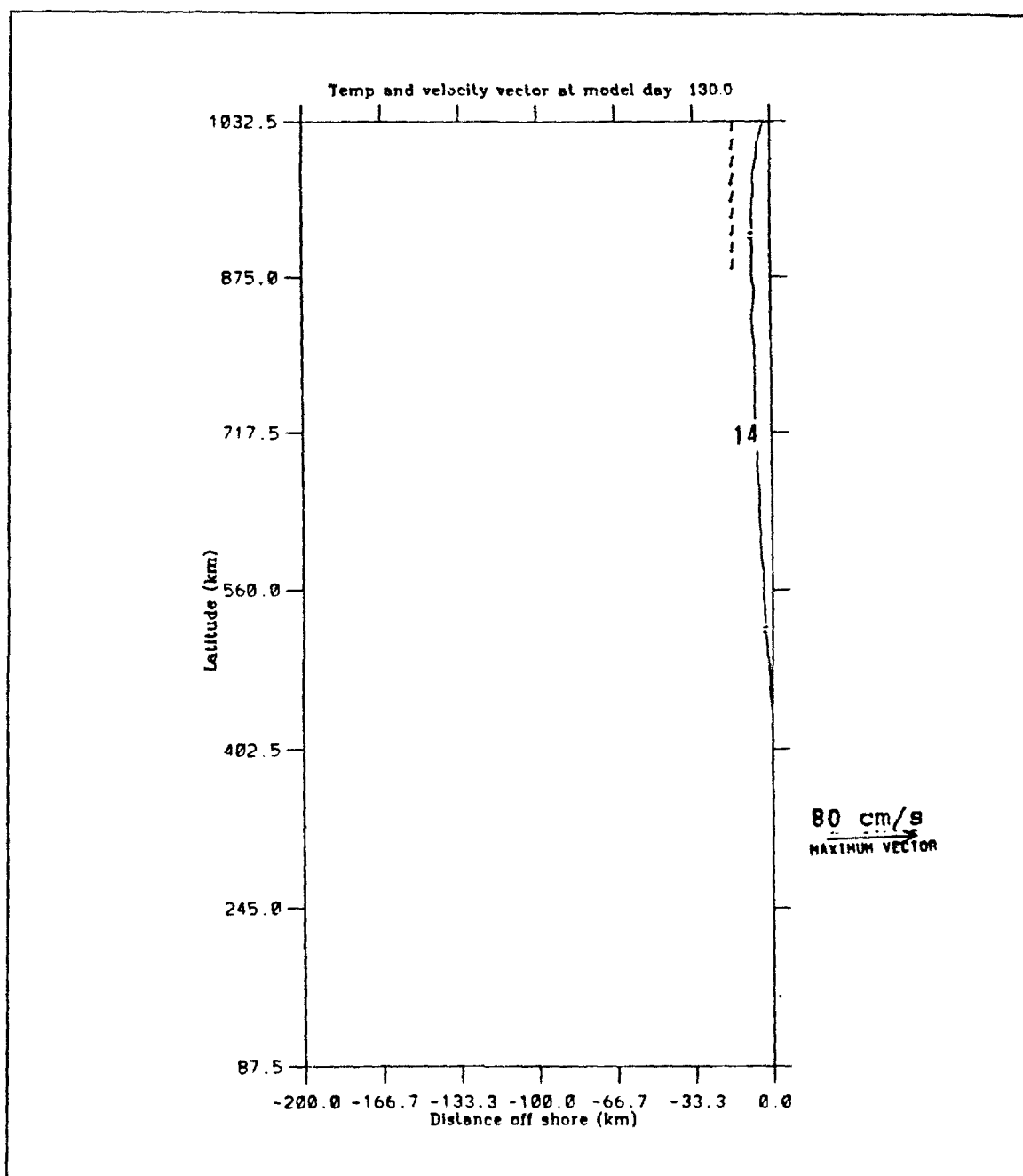
Figure 4.5 b) Experiment 1: Surface velocity vectors superimposed on temperatures at day 180. The contour interval is 0.5° C. The temperature decreases toward the coast.
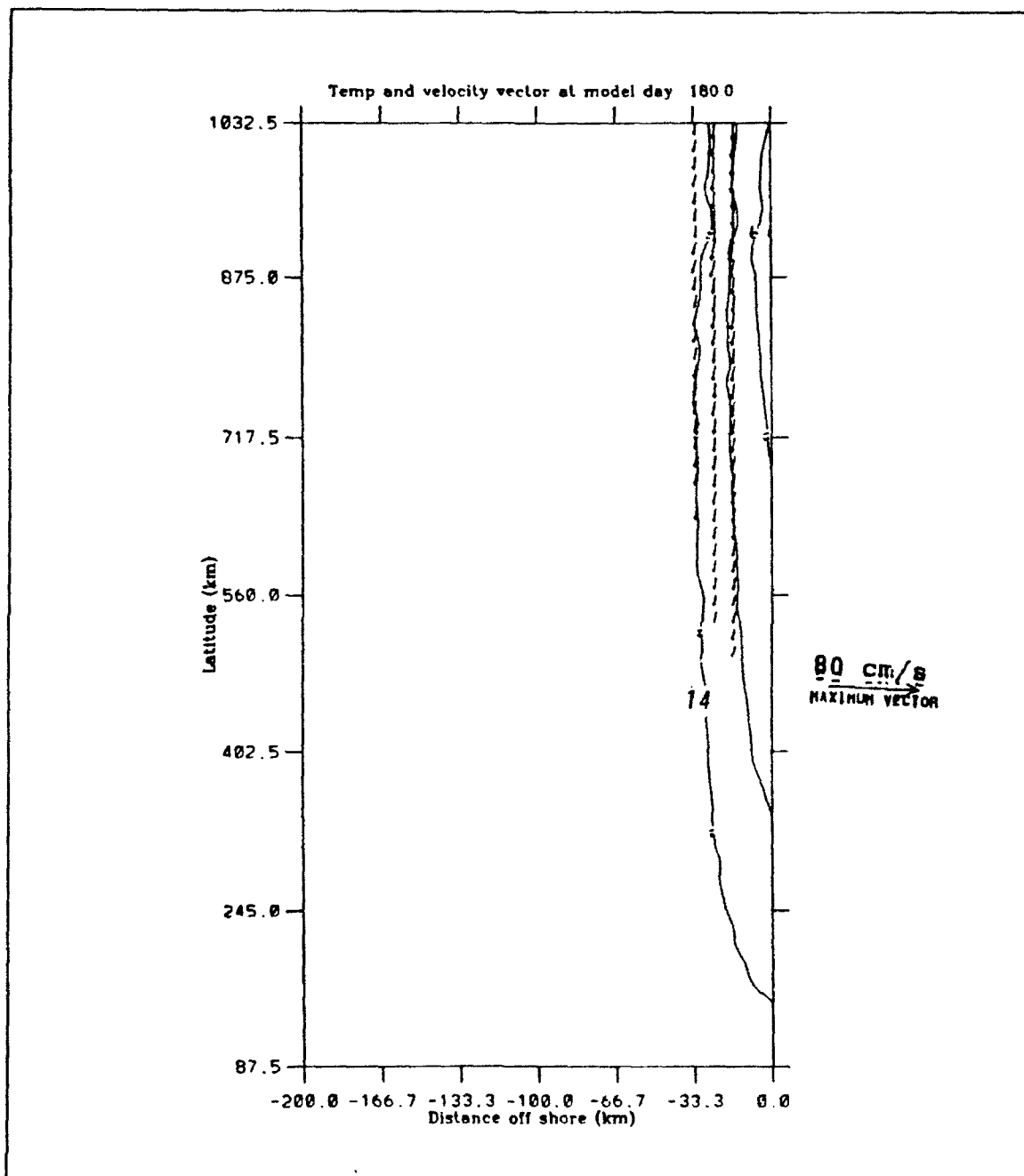
34
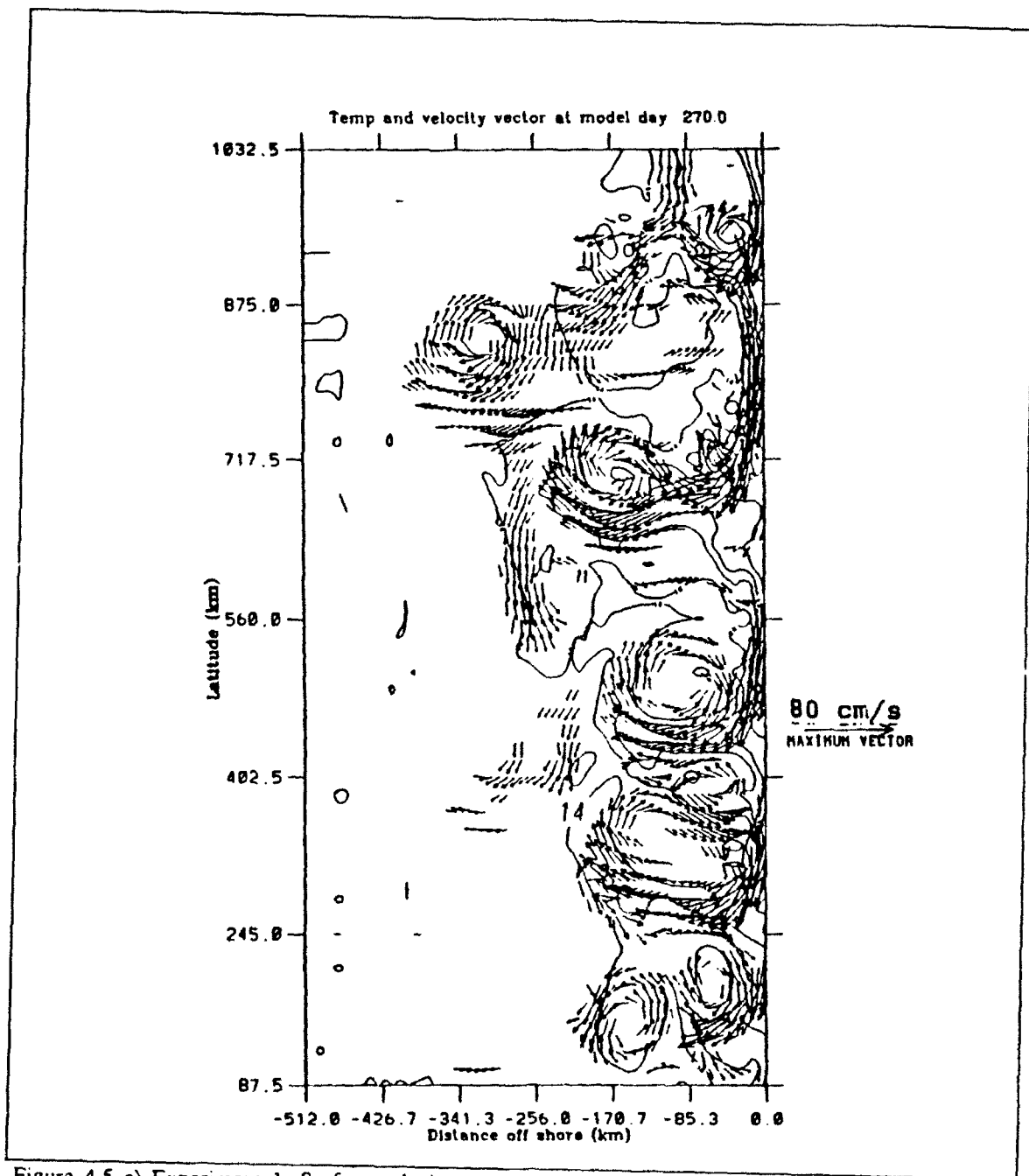
Figure 4.5 c) Experiment 1: Surface velocity vectors superimposed on temperatures at day 270. The contour interval is 0.5° C. The temperature decreases toward the coast.

35
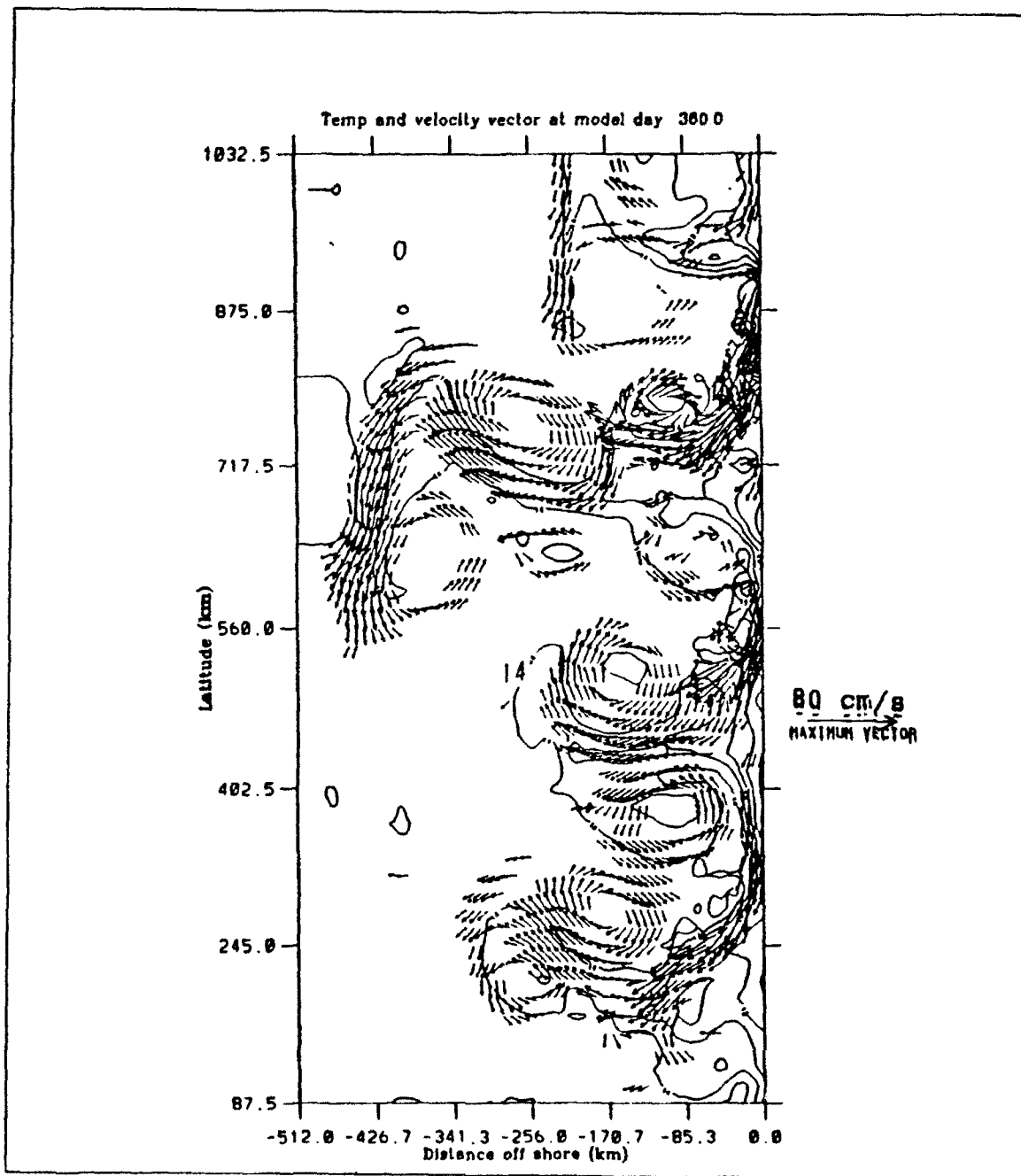
Figure 4.5 d)Experiment 1: Surface velocity vectors superimposed on temperatures at day 360. The contour interval is 0.5° C. The temperature decreases toward the coast.

36
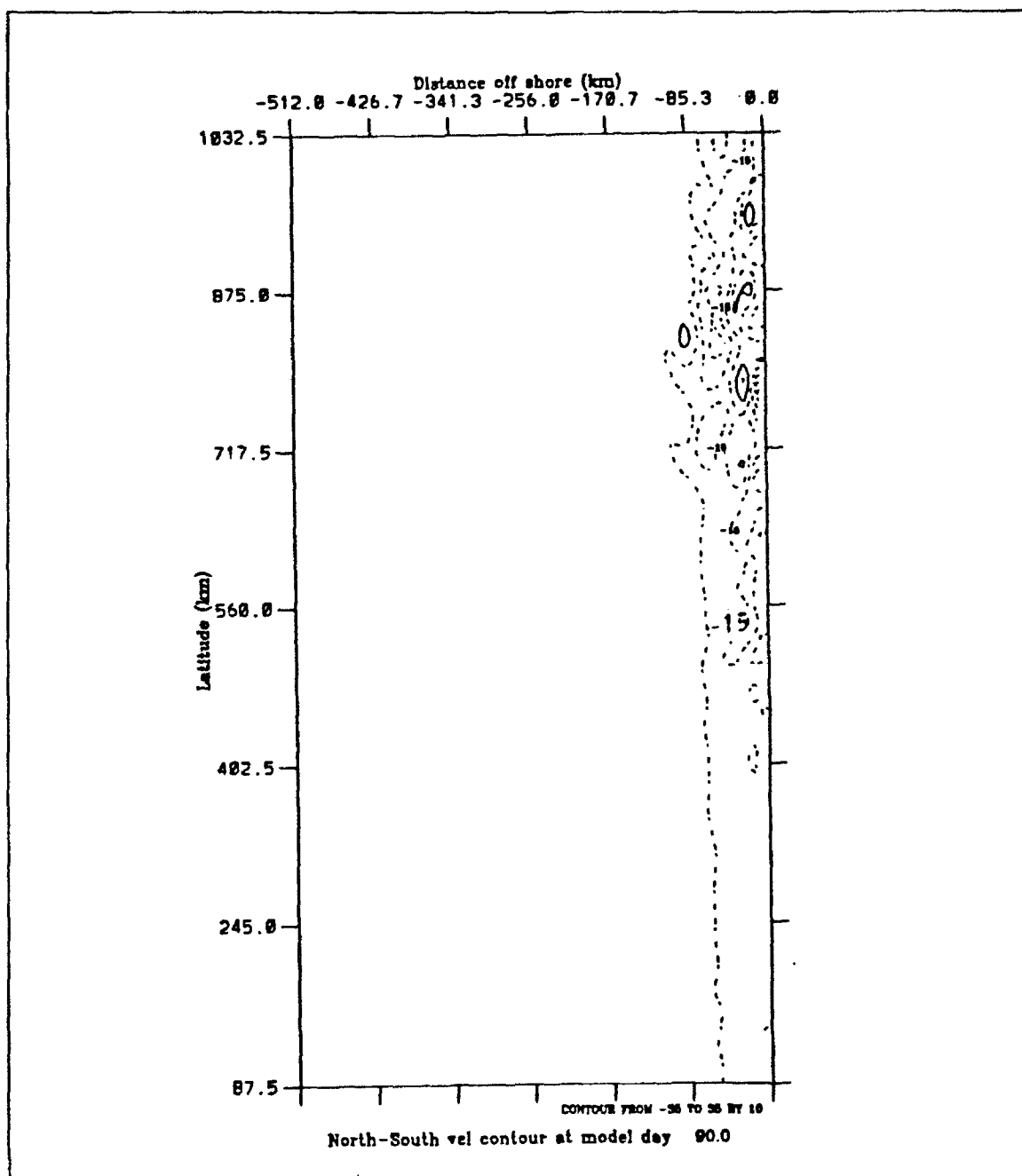
Figure 4.6 a) Experiment 1: Surface meridional velocities at day 90. The contour interval is 10 cm s^{-1}. The dashed lines indicate southward velocities. Closed contours show the locations of eddies.
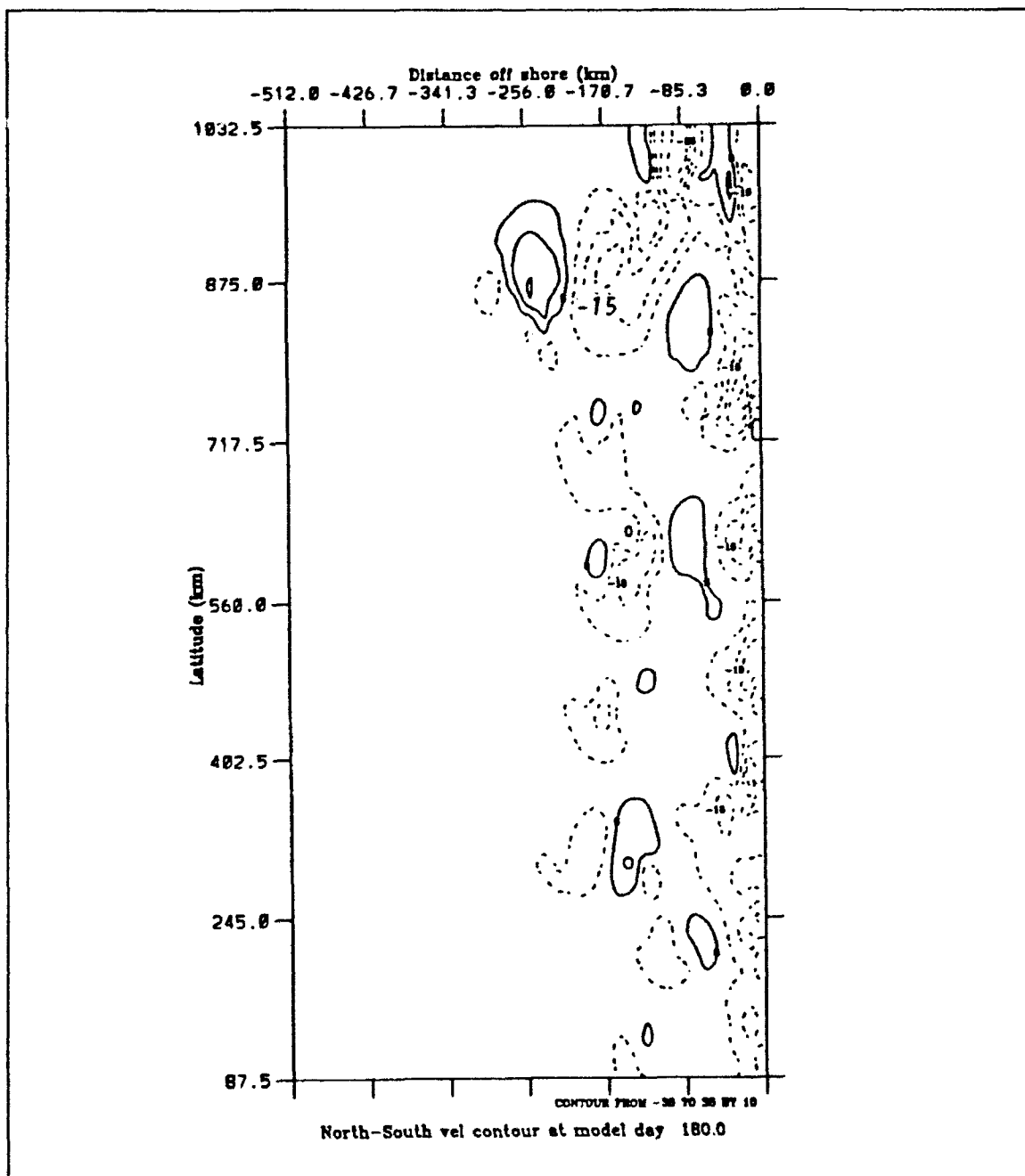
Figure 4.6 b) Experiment 1: Surface meridional velocities at day 180. The contour interval is 10 cm s^{-1}. The dashed lines indicate southward velocities. Closed contours show the locations of eddies.
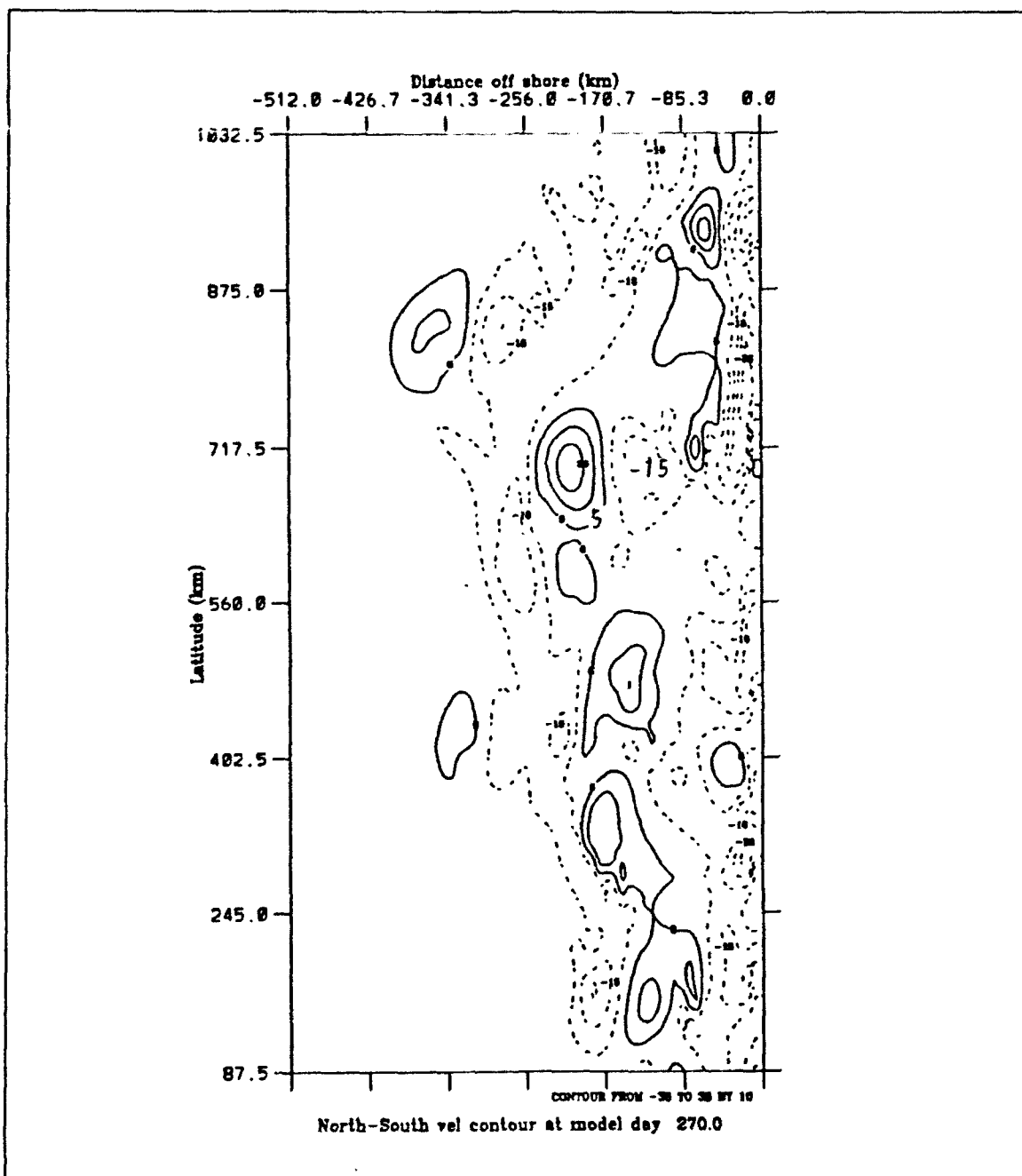
Figure 4.6 c) Experiment 1: Surface meridional velocities at day 270. The contour interval is 10 cm s^{-1}. The dashed lines indicate southward velocities. Closed contours show the locations of eddies.

Figure 4.6 d) Experiment 1: Surface meridional velocities at day 360. The contour interval is 10 cm s⁻¹.
The dashed lines indicate southward velocities. Closed contours show the locations of eddies.
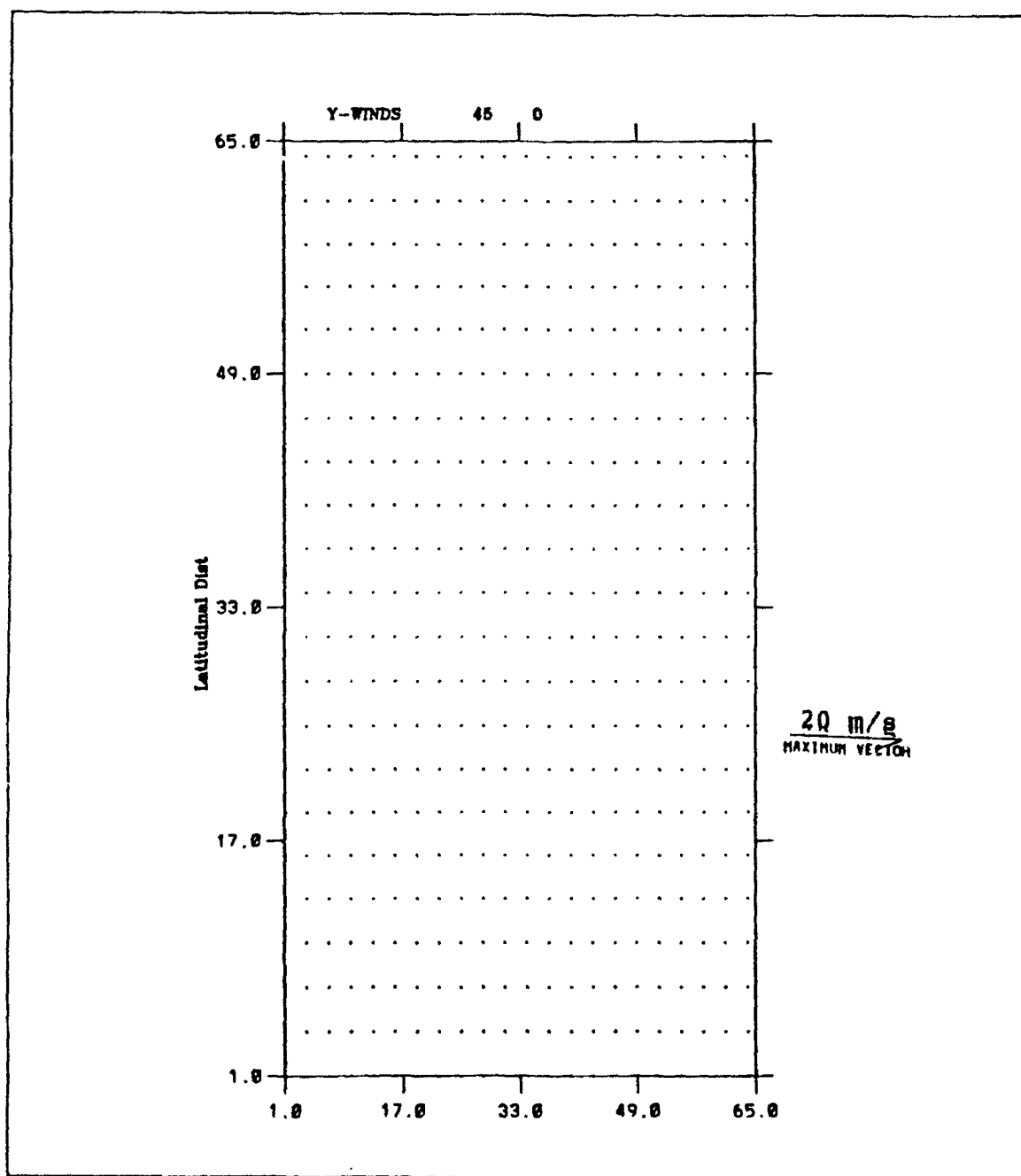
Figure 4.7a) Experiment 2: Wind forcing in m s⁻¹ at day 45.

41
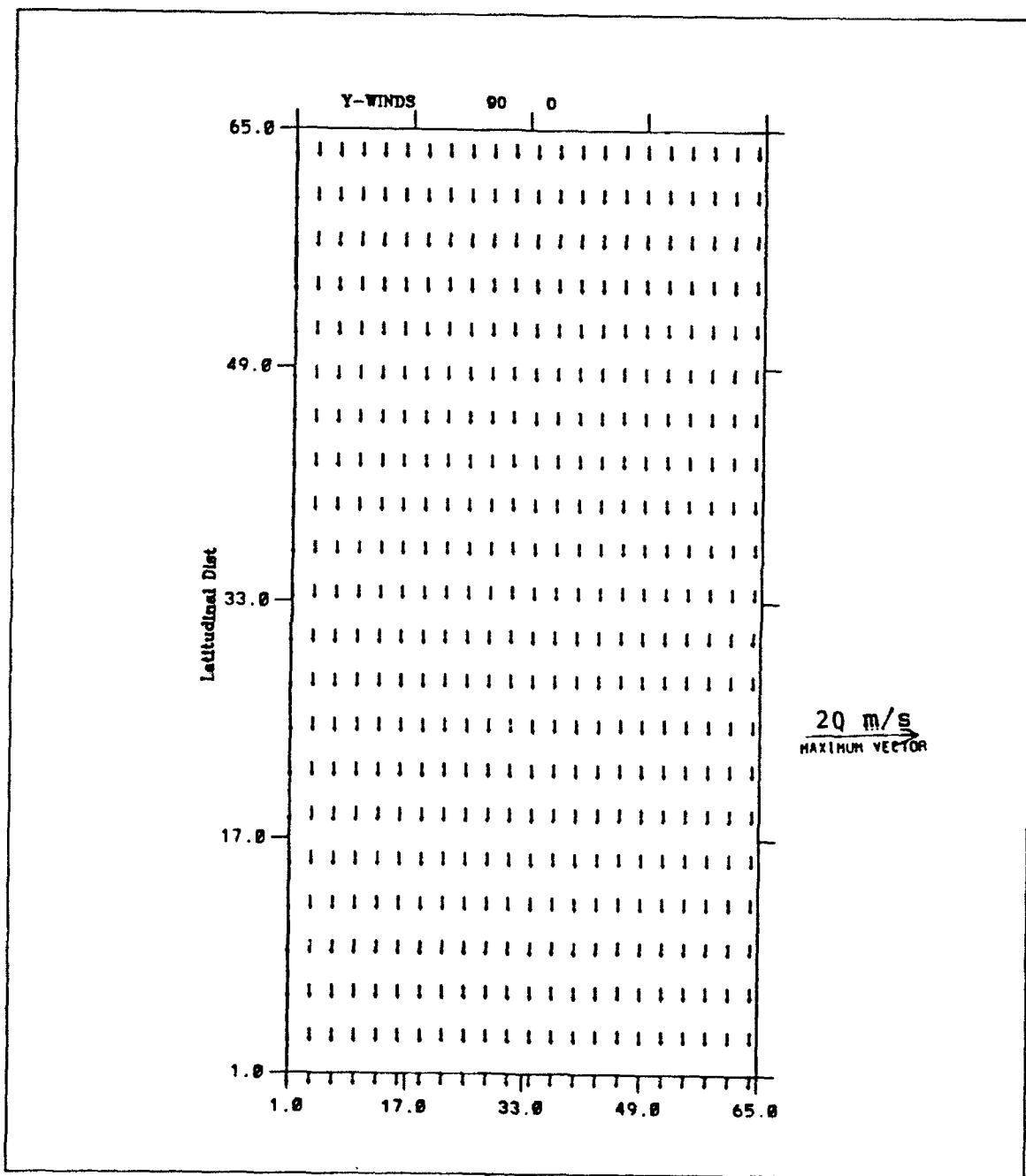
Figure 4.7 b) Experiment 2: Wind forcing in m s⁻¹ at day 90.
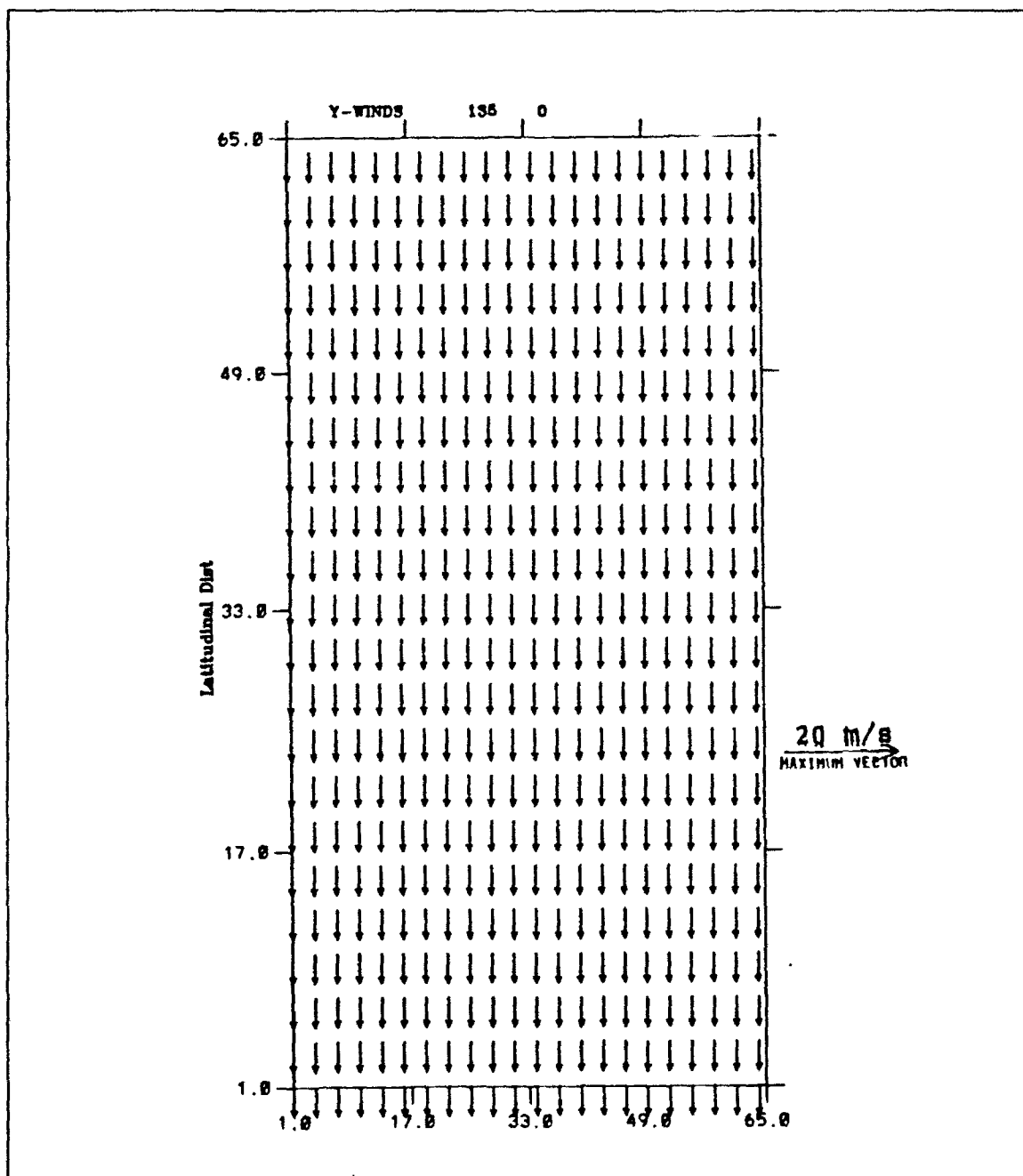
Figure 4.7 c) Experiment 2: Wind forcing in m s^{-1} at day 135.
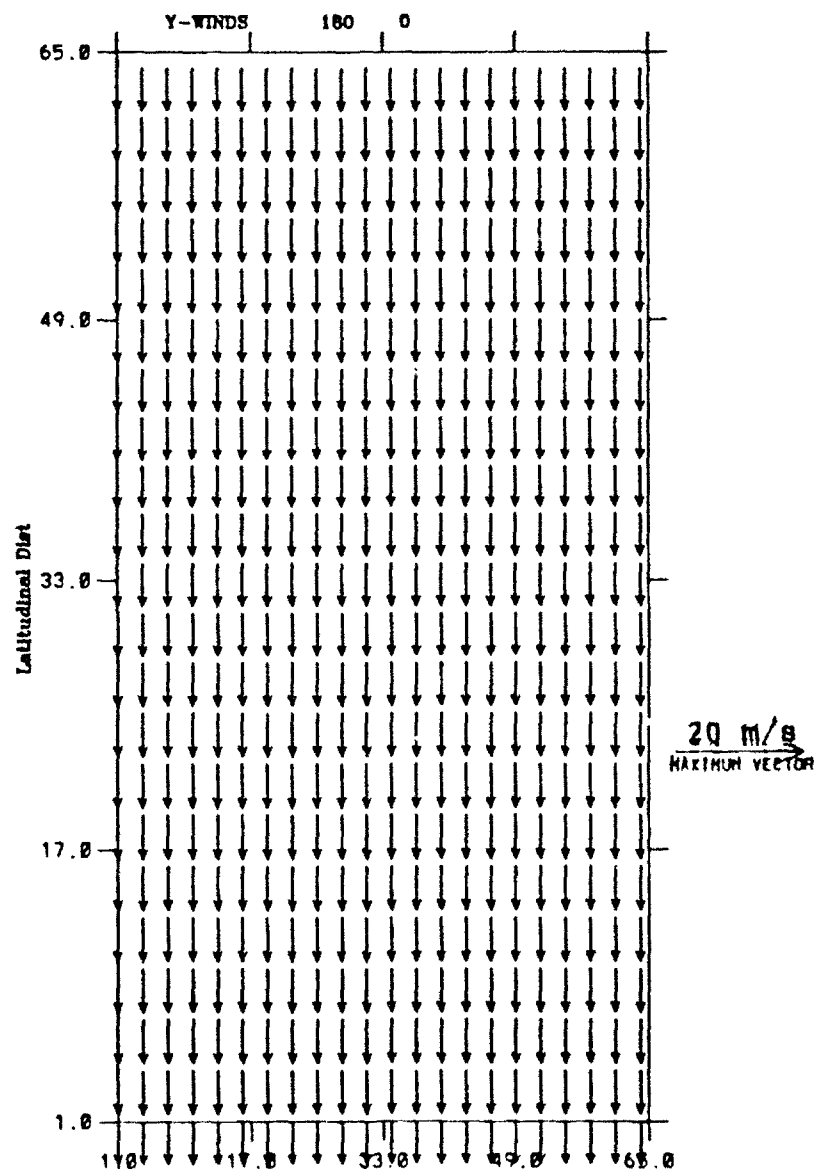
Figure 4.7 d) Experiment 2: Wind forcing in m s^{-1} at day 180.
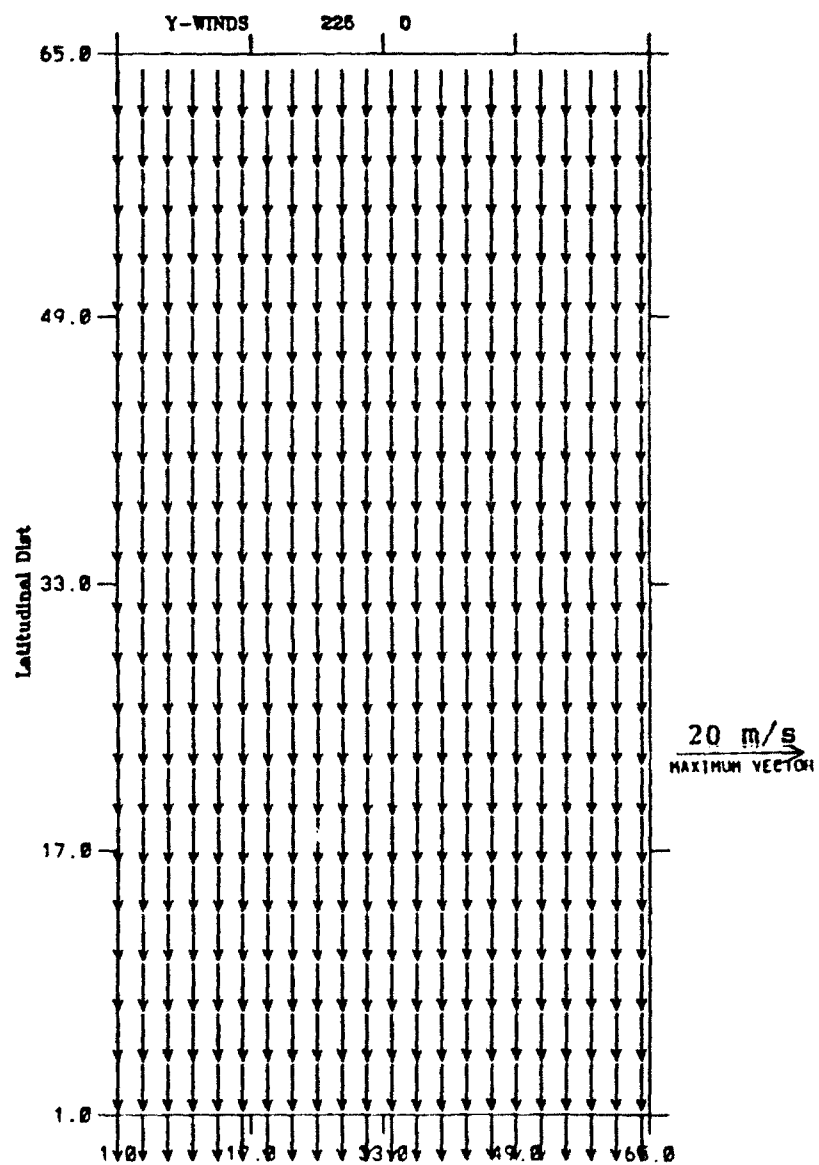
Figure 4.8 a) Experiment 2: Wind forcing in m s^{-1} at day 225.
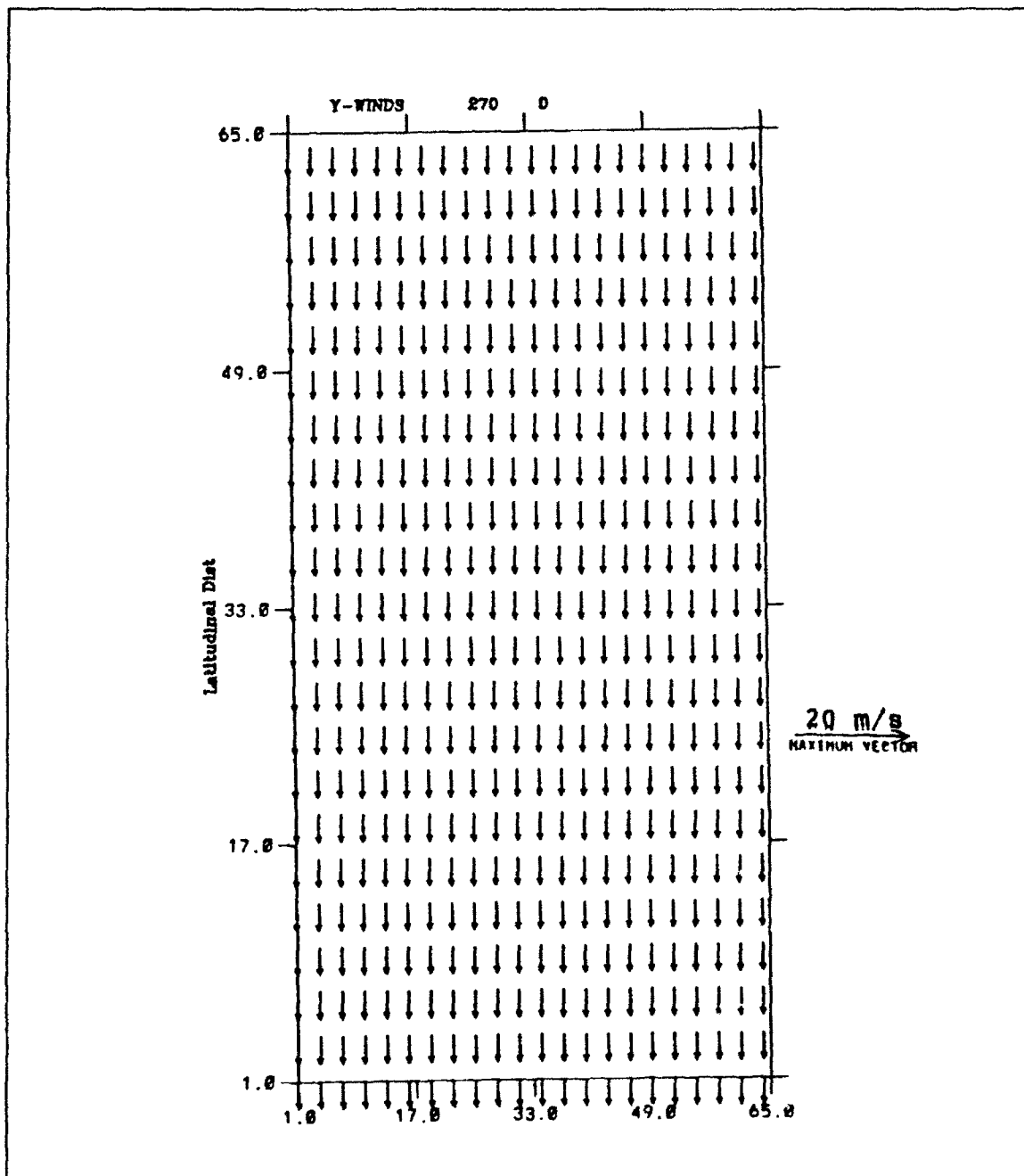
Figure 4.8 b) Experiment 2: Wind forcing in m s^{-1} at day 270.
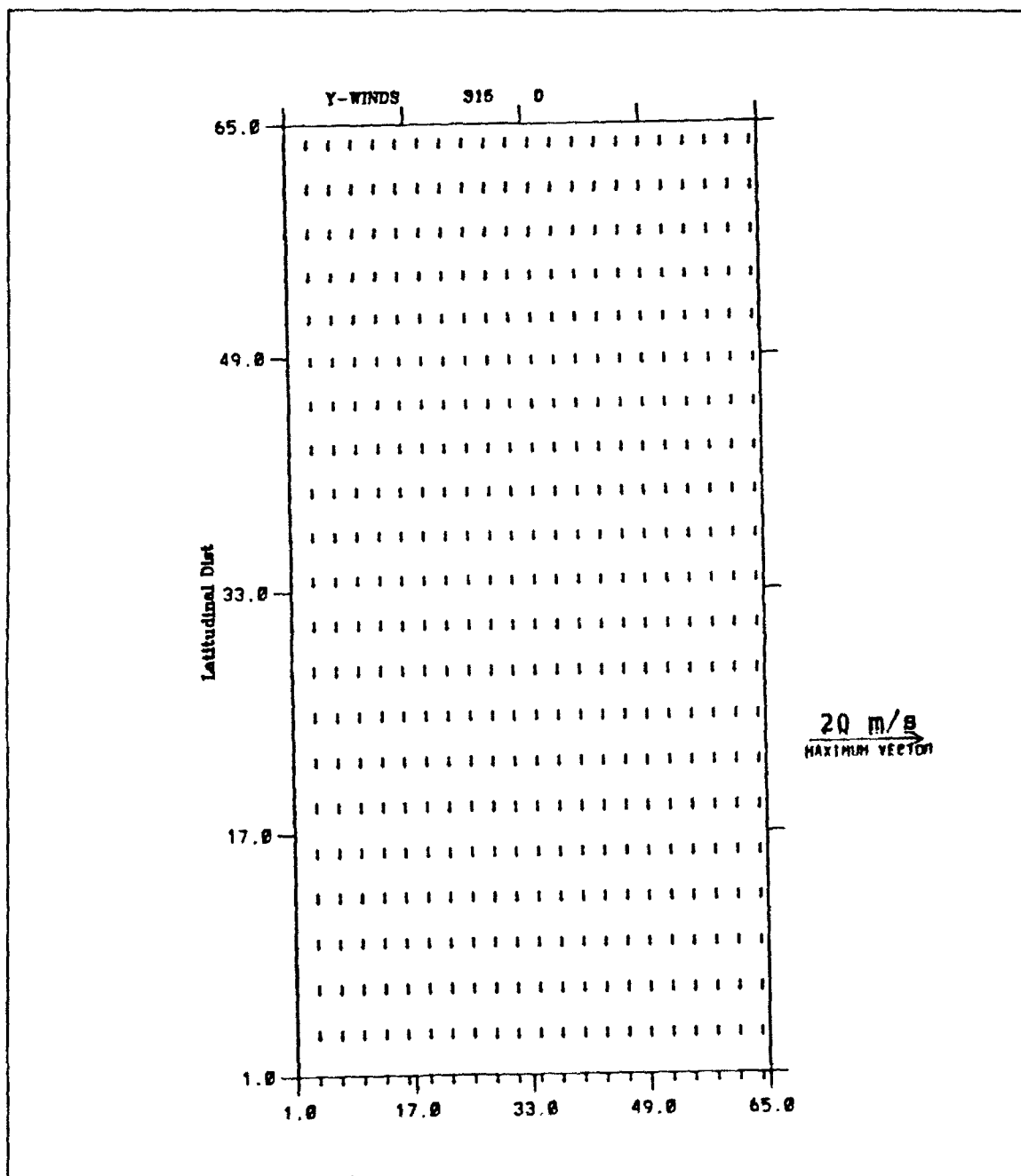
Figure 4.8 c) Experiment 2: Wind forcing in m s^{-1} at day 315.
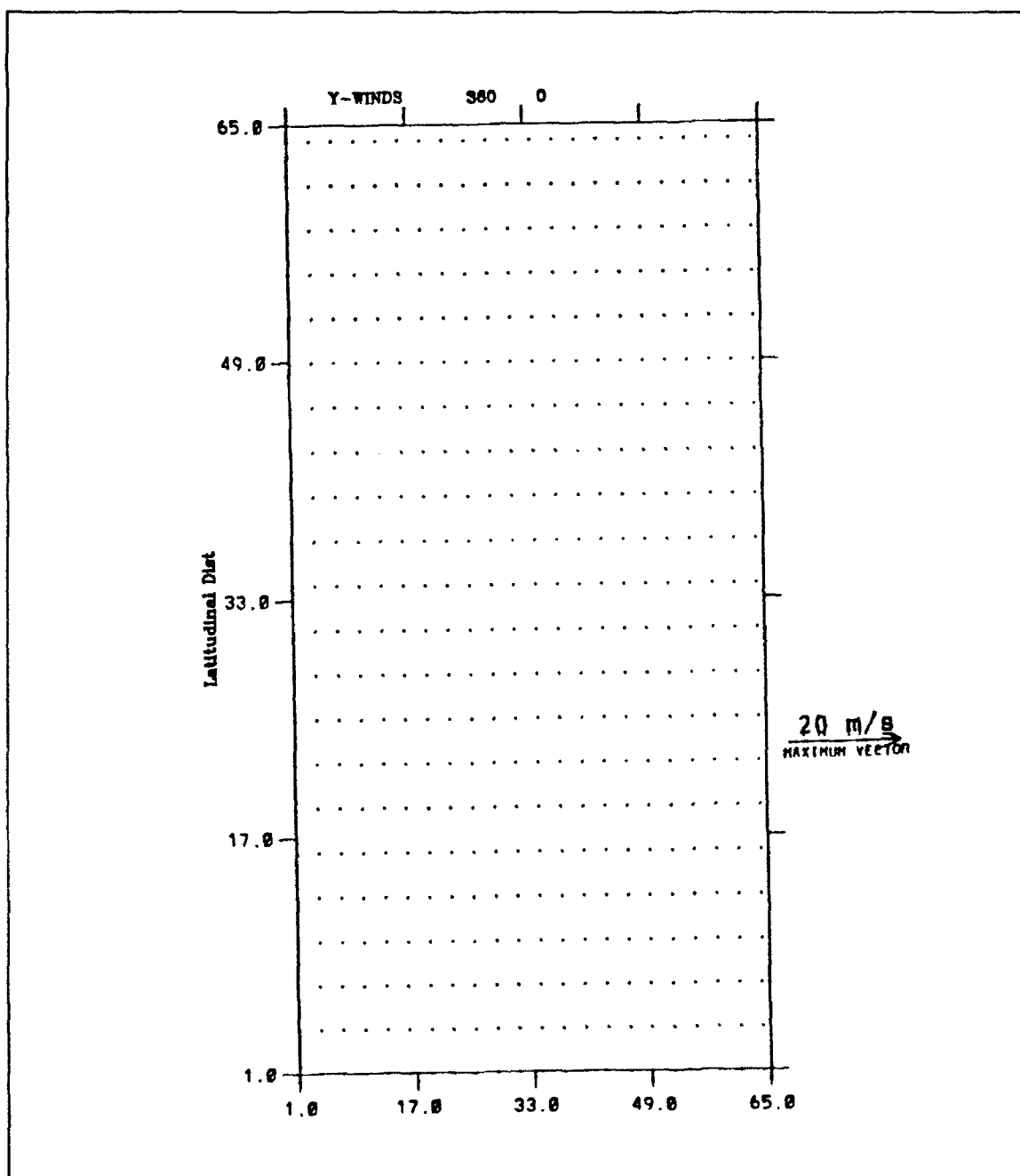
Figure 4.8 d) Experiment 2: Wind forcing in m s^{-1} at day 360.

Figure 4.9 a) Experiment 2: Velocity vectors superimposed on surface temperatures at day 130. The contour interval is 0.5° C. The temperature decreases toward the coast.
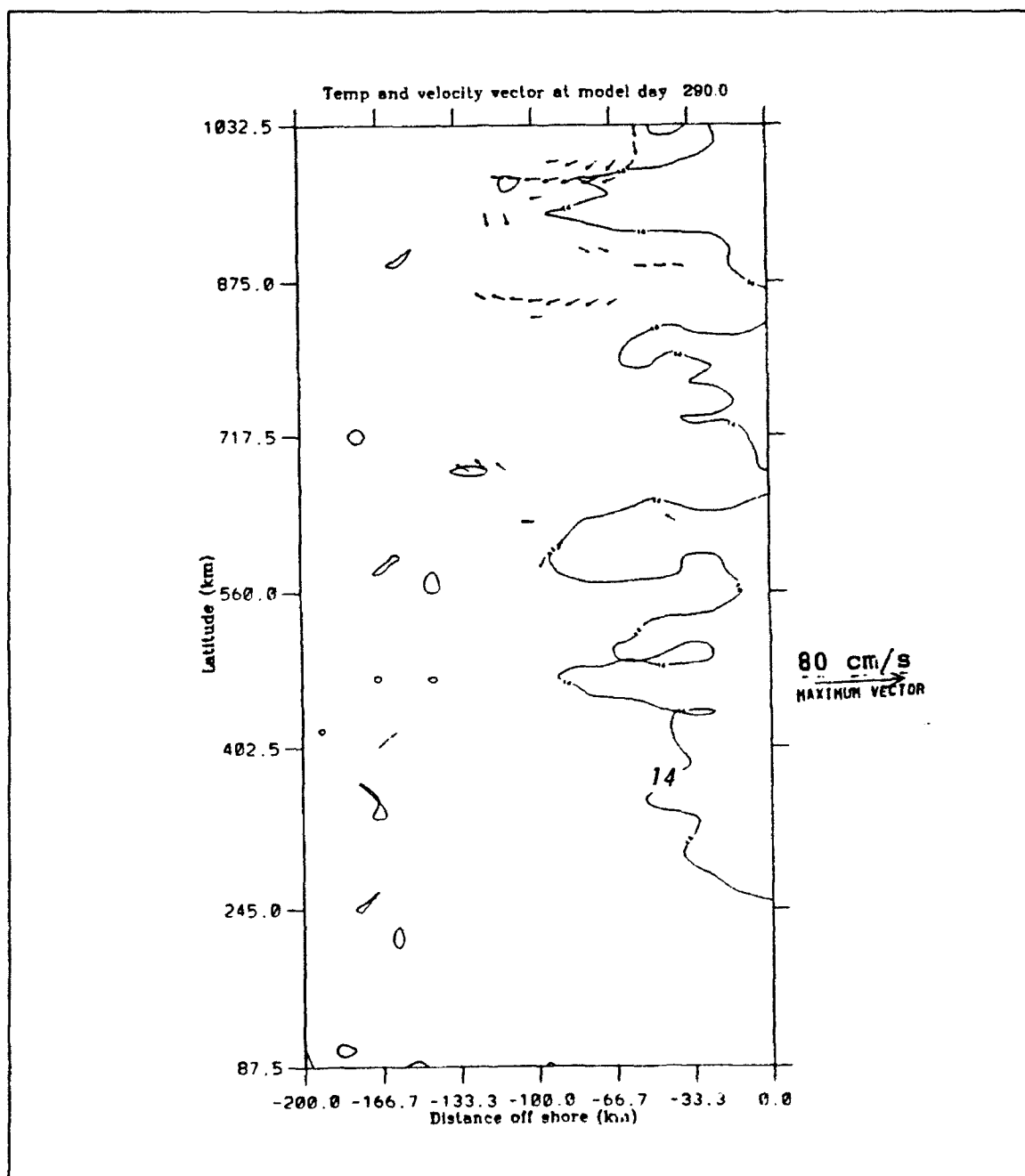
49

Figure 4.9 b) Experiment 2: Velocity vectors superimposed on surface temperatures at day 180. The contour interval is 0.5° C. The temperature decreases toward the coast.
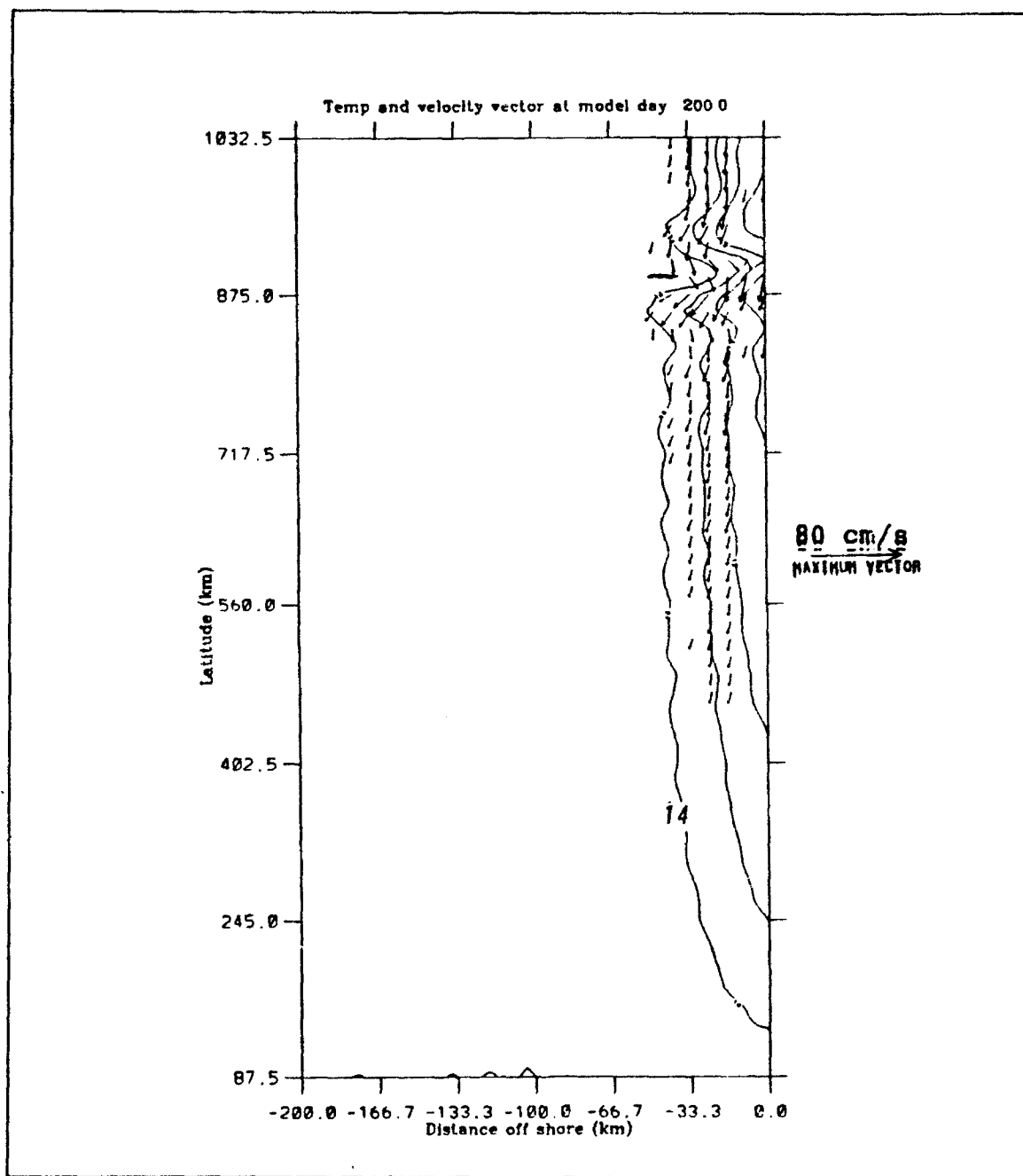
Figure 4.9 c) Experiment 2: Velocity vectors superimposed on surface temperatures at day 200. The contour interval is 0.5° C. The temperature decreases toward the coast.

51
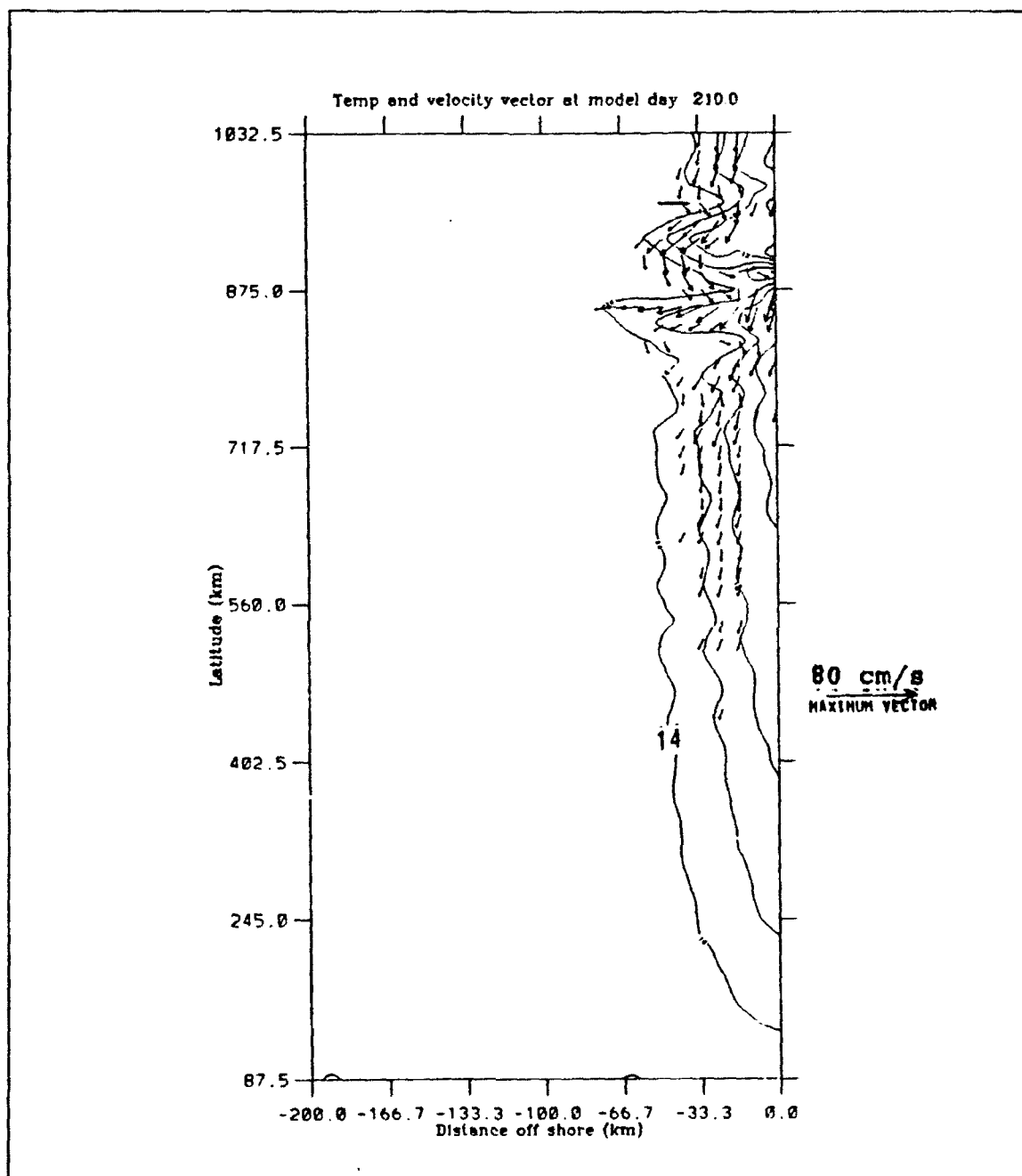
Figure 4.9 d) Experiment 2: Velocity vectors superimposed on surface temperatures at day 210. The contour interval is 0.5° C. The temperature decreases toward the coast.
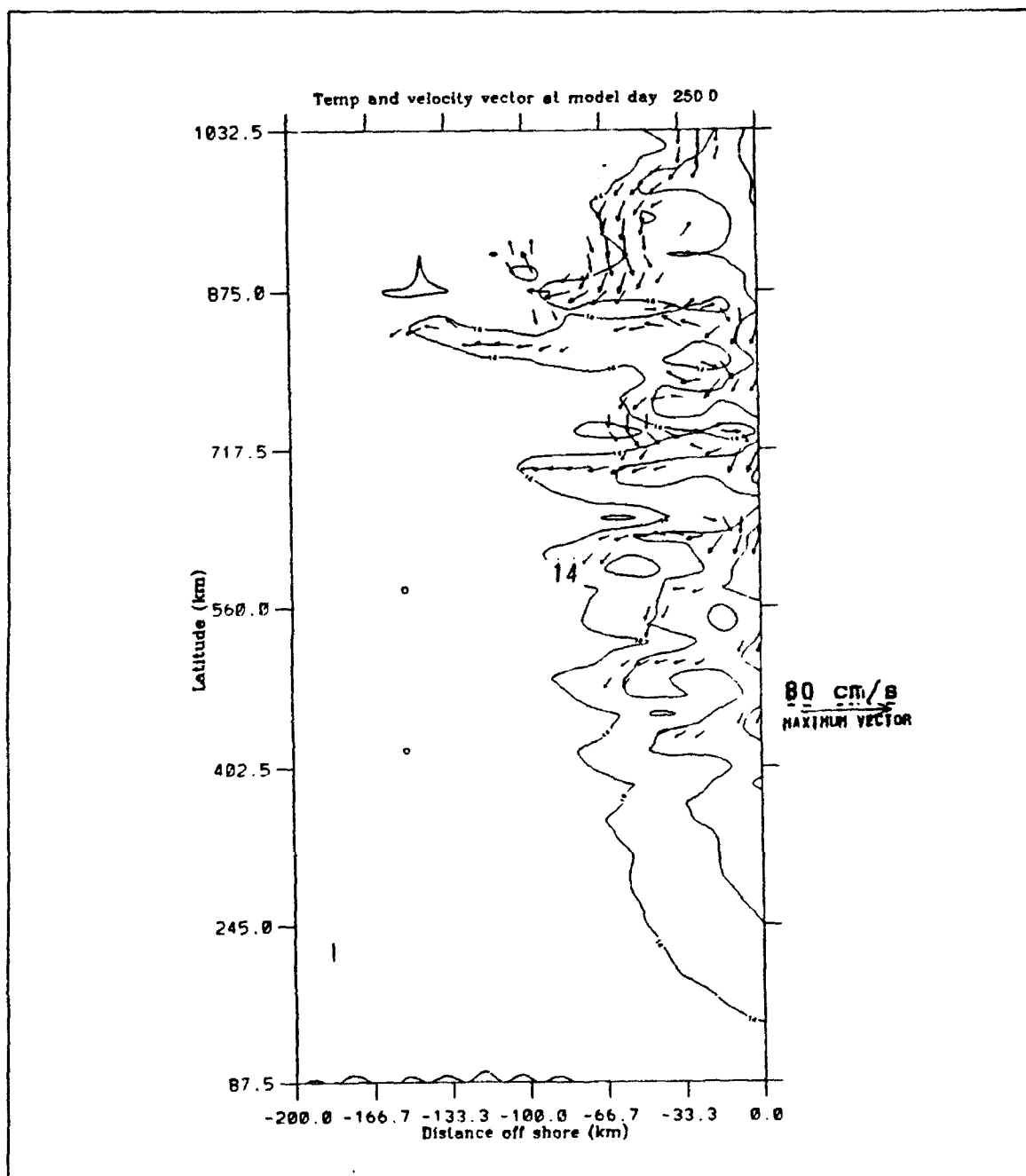
Figure 4.10 a) Experiment 2: Velocity vectors superimposed on surface temperatures at day 250. The contour interval is 0.5° C. The temperature decreases toward the coast.

53
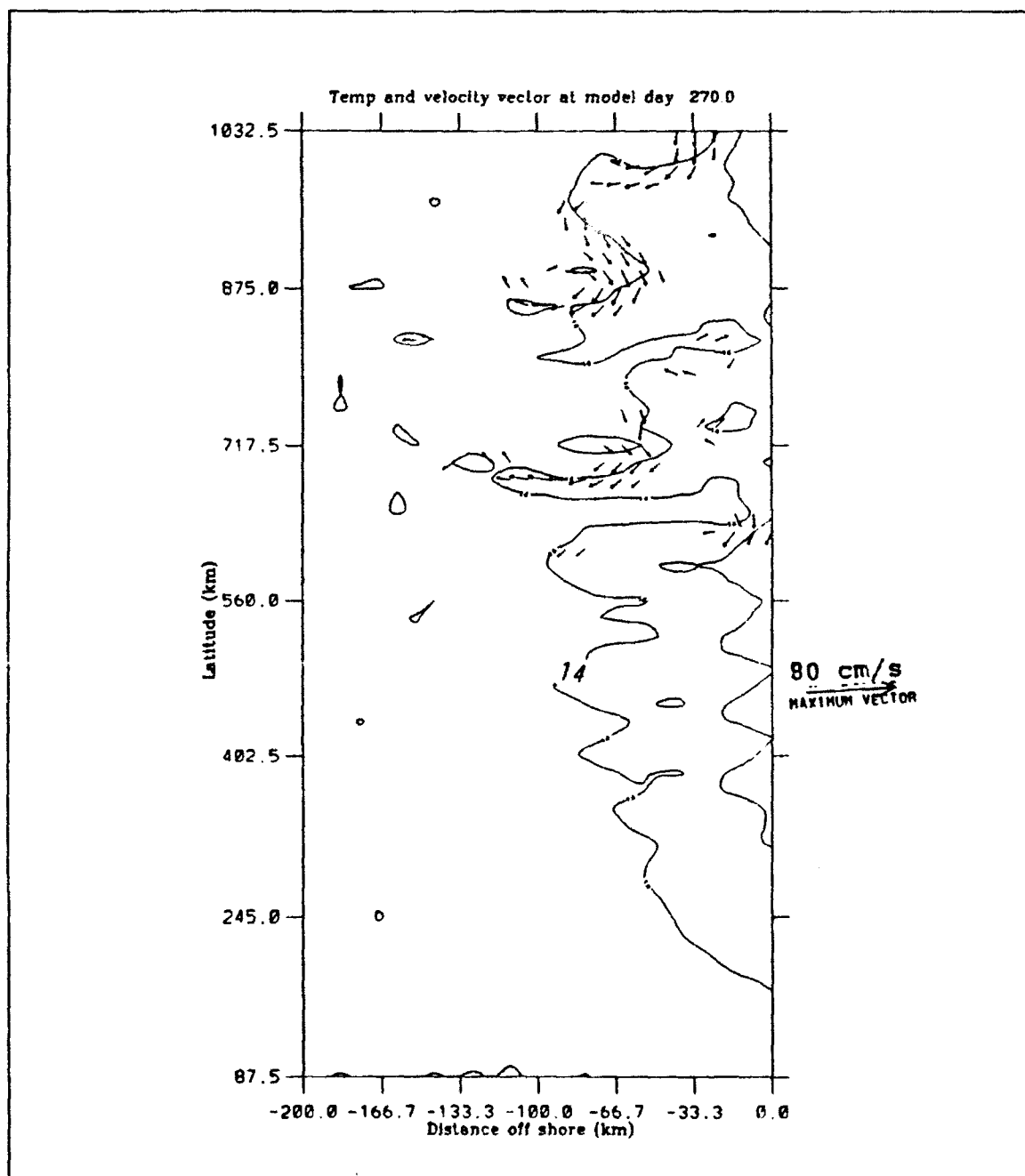
Figure 4.10 b) Experiment 2: Velocity vectors superimposed on surface temperatures at day 270. The contour interval is 0.5° C. The temperature decreases toward the coast.
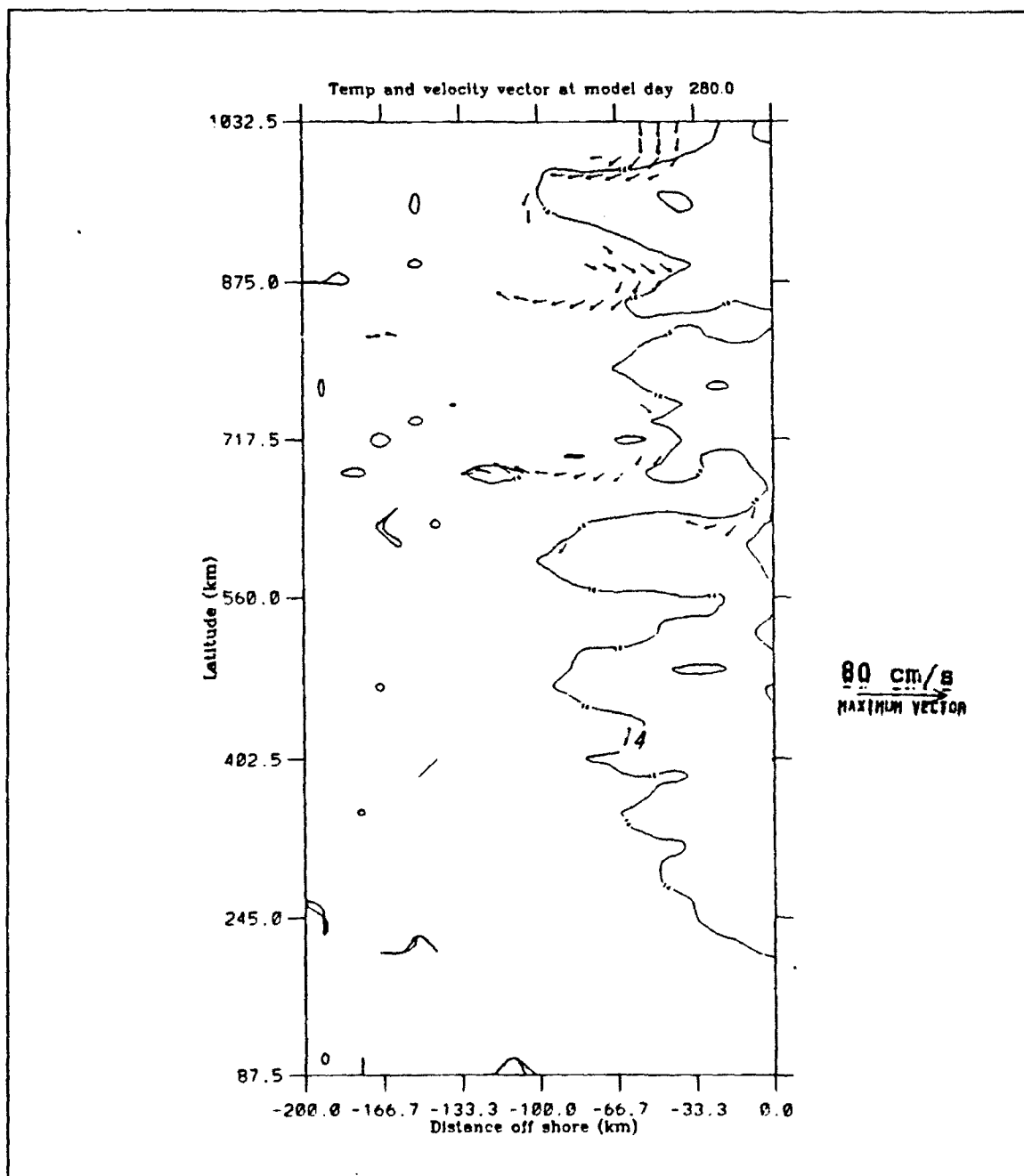
Figure 4.10 c) Experiment 2: Velocity vectors superimposed on surface temperatures at day 280. The contour interval is 0.5° C. The temperature decreases toward the coast.

Figure 4.10 d) Experiment 2: Velocity vectors superimposed on surface temperatures at day 290. The contour interval is 0.5° C. The temperature decreases toward the coast.
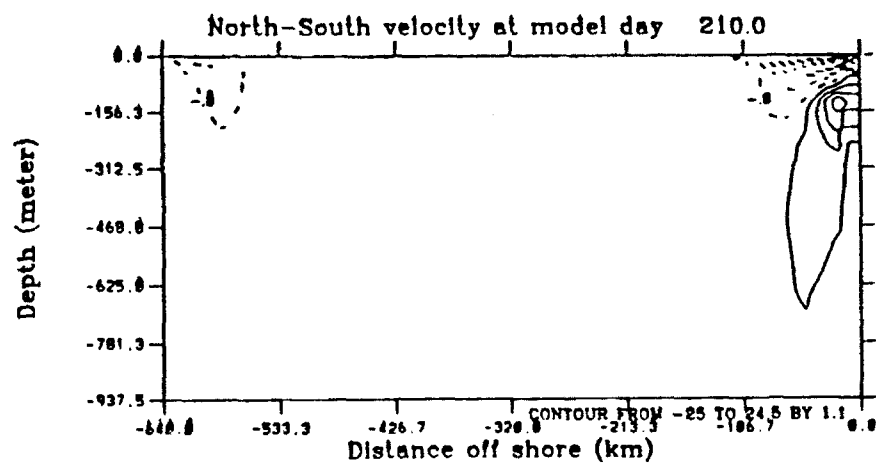
Figure 4.11 Experiment 2: Cross-section at 40° N latitude of meridional velocities at day 210. The contour interval is 1.1 cm s⁻¹. The dashed lines indicate southward velocities and show the surface equatorward current. The solid lines indicate northward flow and show the poleward undercurrent.
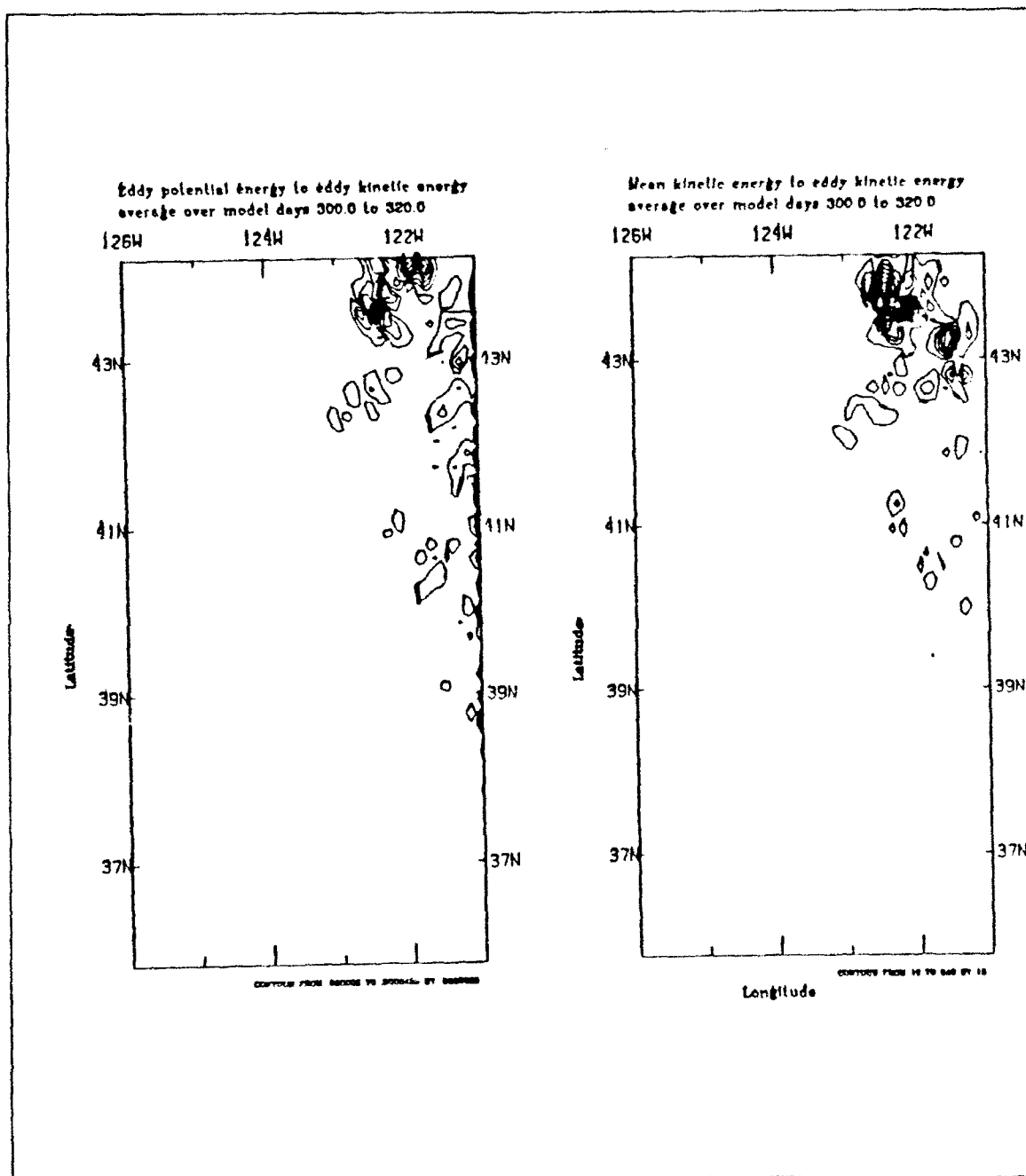
Figure 4.12 Experiment 2 Transfers of energy (as defined in equations 3.18 and 3.19) from: a) P to K (eddy available to eddy kinetic energy), and b) $\overline{K}$ to K (mean to eddy kinetic energy). Transfers of energy are averaged over the days 300-320 and summed over the upper five layers. The contour intervals are 0.0000025 ergs cm^{-3} s^{-1} in a) and 10 ergs cm^{-3} s^{-1} in b).

58
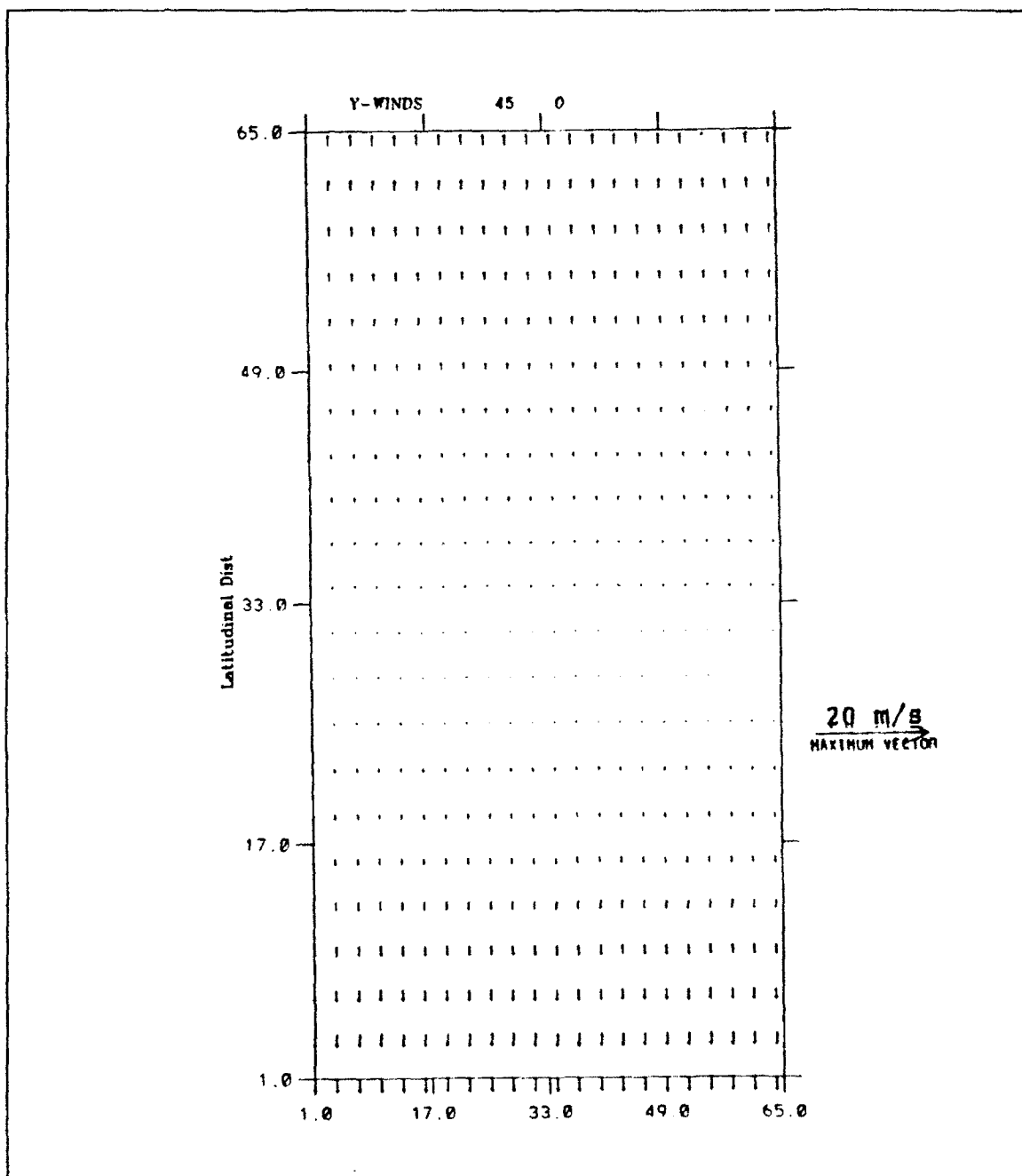
Figure 4.13a) Experiment 3: Wind forcing in m s^{-1} at day 45.
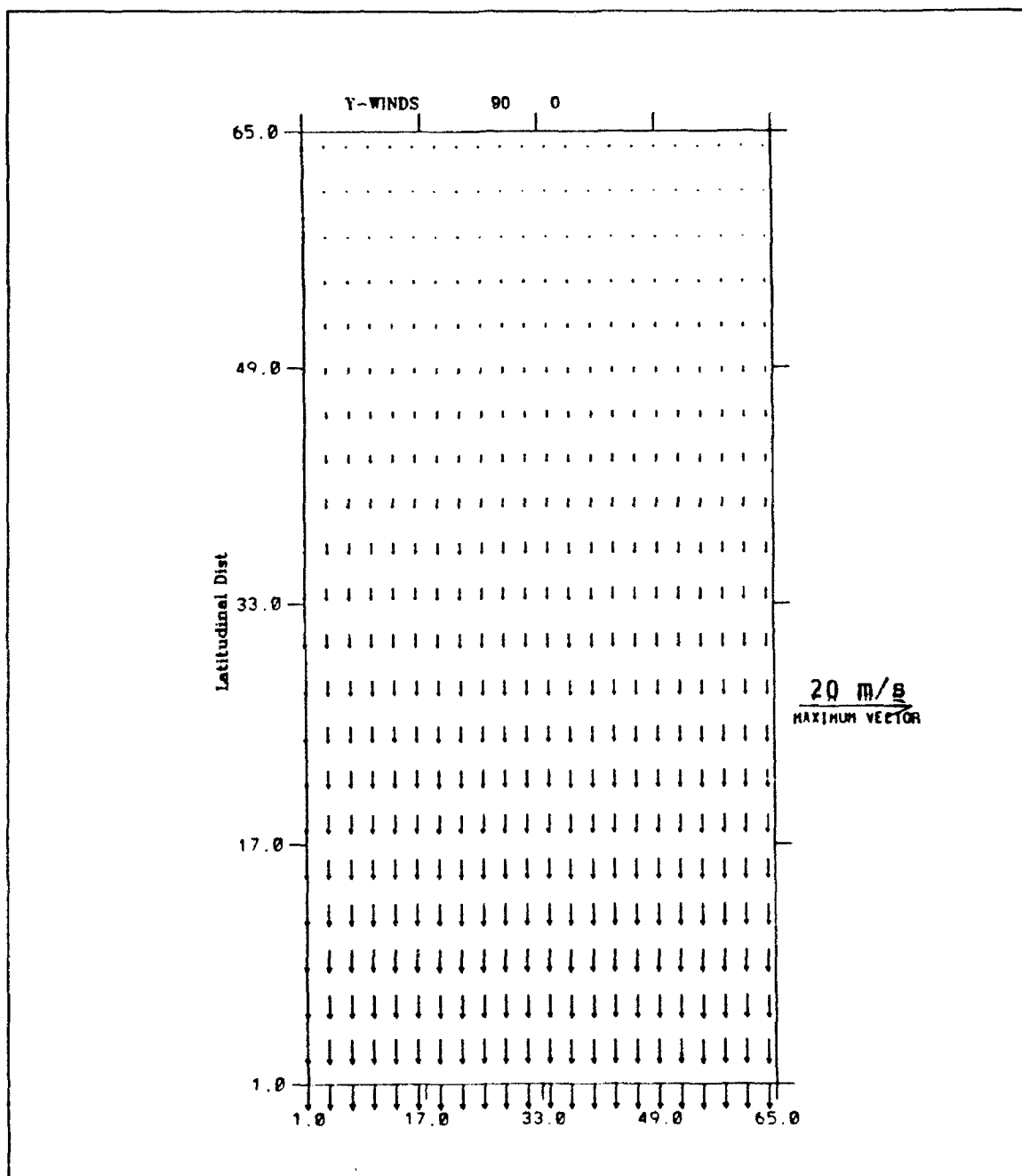
Figure 4.13 b) Experiment 3: Wind forcing in m s^{-1} at day 90.
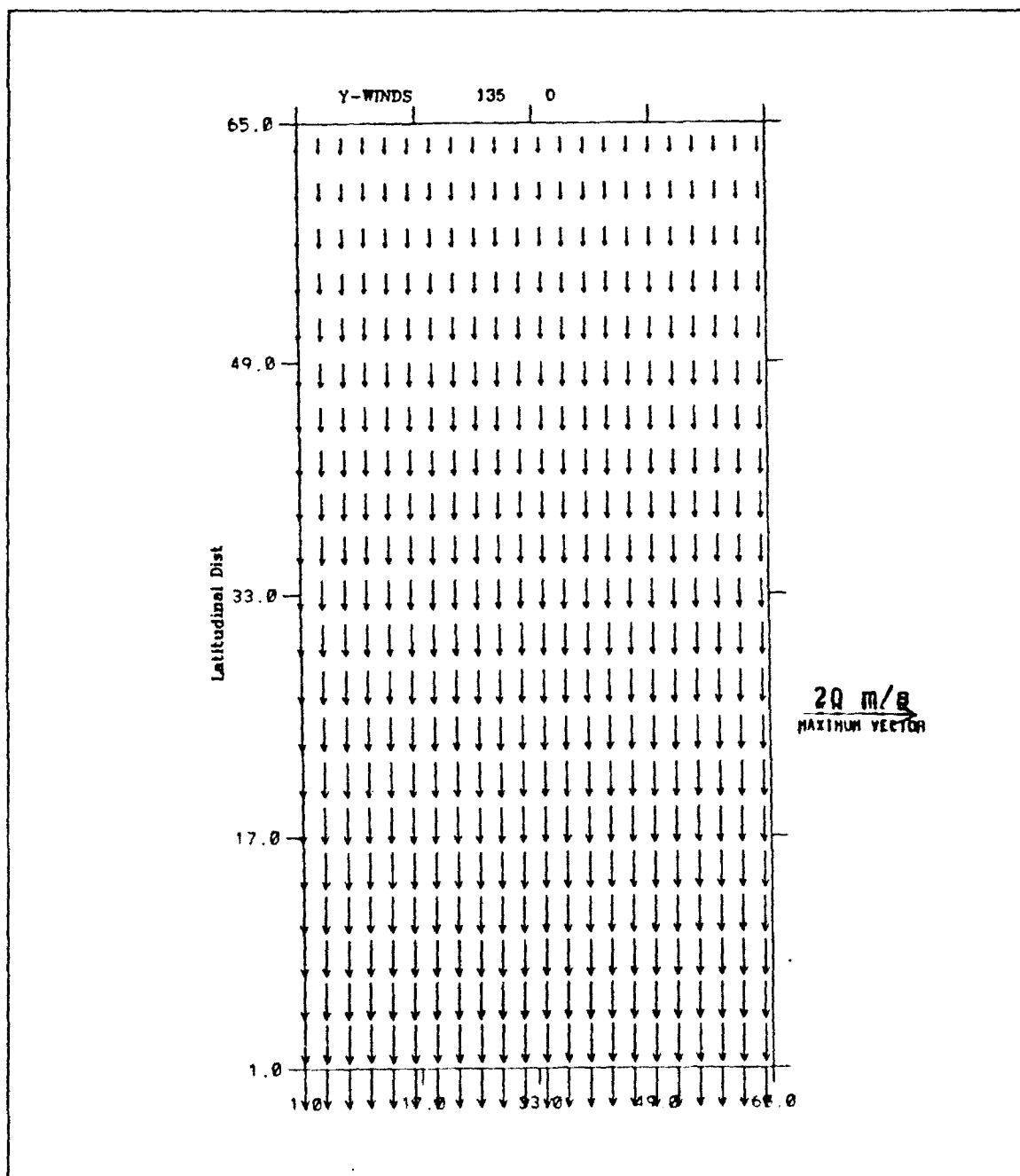
Figure 4.13 c) Experiment 3: Wind forcing in m s^{-1} at day 135.
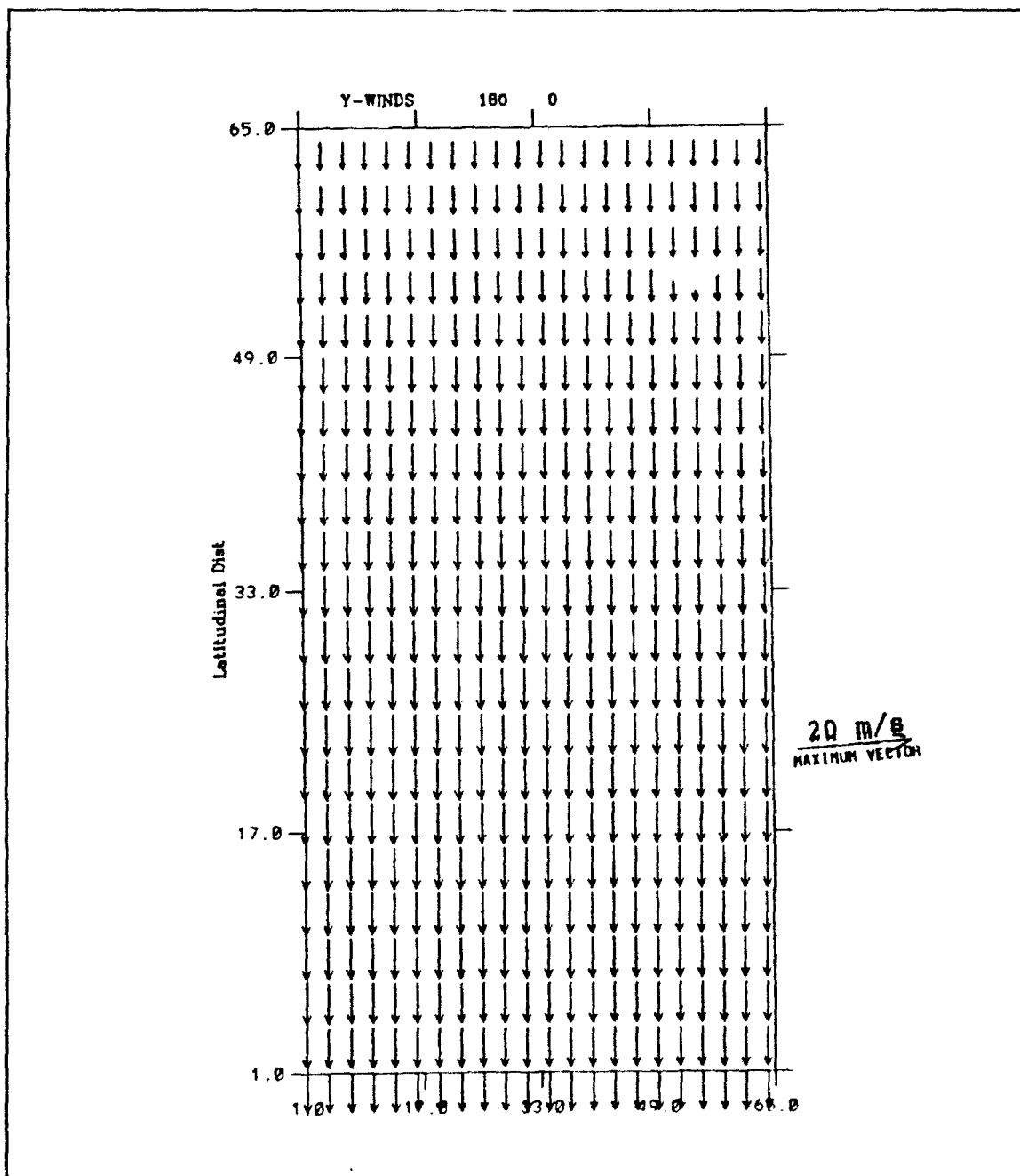
Figure 4.13 d) Experiment 3: Wind forcing in m s^{-1} at day 180.
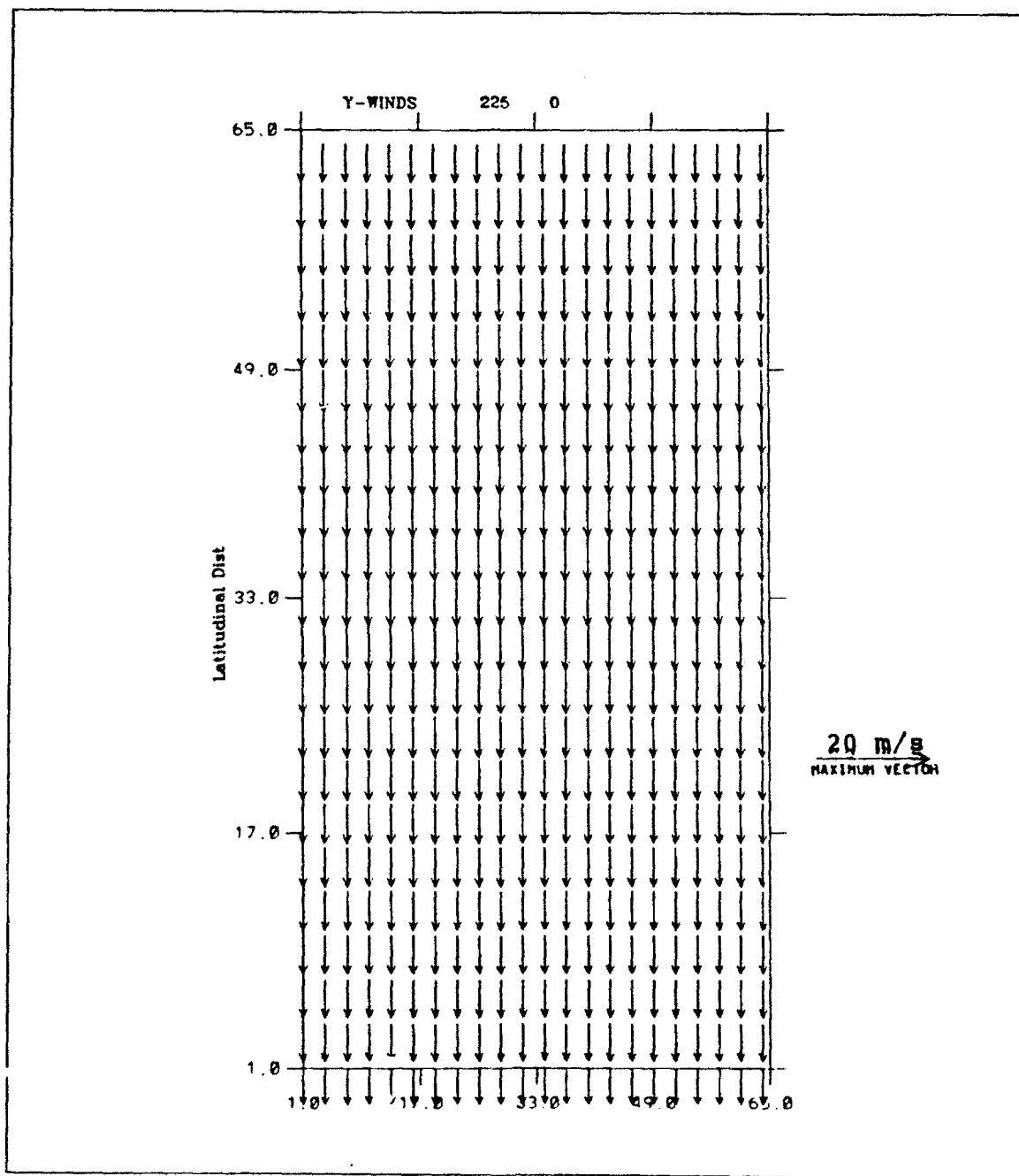
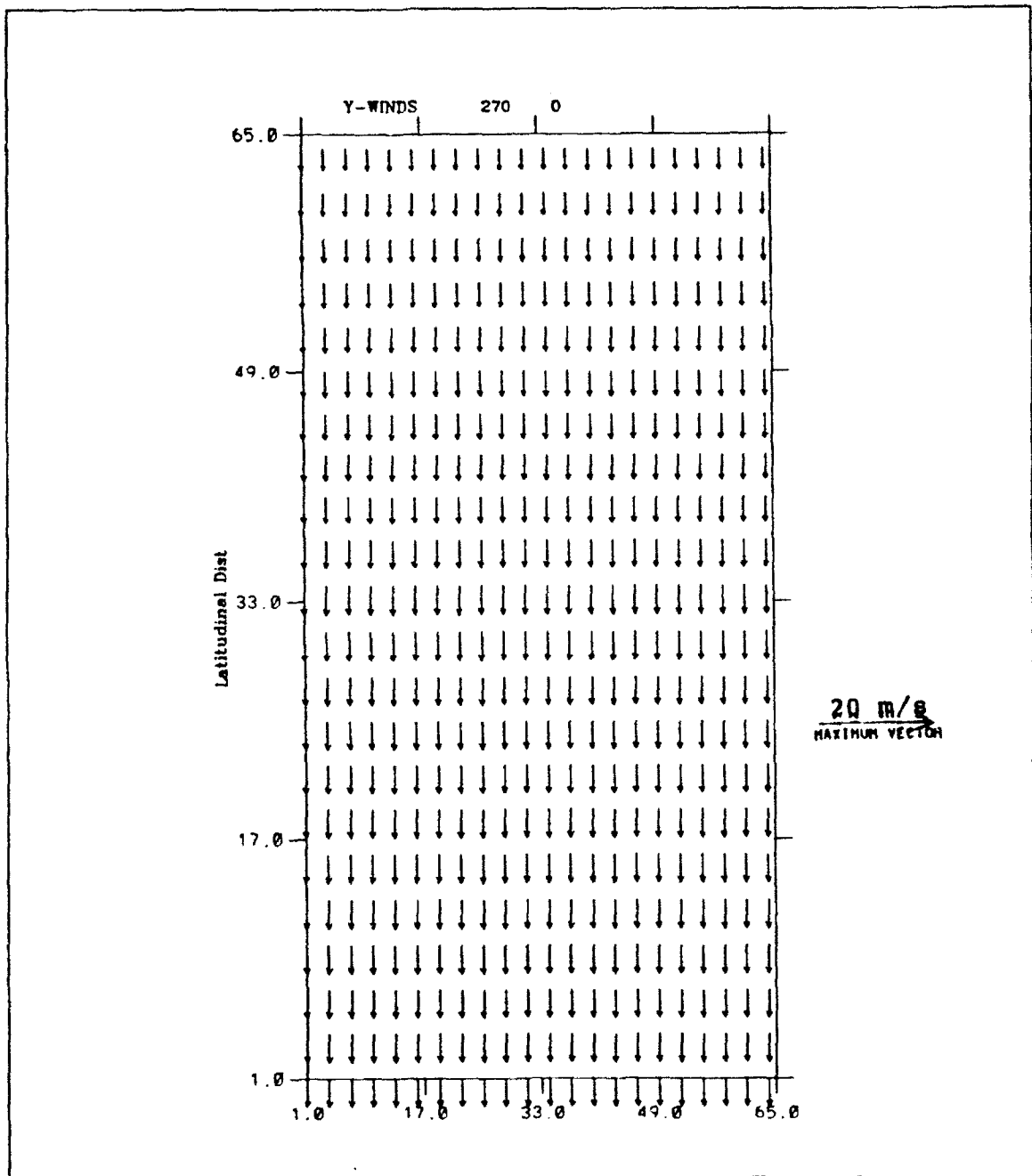Figure 4.14 a) Experiment 3: Wind forcing in m s^{-1} at day 225.

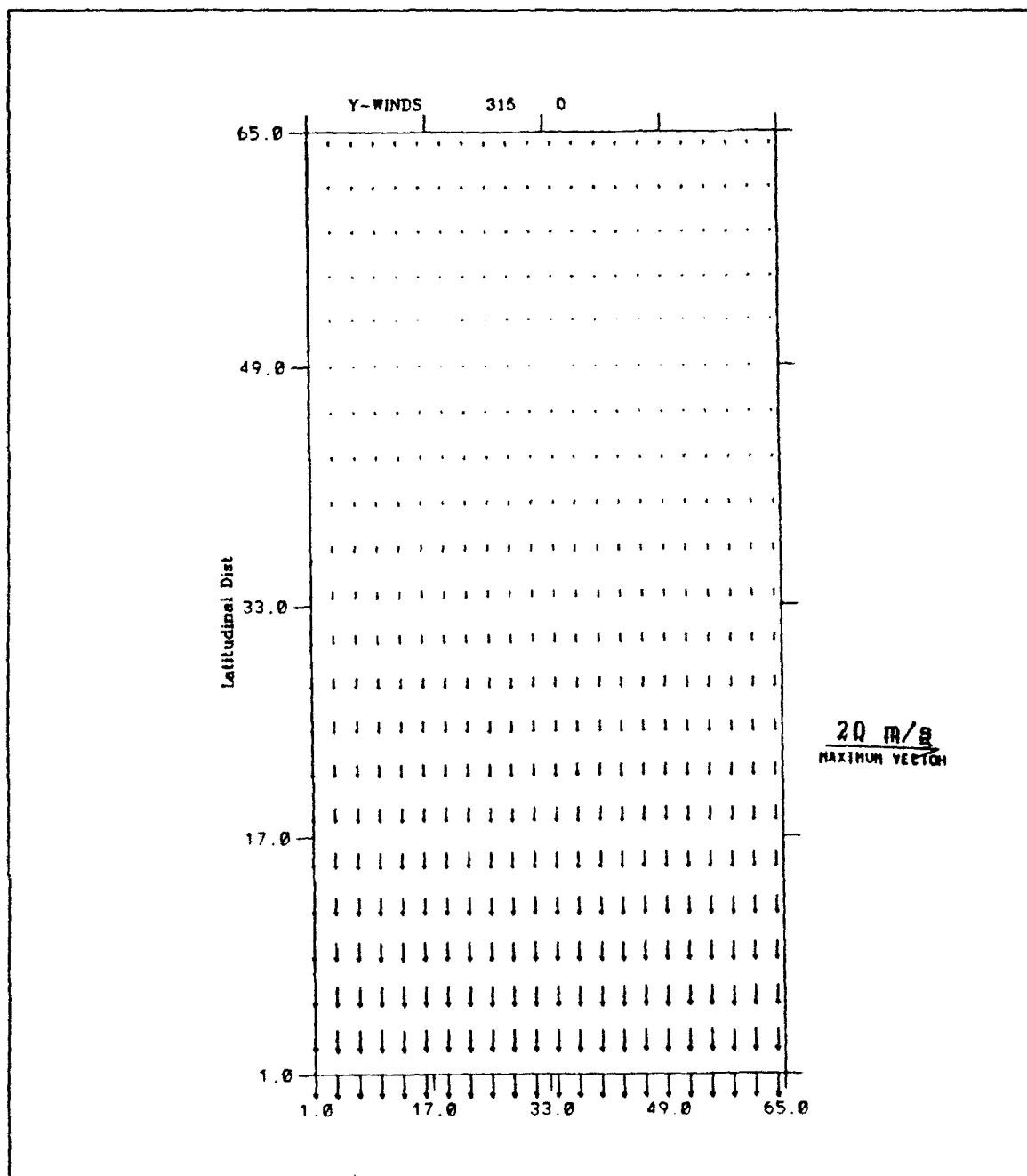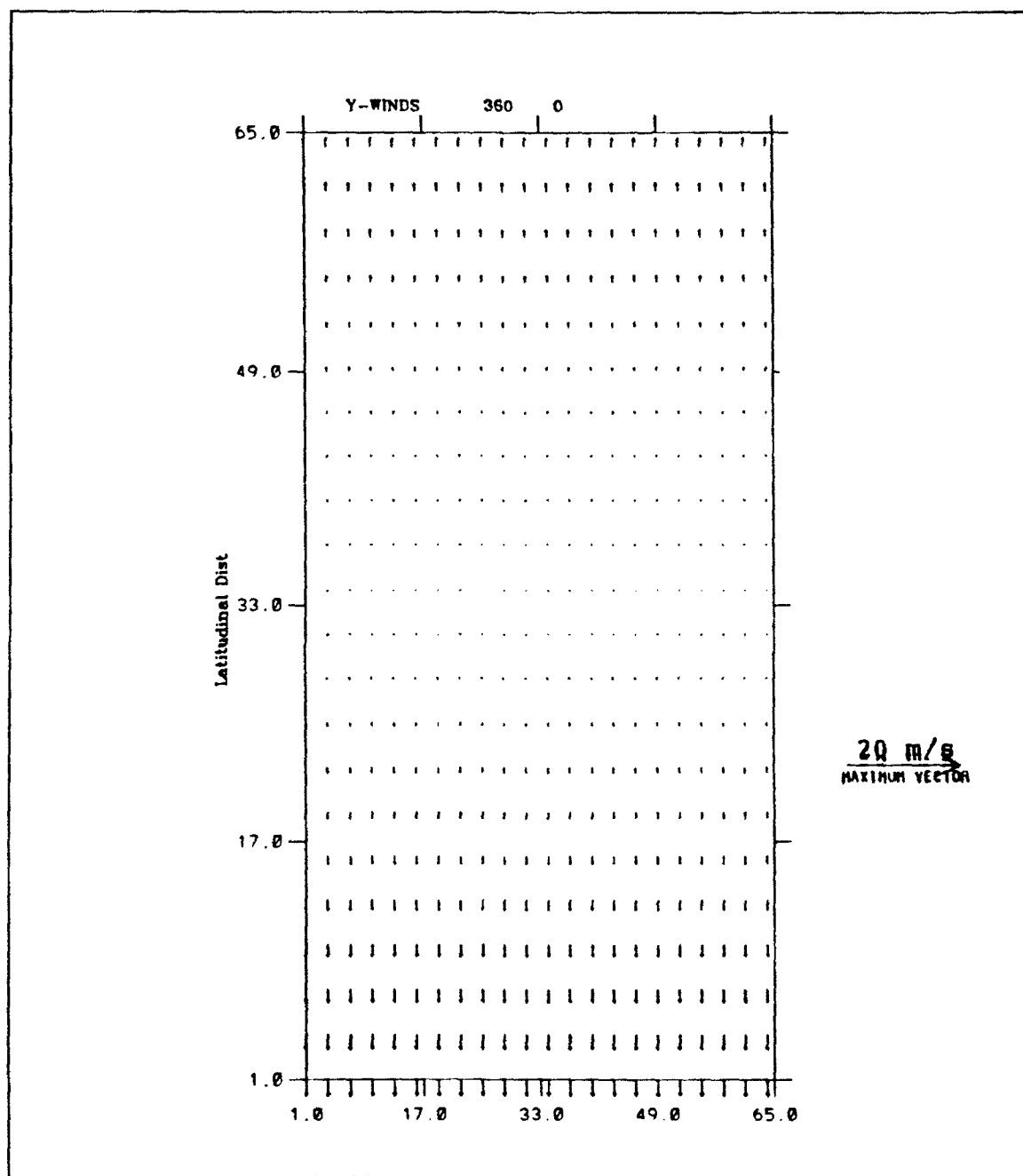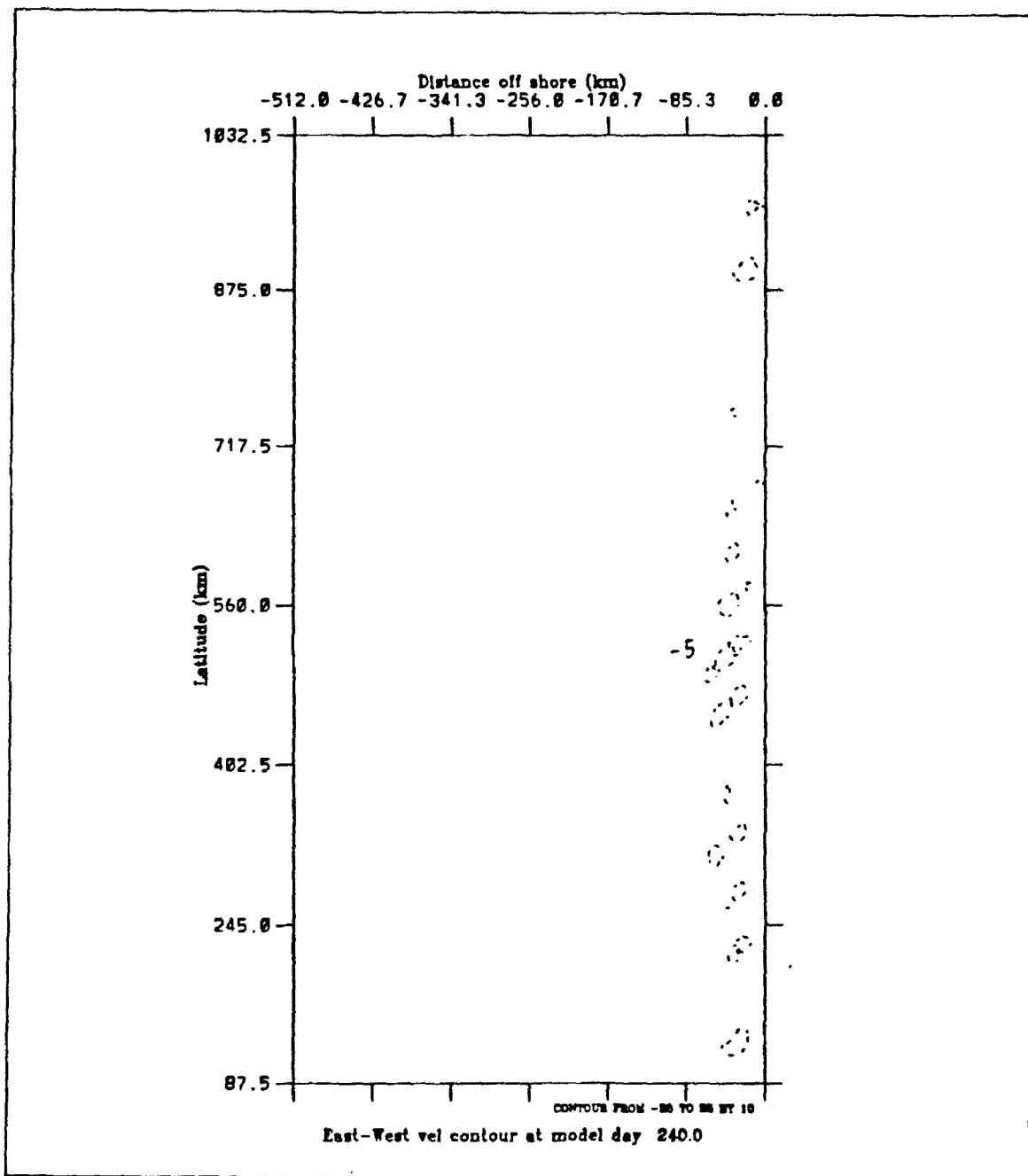Figure 4.14 b) Experiment 3: Wind forcing in m s^{-1} at day 270.

Figure 4.14 c) Experiment 3: Wind forcing in m s^{-1} at day 315.

Figure 4.14 d) Experiment 3: Wind forcing in m s^{-1} at day 360.

Figure 4.15 a) Experiment 3: Surface Zonal velocities at day 240. The contour interval is 10 cm s^{-1}. The dashed lines indicate westward velocities. Closed contours show the locations of eddies.
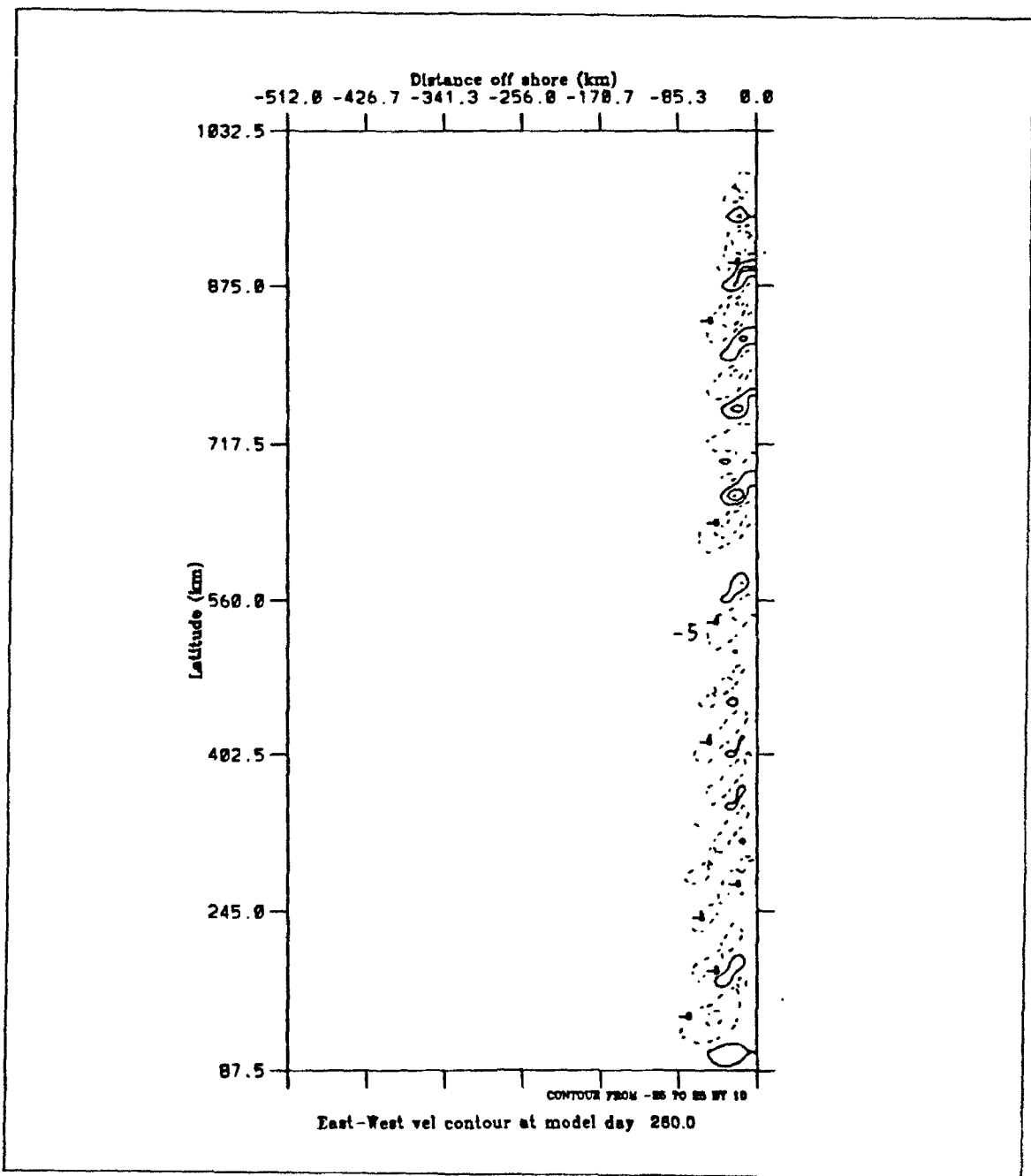
Figure 4.15 b) Experiment 3: Surface Zonal velocities at day 260. The contour interval is 10 cm s^{-1}. The dashed lines indicate westward velocities. Closed contours show the locations of eddies.
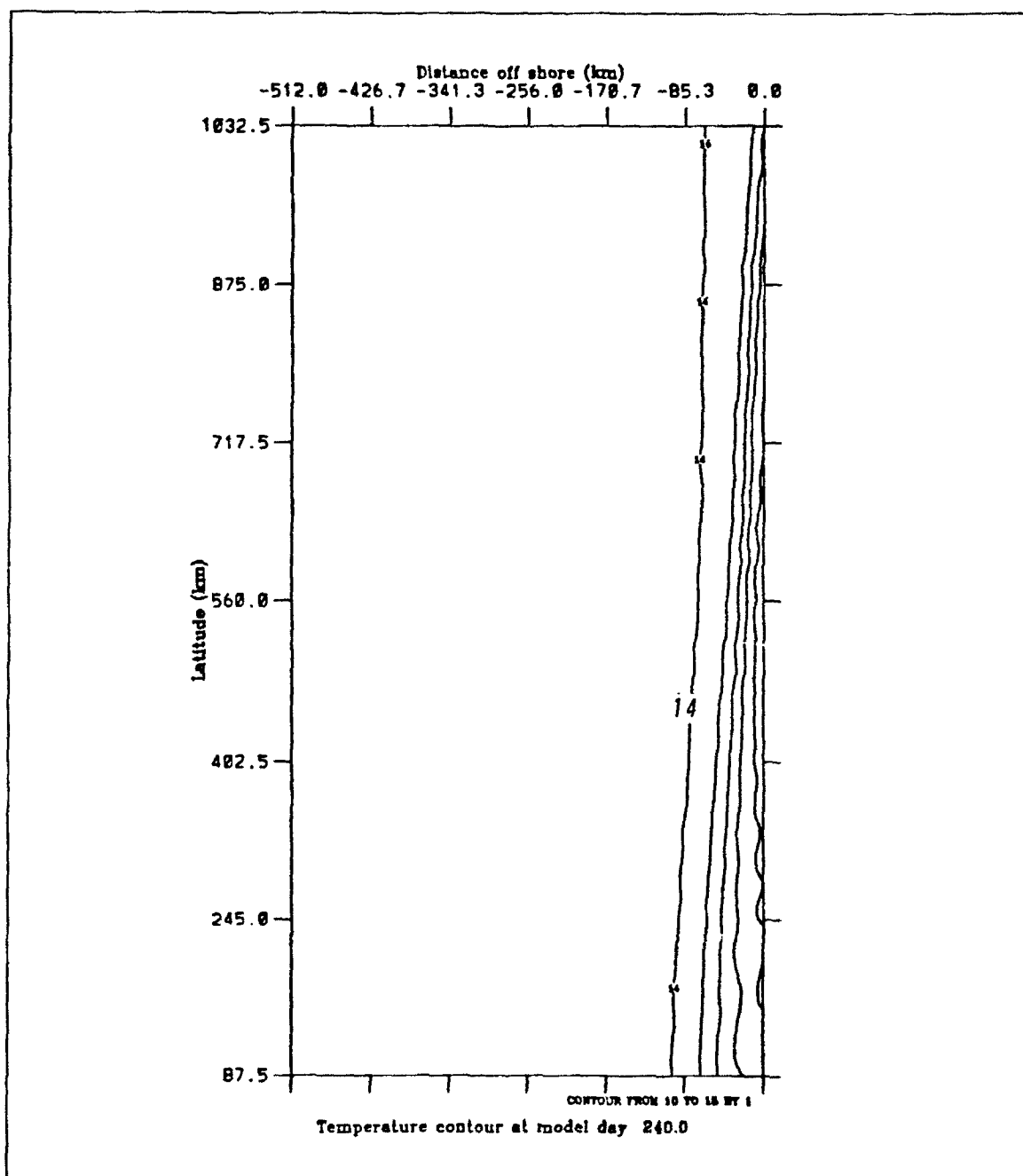
68

Figure 4.15 c) Experiment 3: Surface temperatures at day 240. The contour interval is 1° C. The temperature decreases toward the coast.
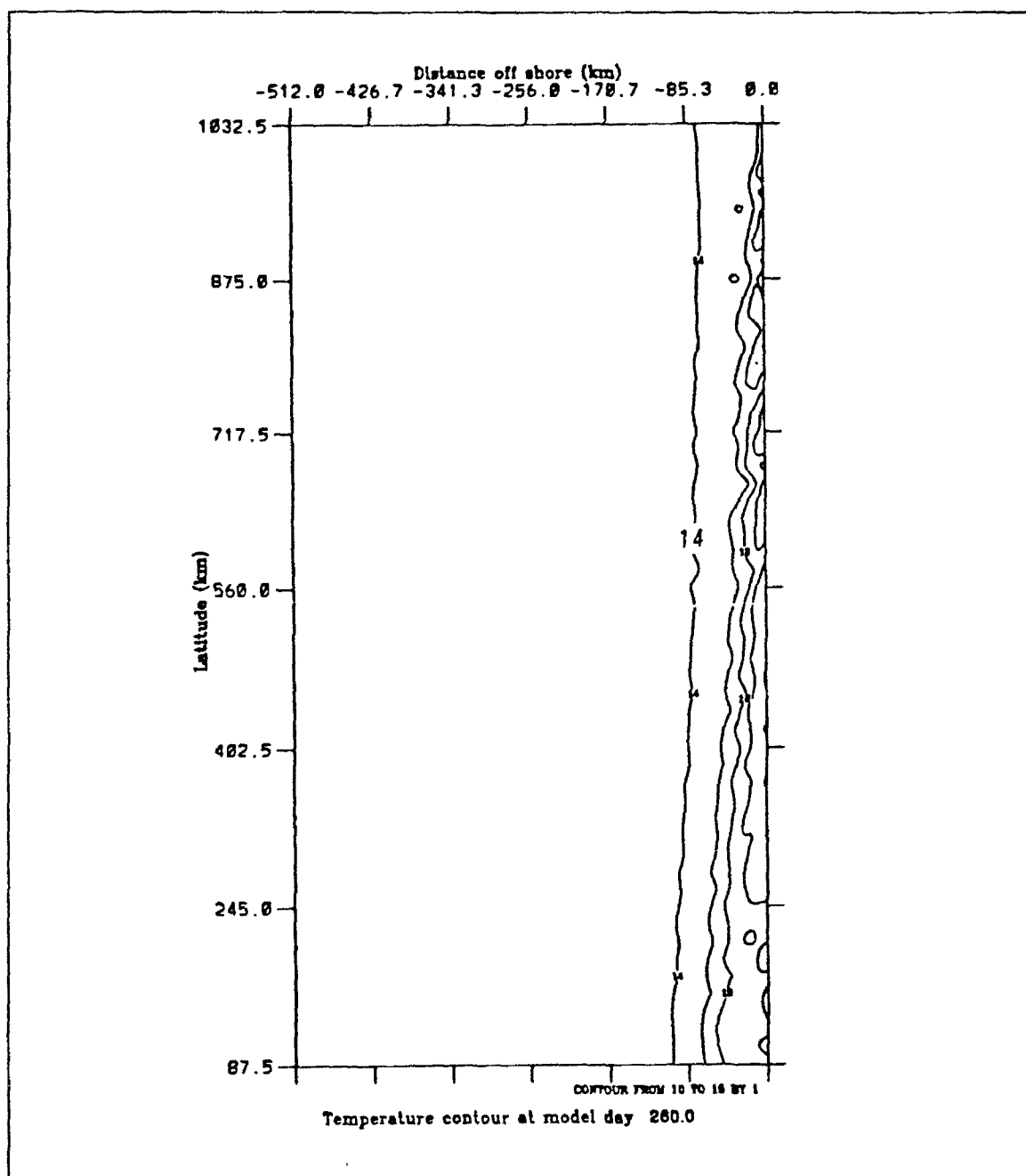
Figure 4.15 d) Experiment 3: Surface temperatures at day 260. The contour interval is 1° C. The temperature decreases toward the coast.
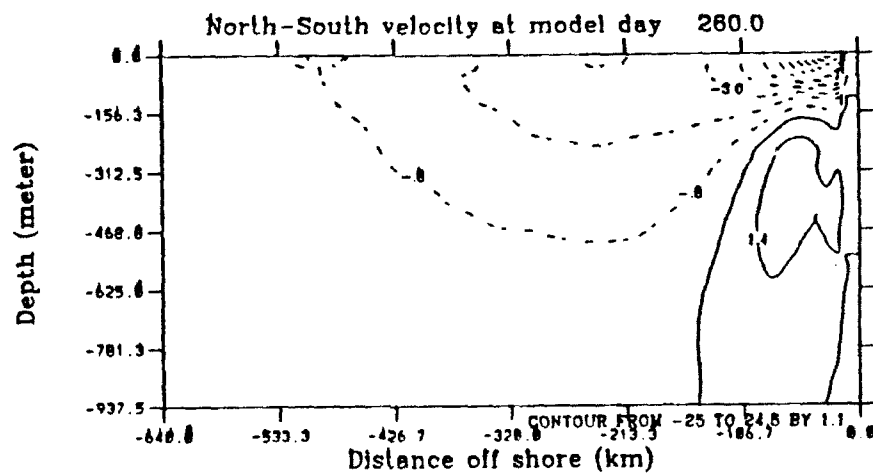
Figure 4.16 Experiment 3: Cross-section at 40° N latitude of meridional velocities at day 260. The contour interval is 1.1 cm s⁻¹. The dashed lines indicate southward velocities and show the surface equatorward current. The solid lines indicate northward flow and show the poleward undercurrent.
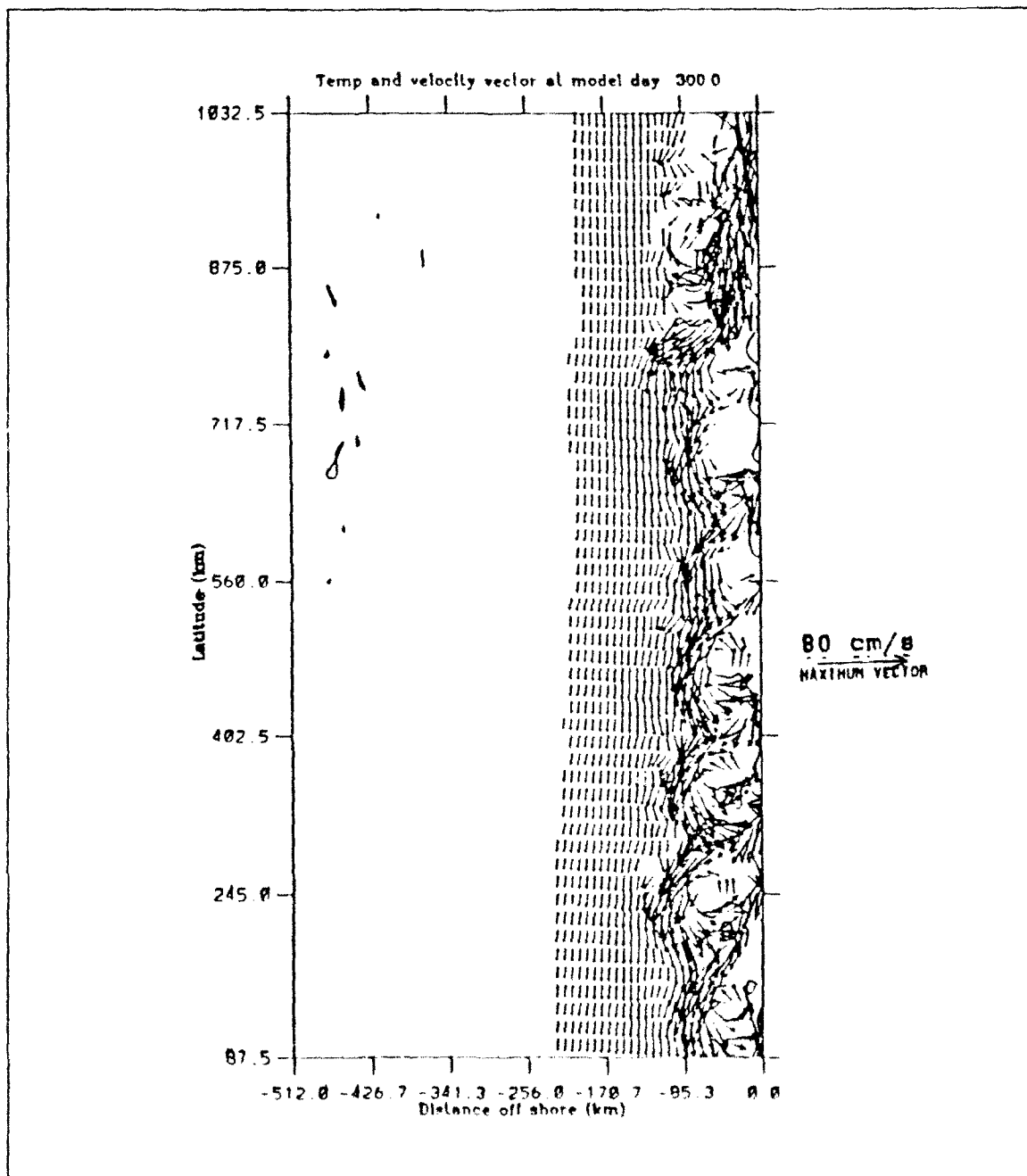
71

Figure 4.17 a) Experiment 3: Surface velocity vectors superimposed on temperatures at day 300. The contour interval is 0.5° C. The temperature decreases toward the coast.
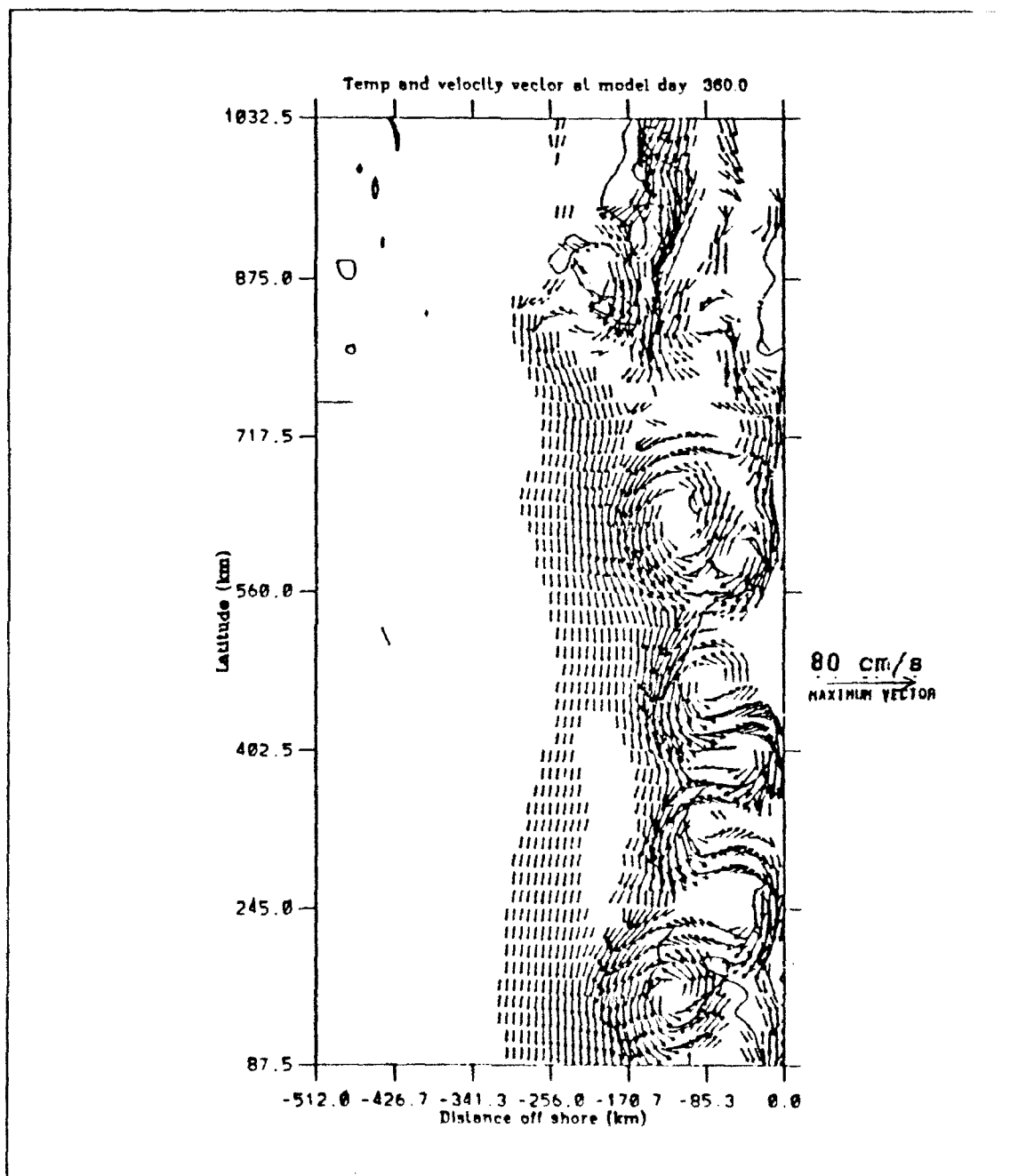
Figure 4.17 b) Experiment 3: Surface velocity vectors superimposed on temperatures at day 360. The contour interval is 0.5° C. The temperature decreases toward the coast.
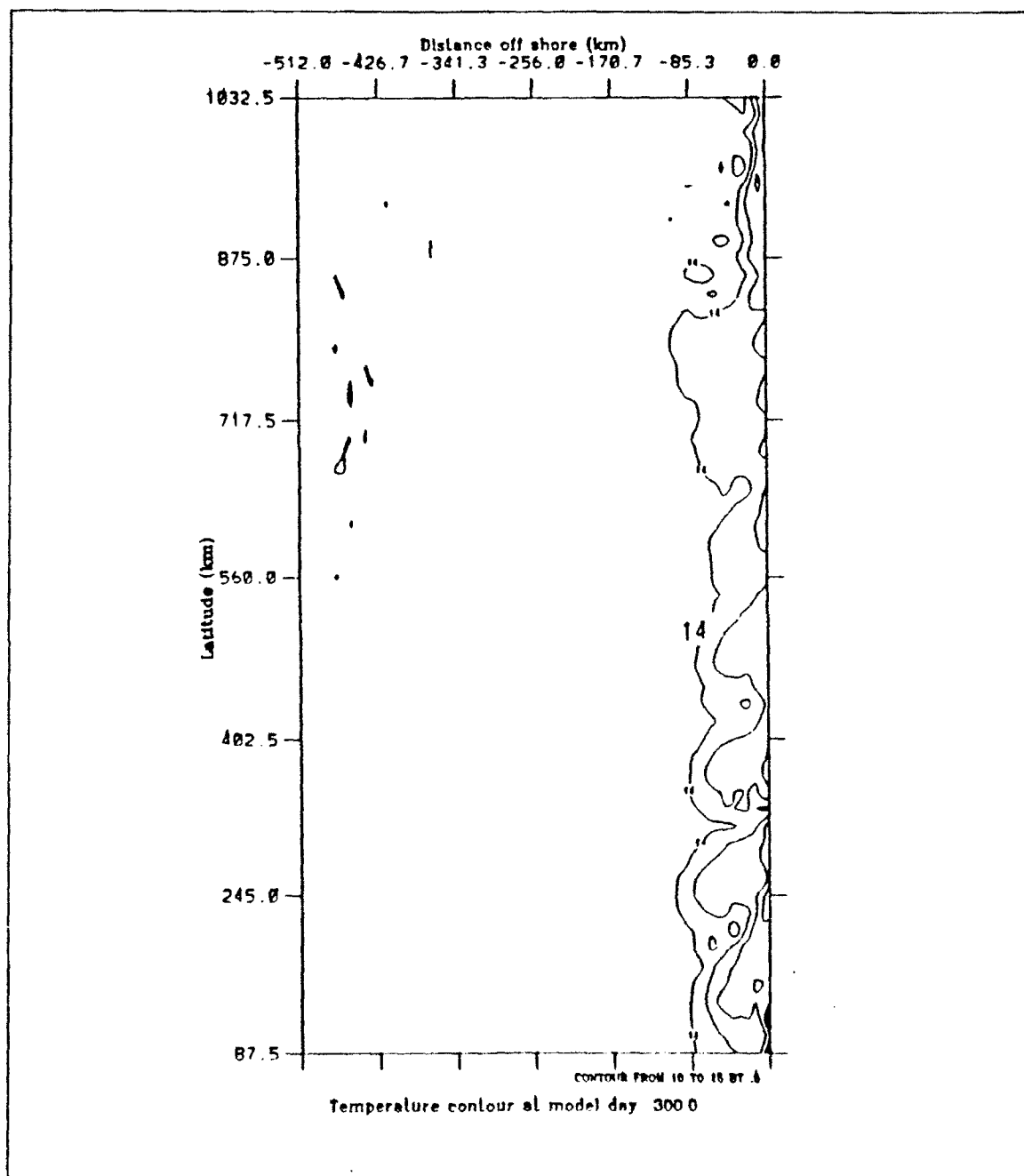
Figure 4.17 c) Experiment 3: Surface temperatures at day 300. The contour interval is 0.5° C. The temperature decreases toward the coast.
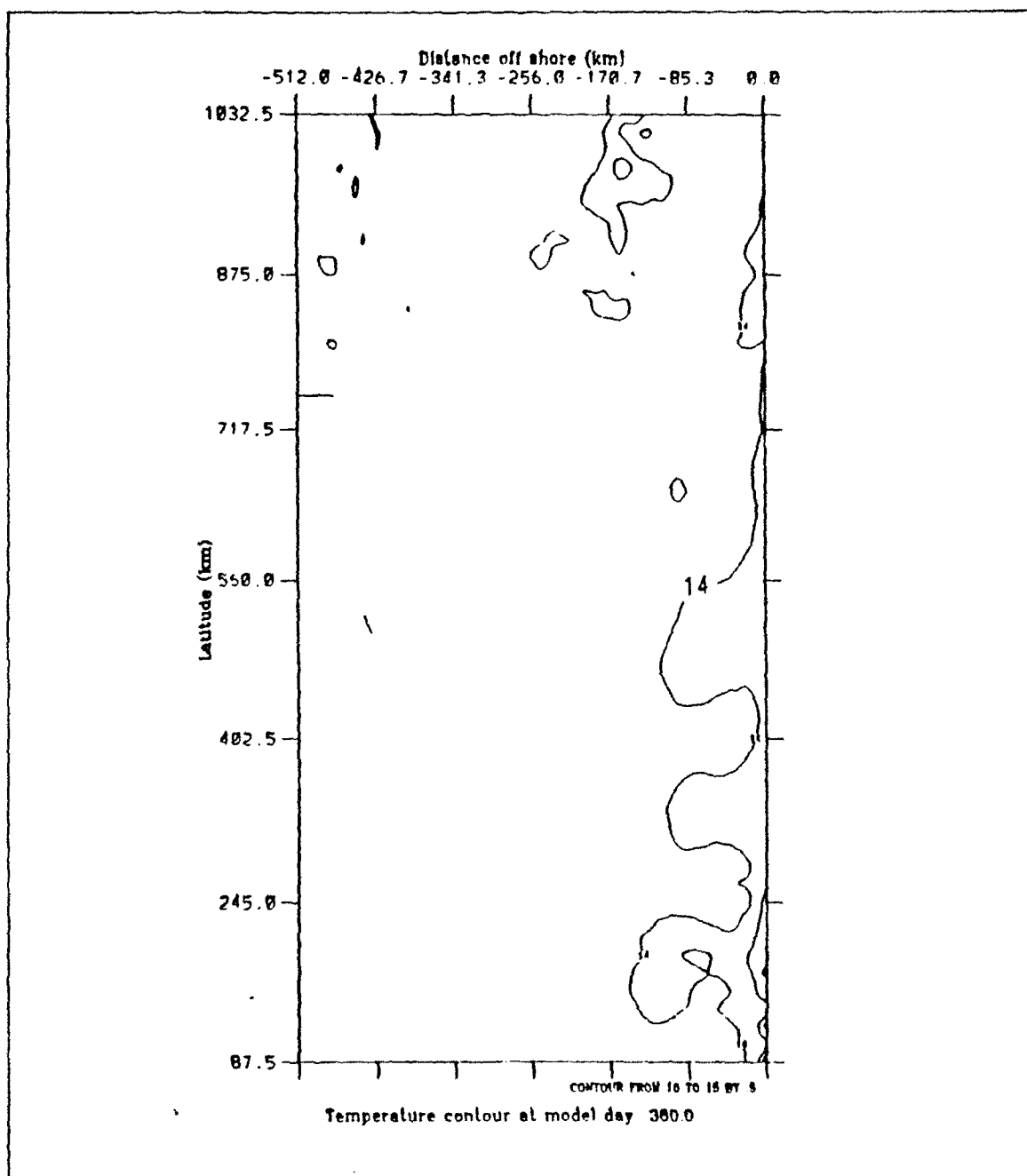
Figure 4.17 d) Experiment 3: Surface temperatures at day 360. The contour interval is 0.5⁰ C. The temperature decreases toward the coast.
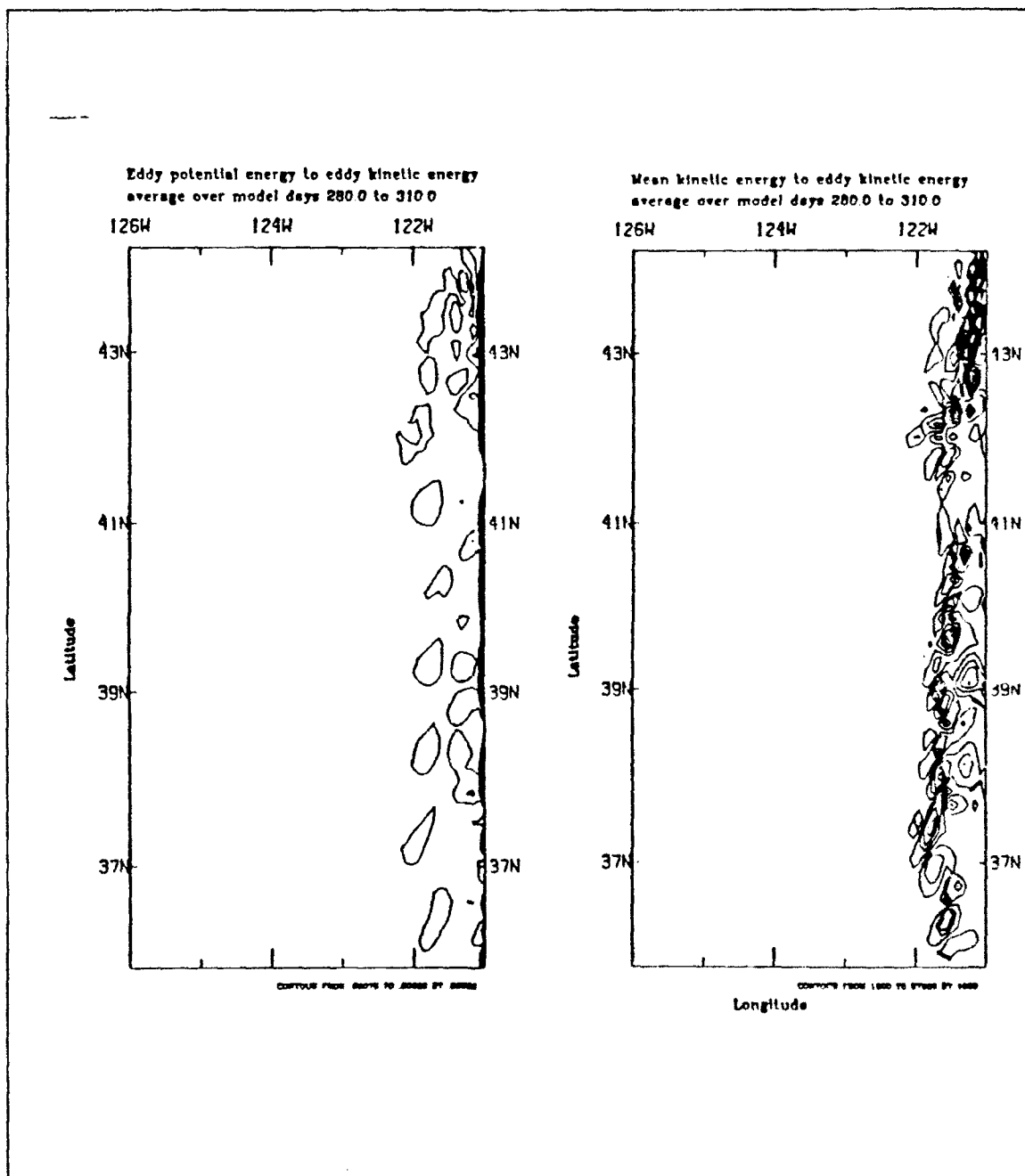
Figure 4.18 Experiment 3 Transfers of energy (as defined in equations 3.18 and 3.19) from: a) P to K (eddy available to eddy kinetic energy), and b) $\overline{K}$ to K' (mean to eddy kinetic energy). Transfers of energy are averaged over the days 280-310 and summed over the upper five layers. The contour intervals are 0.00025 ergs cm^{-3} s^{-1} in a) and 1000 ergs cm^{-3} s^{-1} in b).

76

Figure 4.19a) Experiment 4: Wind forcing in m s^{-1} at day 45.

Figure 4.19 b) Experiment 4: Wind forcing in m s^{-1} at day 90.

Figure 4.19 c) Experiment 4: Wind forcing in m s^{-1} at day 135.
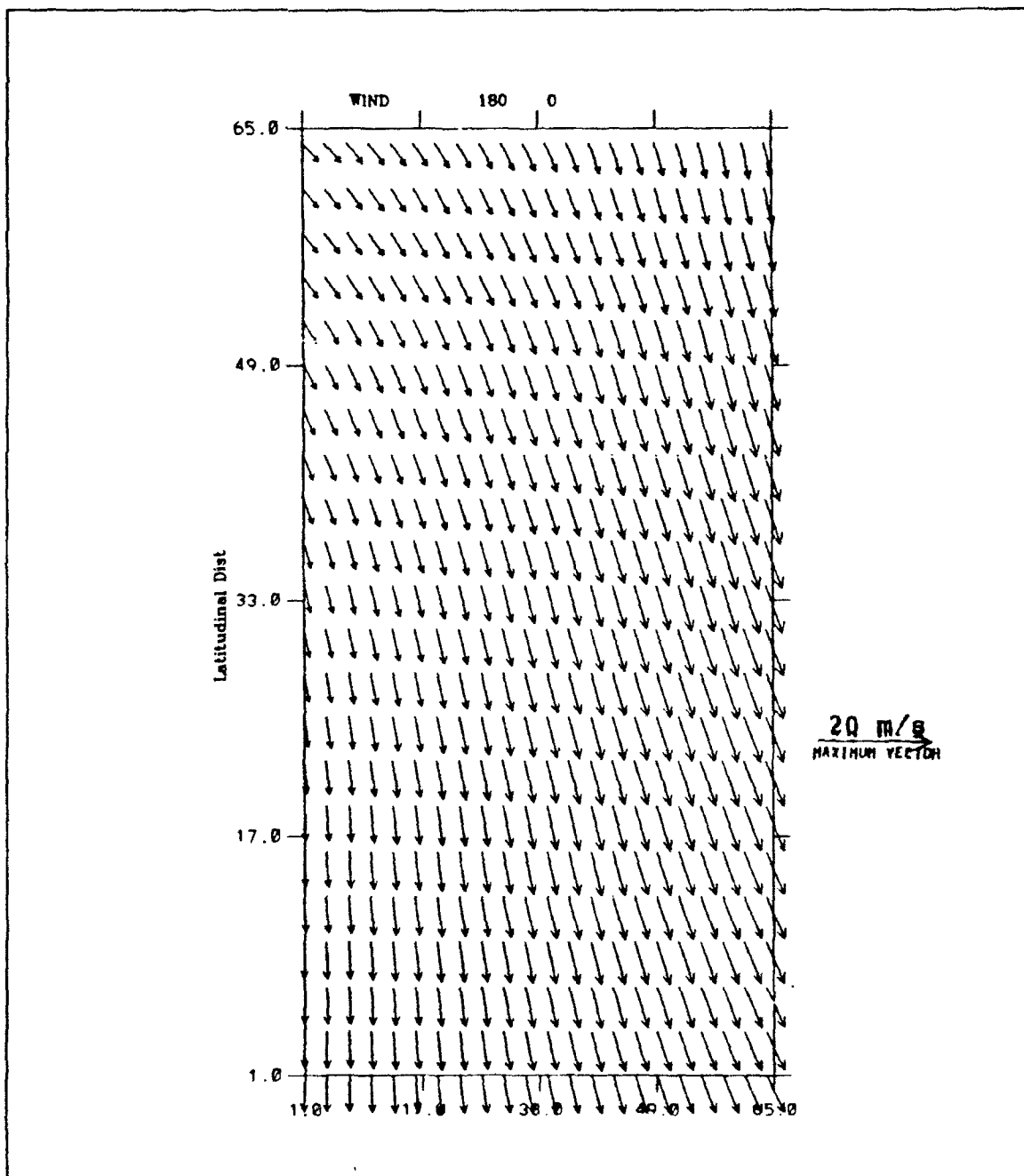
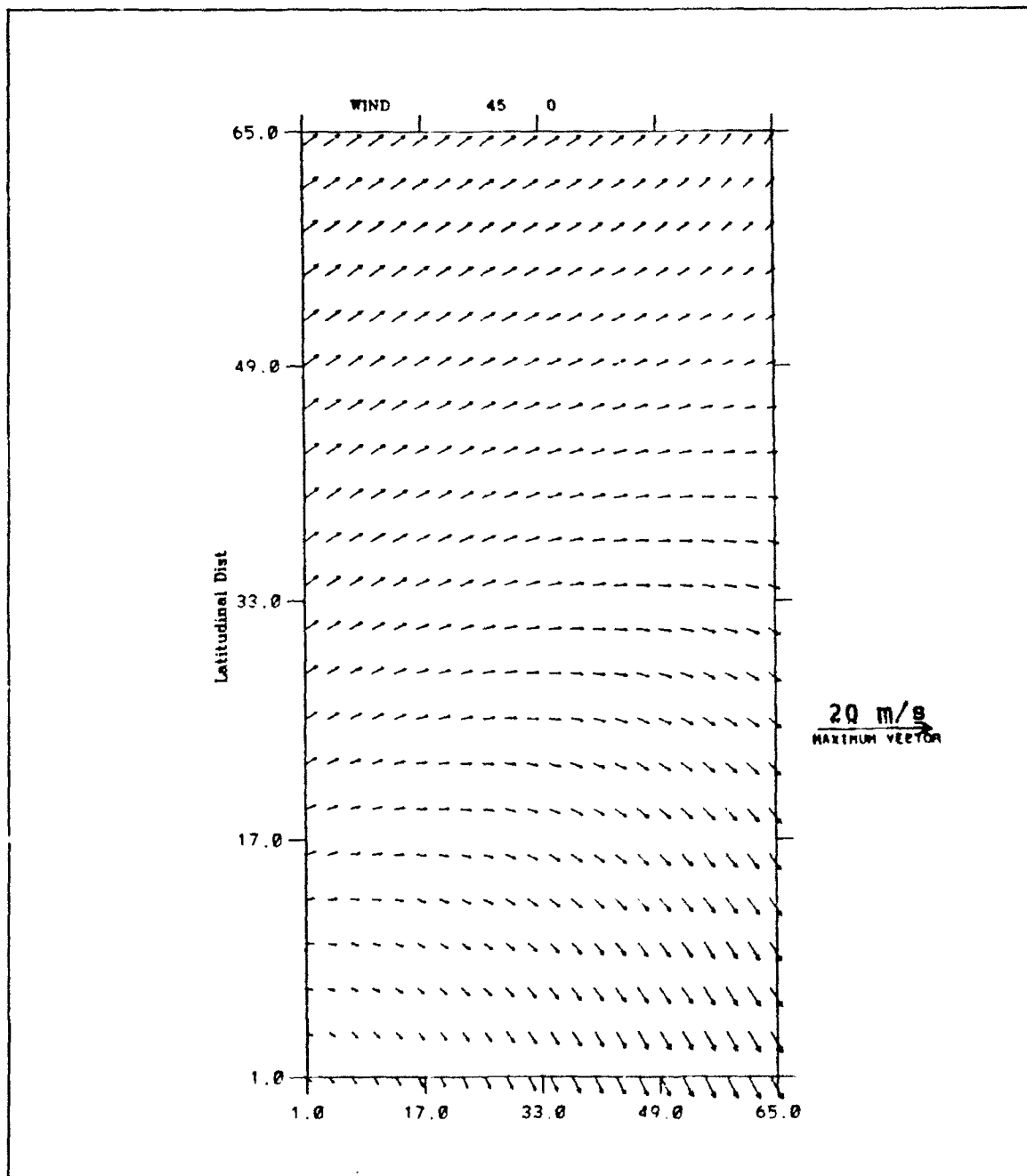Figure 4.19 d) Experiment 4: Wind forcing in m s^{-1} at day 180.
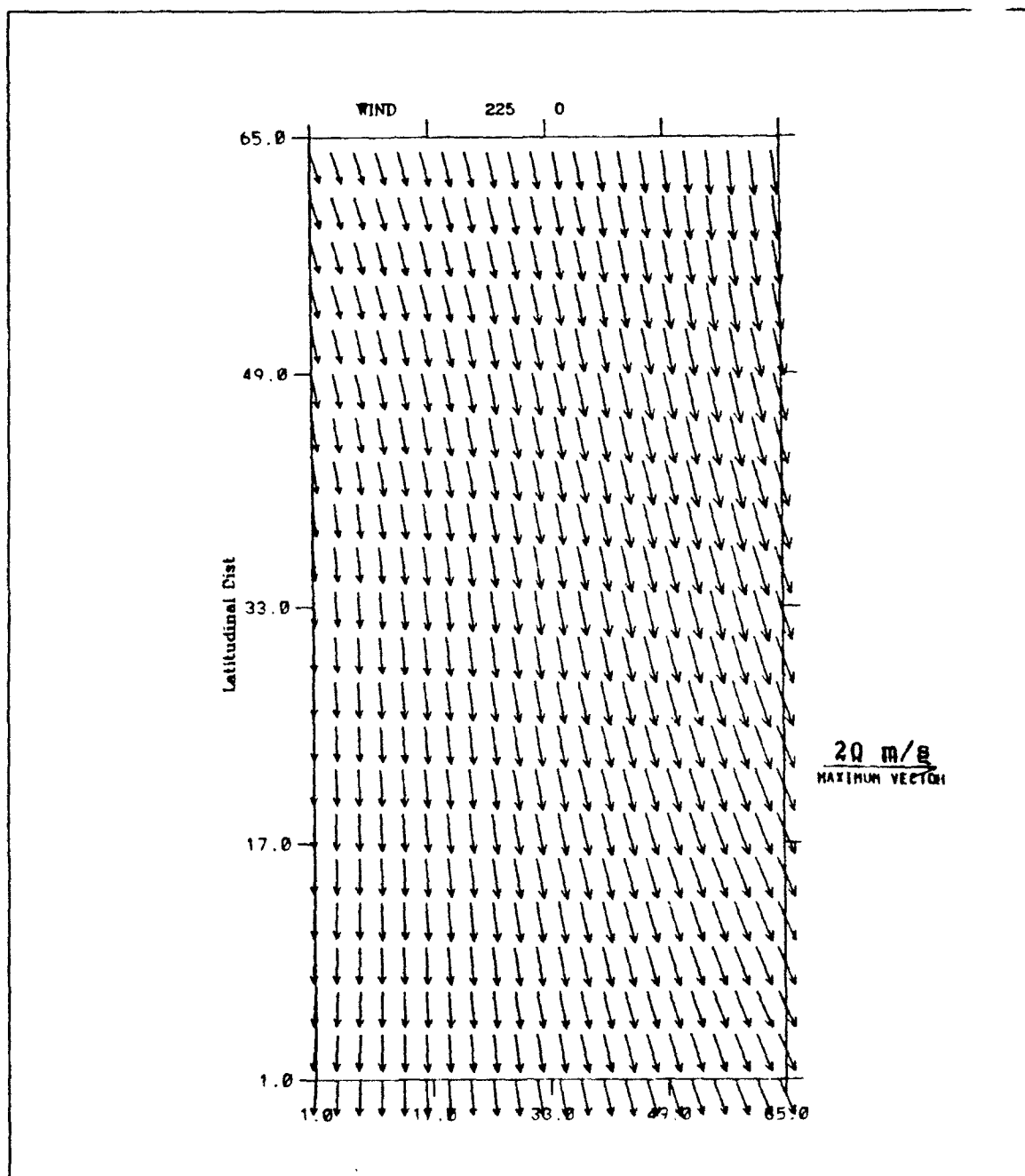
Figure 4.20 a) Experiment 4: Wind forcing in m s^{-1} at day 225.
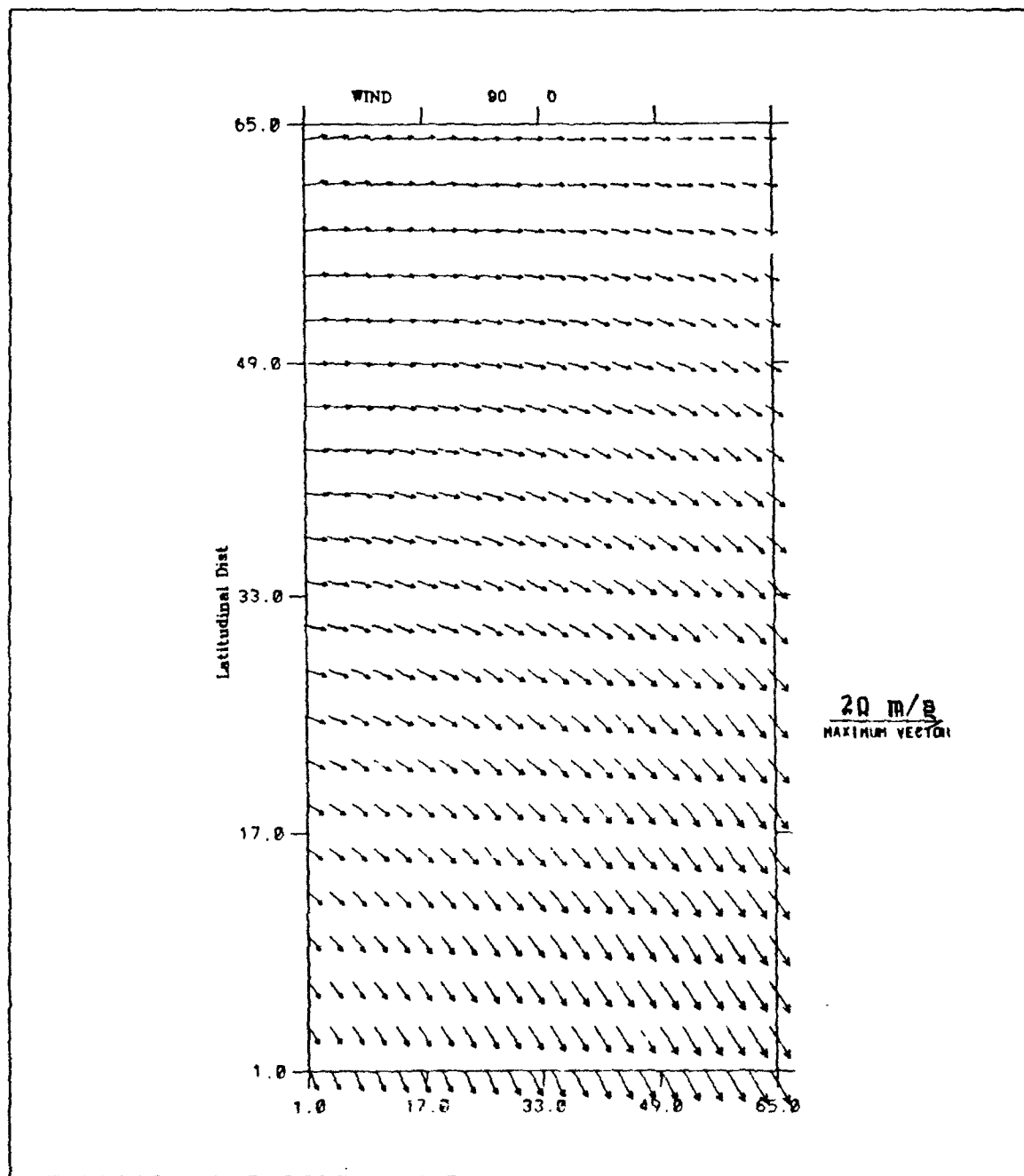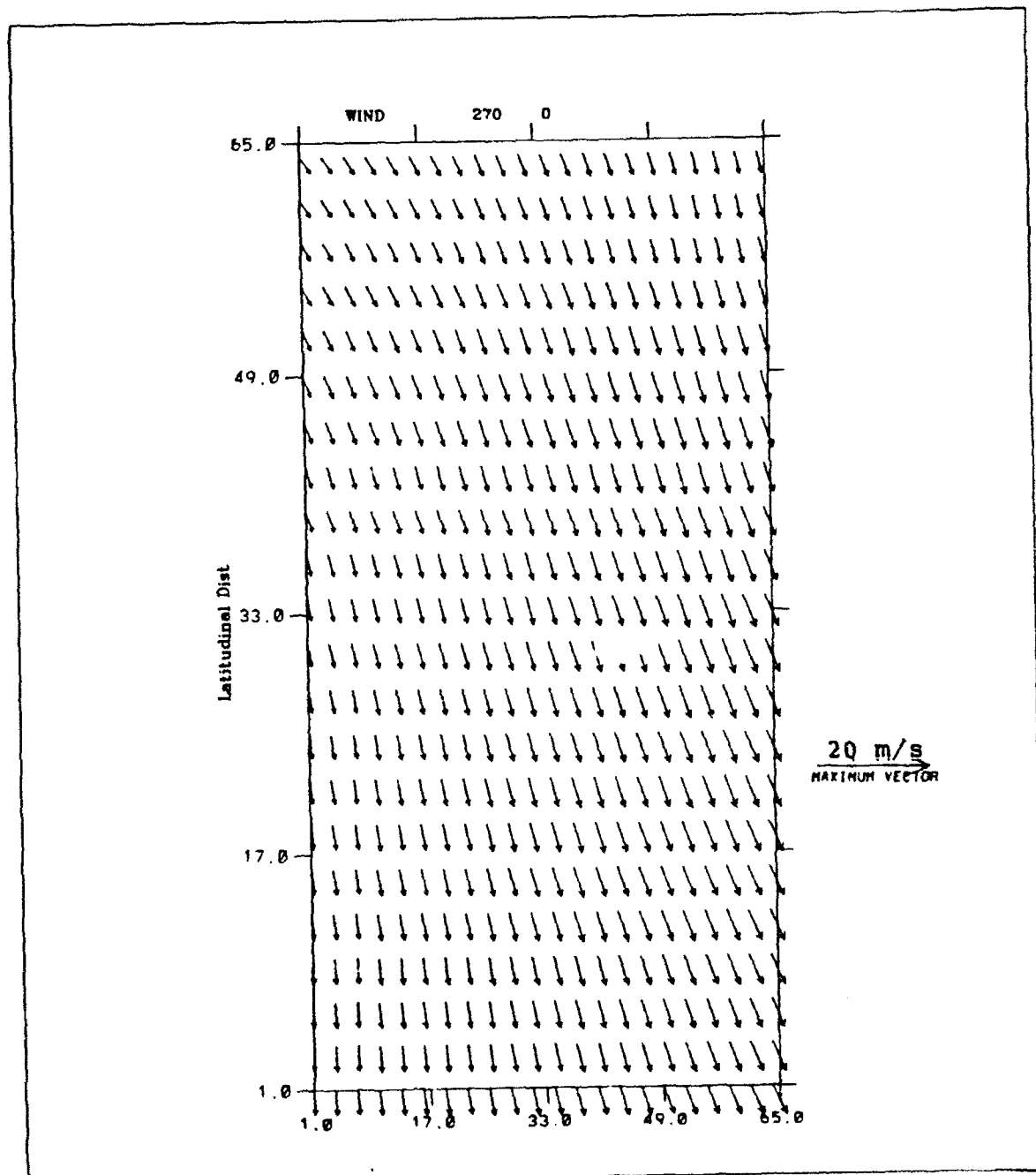
Figure 4.20 b) Experiment 4: Wind forcing in m s^{-1} at day 270.
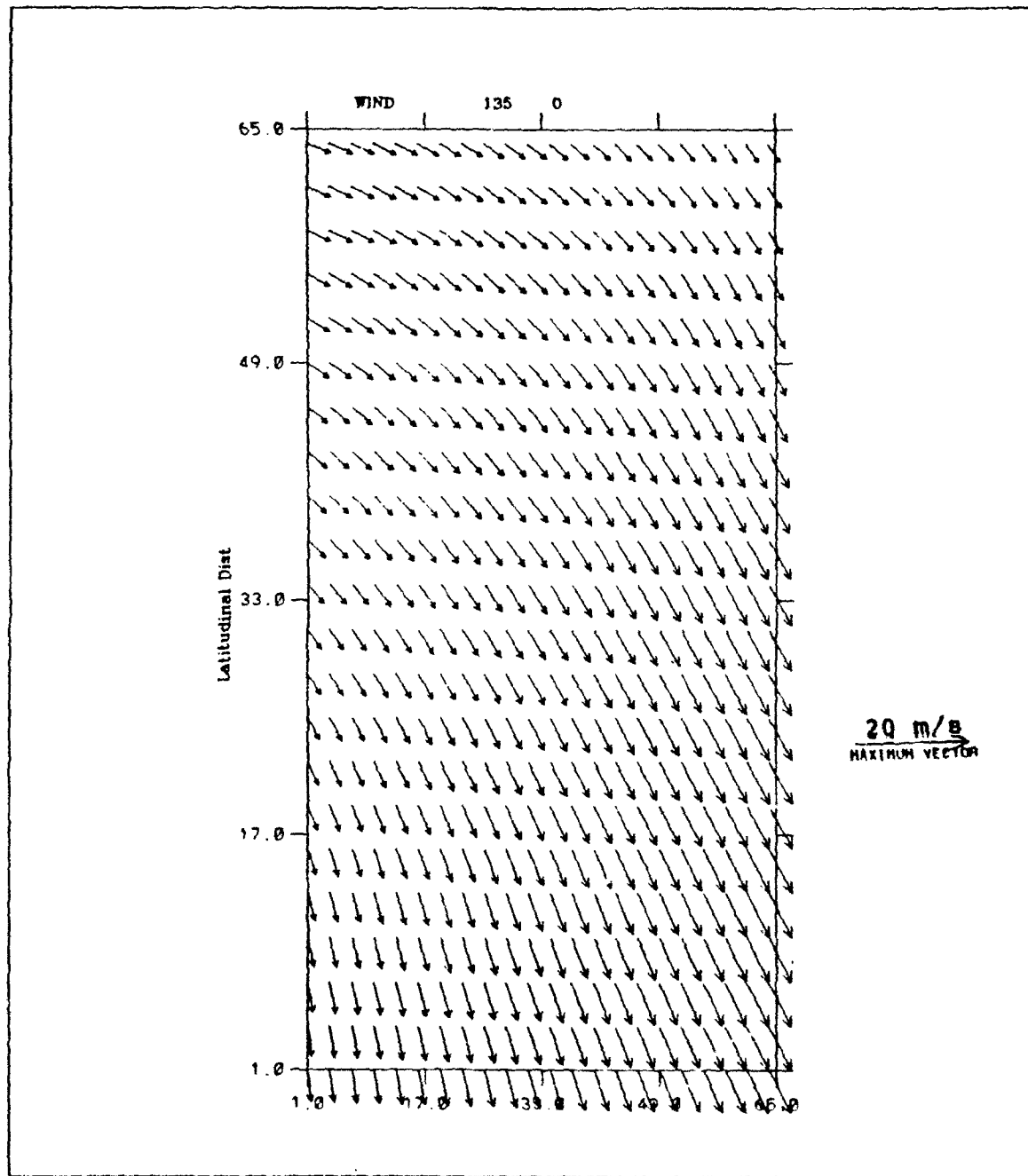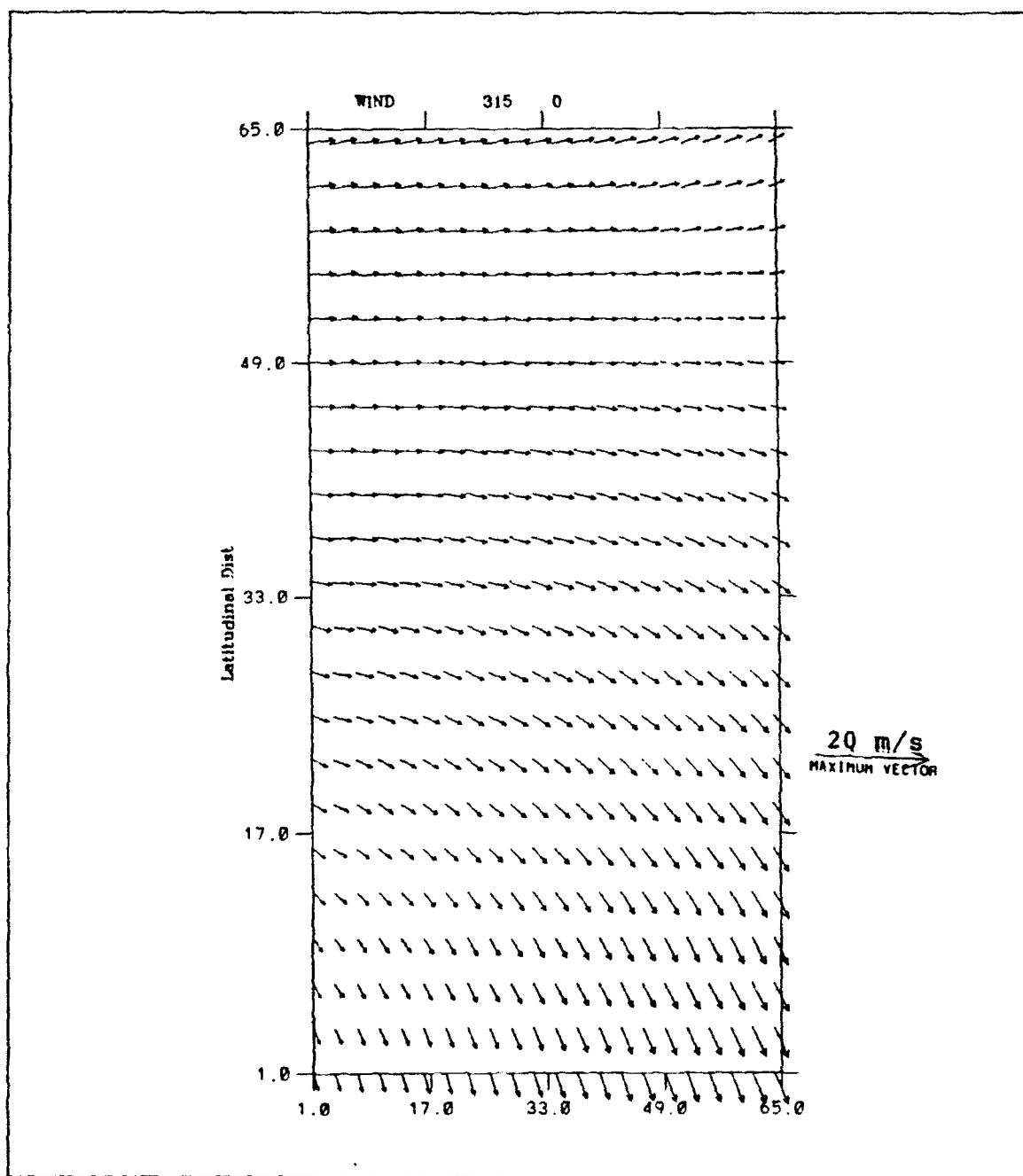
Figure 4.20 c) Experiment 4: Wind forcing in m s^{-1} at day 315.
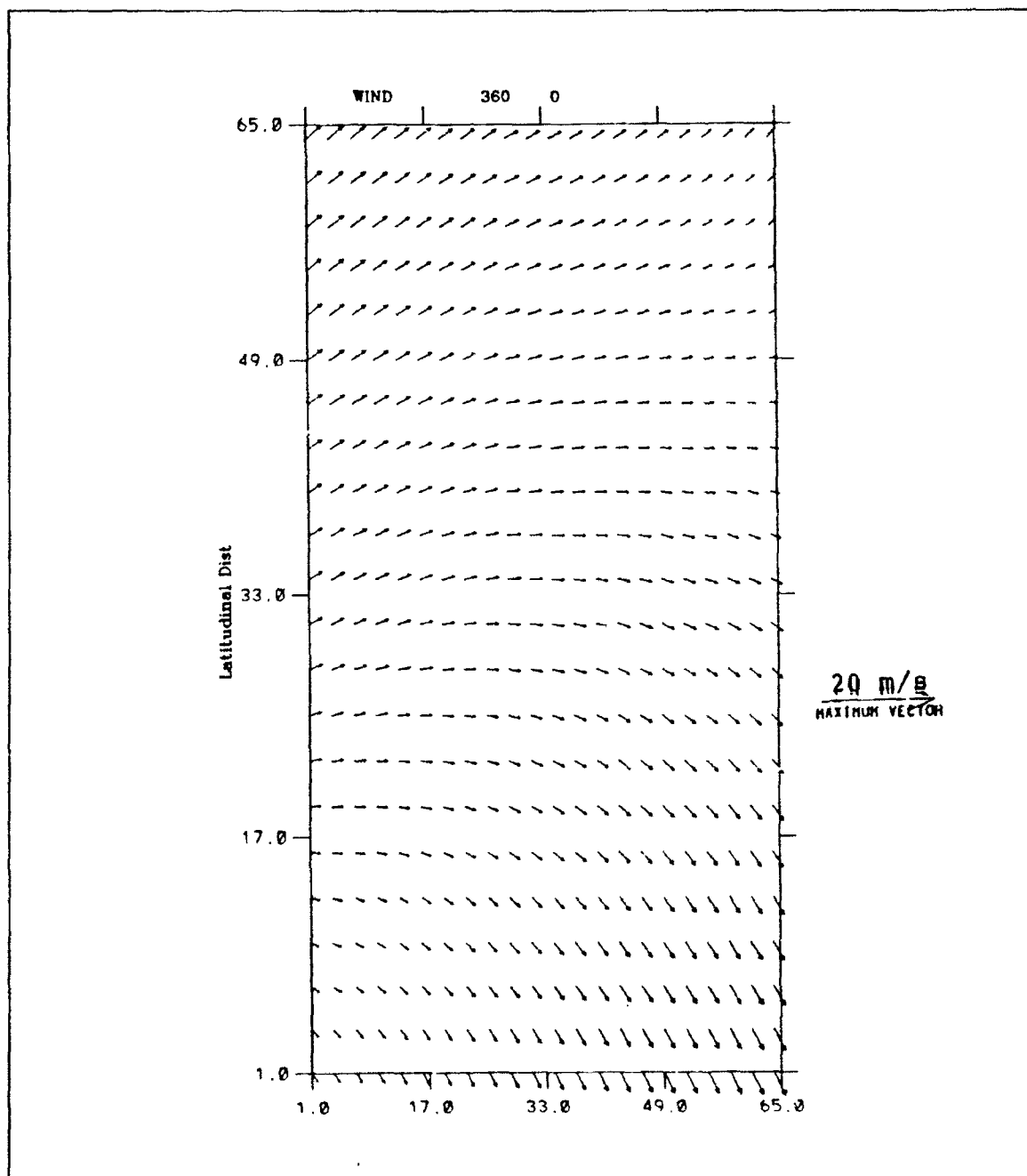
Figure 4.20 d) Experiment 4: Wind forcing in m s^{-1} at day 360.

Figure 4.21 a) Experiment 4: Surface velocity vectors superimposed on temperatures at day 110. The contour interval is 0.5° C. The temperature decreases toward the coast.

Figure 4.21 b) Experiment 4: Cross-section at 40° N latitude of meridional velocities at day 110. The contour interval is 1.1 cm s⁻¹. The dashed lines indicate southward velocities and show the surface equatorward current. The solid lines indicate northward flow and show the poleward undercurrent.
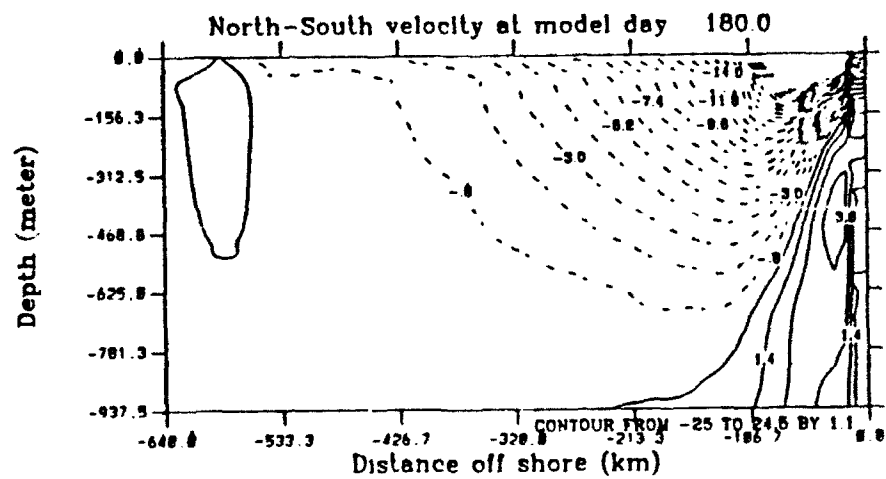
Figure 4.22 Experiment 4: Cross-section at 40° N latitude of meridional velocities at day 180. The contour interval is 1.1 cm s⁻¹. The dashed lines indicate southward velocities and show the surface equatorward current. The solid lines indicate northward flow and show the poleward undercurrent.

Figure 4.23 a) Experiment 4: Surface velocity vectors superimposed on temperatures at day 260. The contour interval is 0.5° C. The temperature decreases toward the coast.

Figure 4.23 b) Experiment 4: Day 260 Meridional velocities. The contour interval is 10 cm s^{-1}. The dashed lines indicate southward velocities. The equatorward velocity increases to ~35 cm s^{-1} near the coast.

Figure 4.23 c) Experiment 4: Surface temperatures at day 260. The contour interval is 1° C. The temperature decreases toward the coast.

Figure 4.23 d) Experiment 4: Surface Zonal velocities at day 260. The contour interval is 10 cm s^{-1}. The dashed lines indicate westward velocities. Closed contours show the locations of eddies.
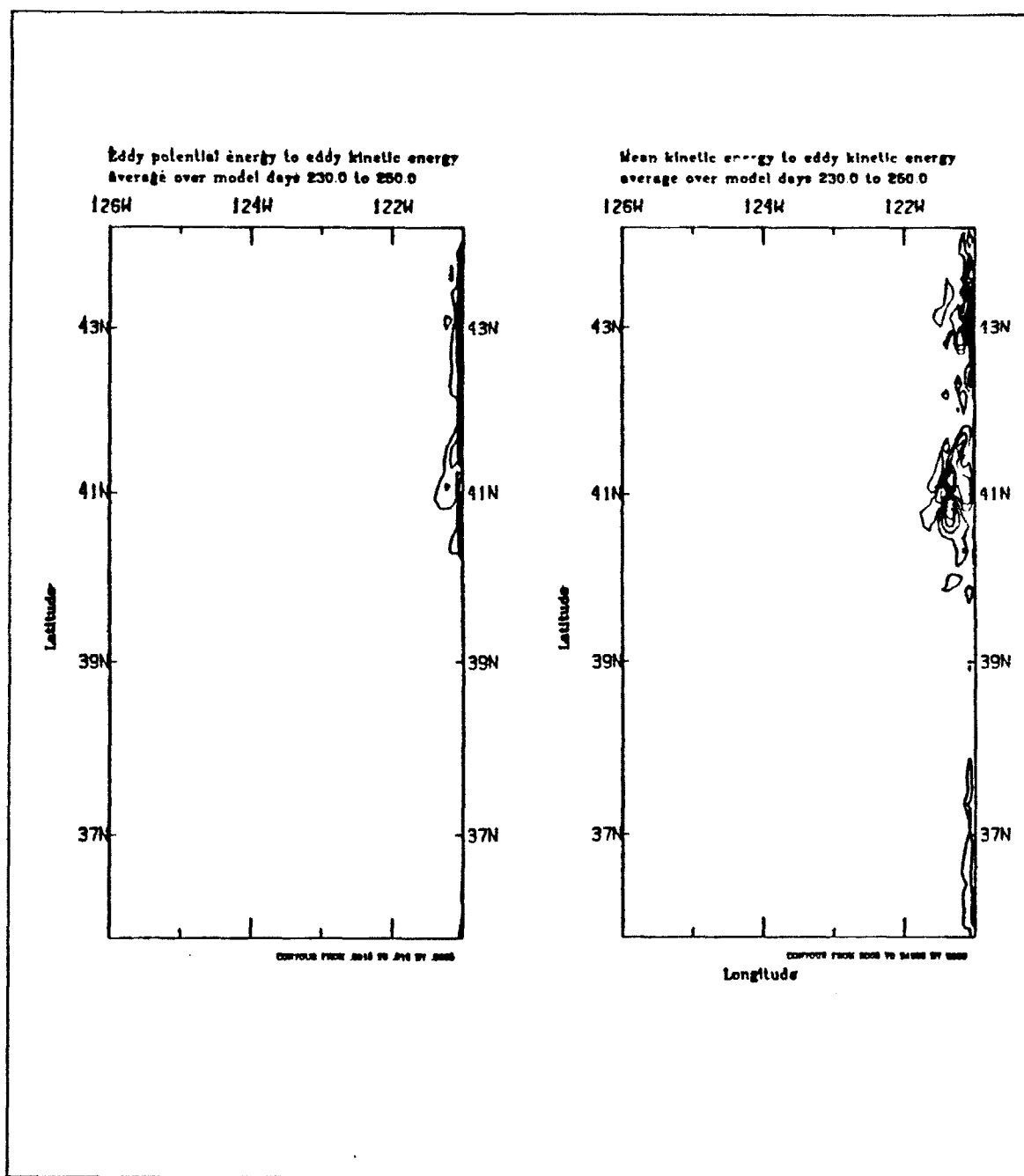
Figure 4.24 Experiment 4 Transfers of energy (as defined in equations 3.18 and 3.19) from: a) P' to K' (eddy available to eddy kinetic energy), and b) $\overline{K}$ to K' (mean to eddy kinetic energy). Transfers of energy are averaged over the days 230-250 and summed over the upper five layers. The contour intervals are 0.0005 ergs cm^{-3} s^{-1} in a) and 2000 ergs cm^{-3} s^{-1} in b).
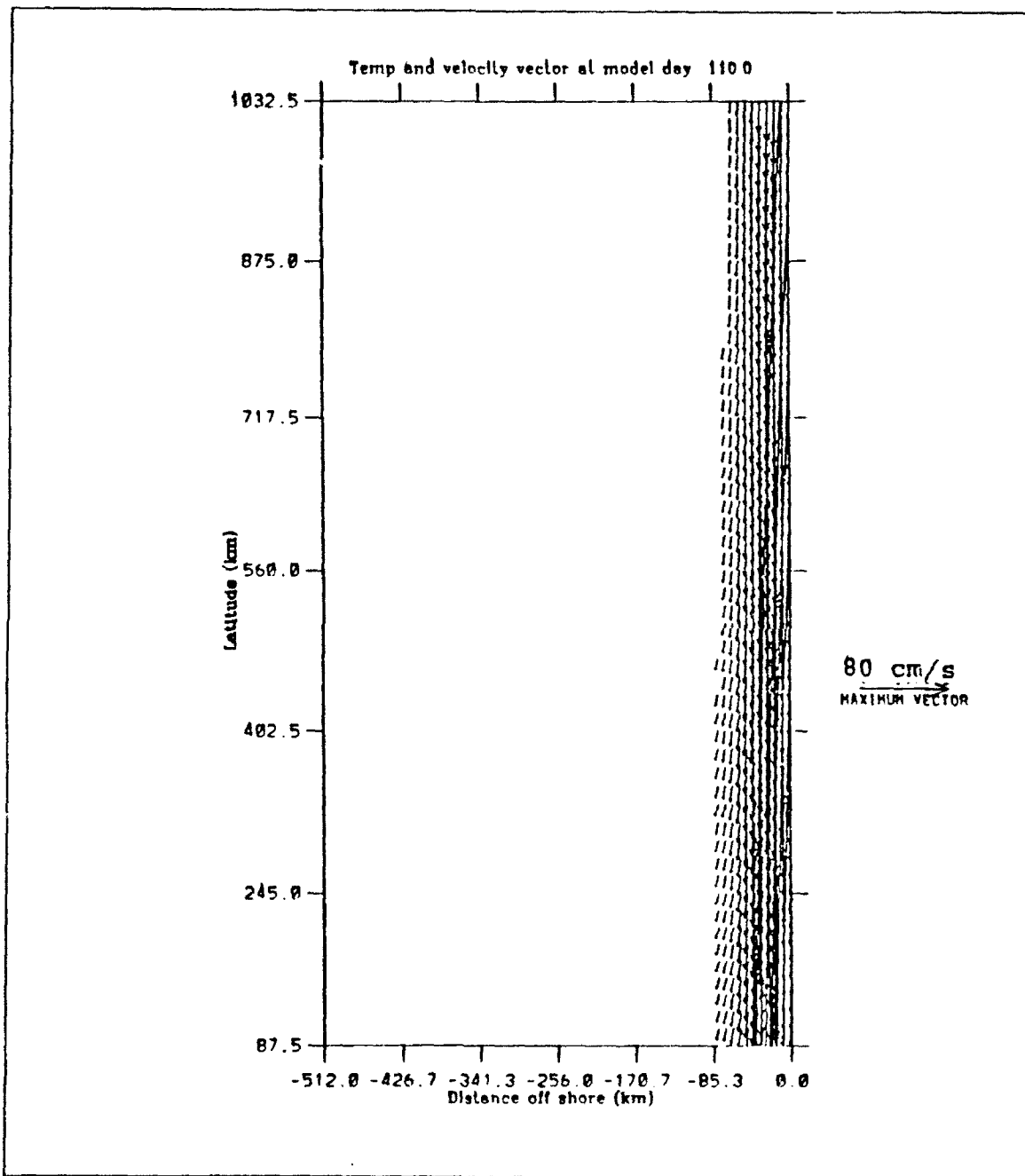
92
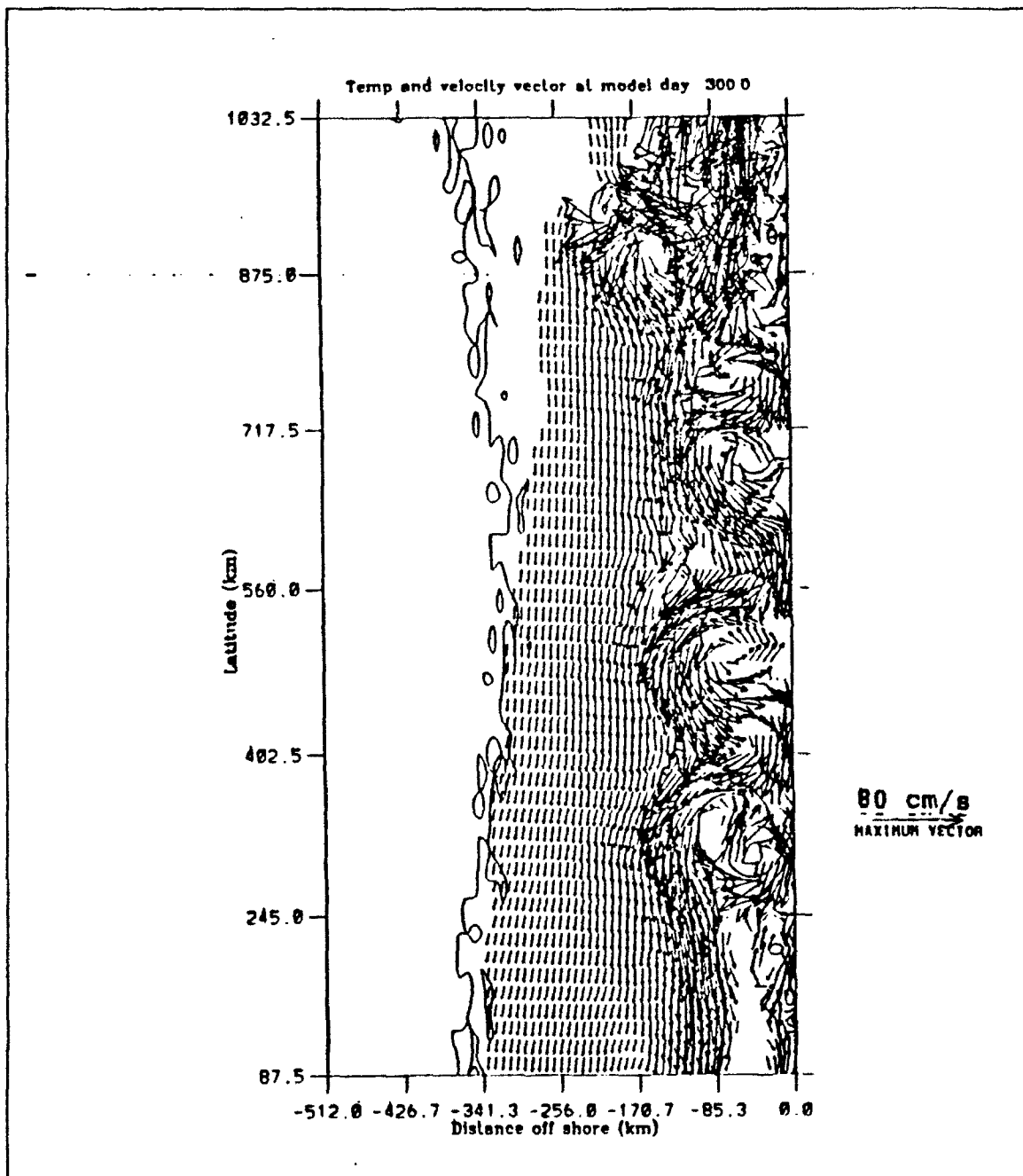
Figure 4.25 a) Experiment 4: Surface velocity vectors superimposed on temperatures at day 300. The contour interval is 0.5° C. The temperature decreases toward the coast.
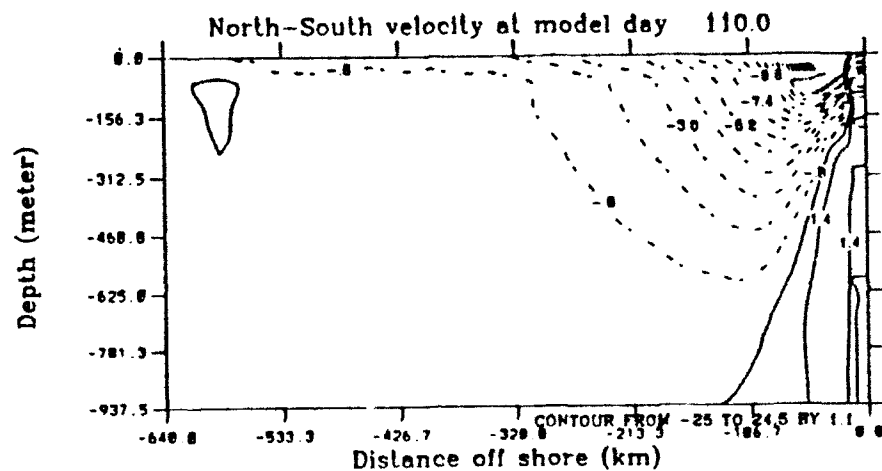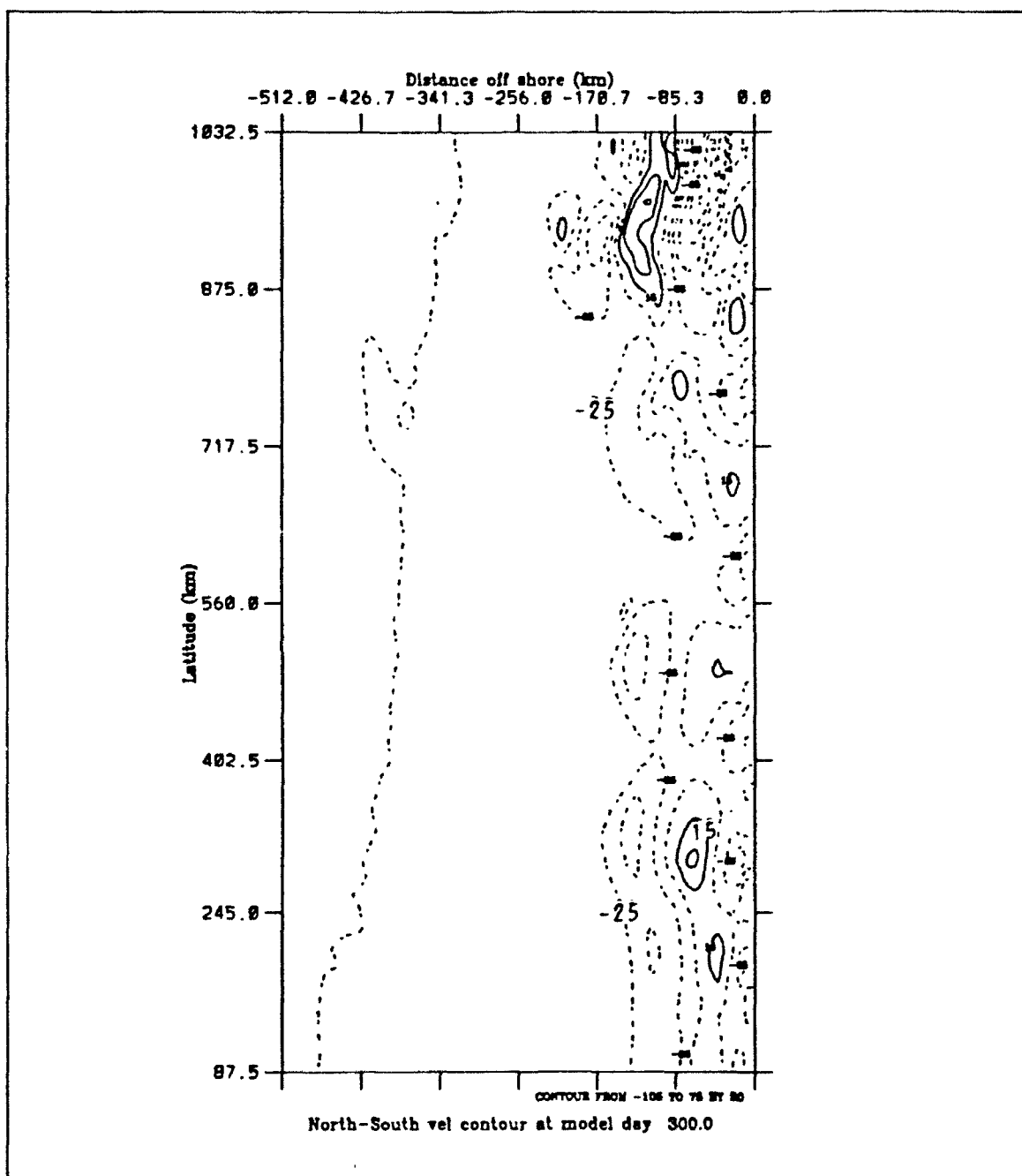
Figure 4.25 b) Experiment 4: Day 300 Meridional velocities. The contour interval is 20 cm s⁻¹. The dashed lines indicate southward velocities.
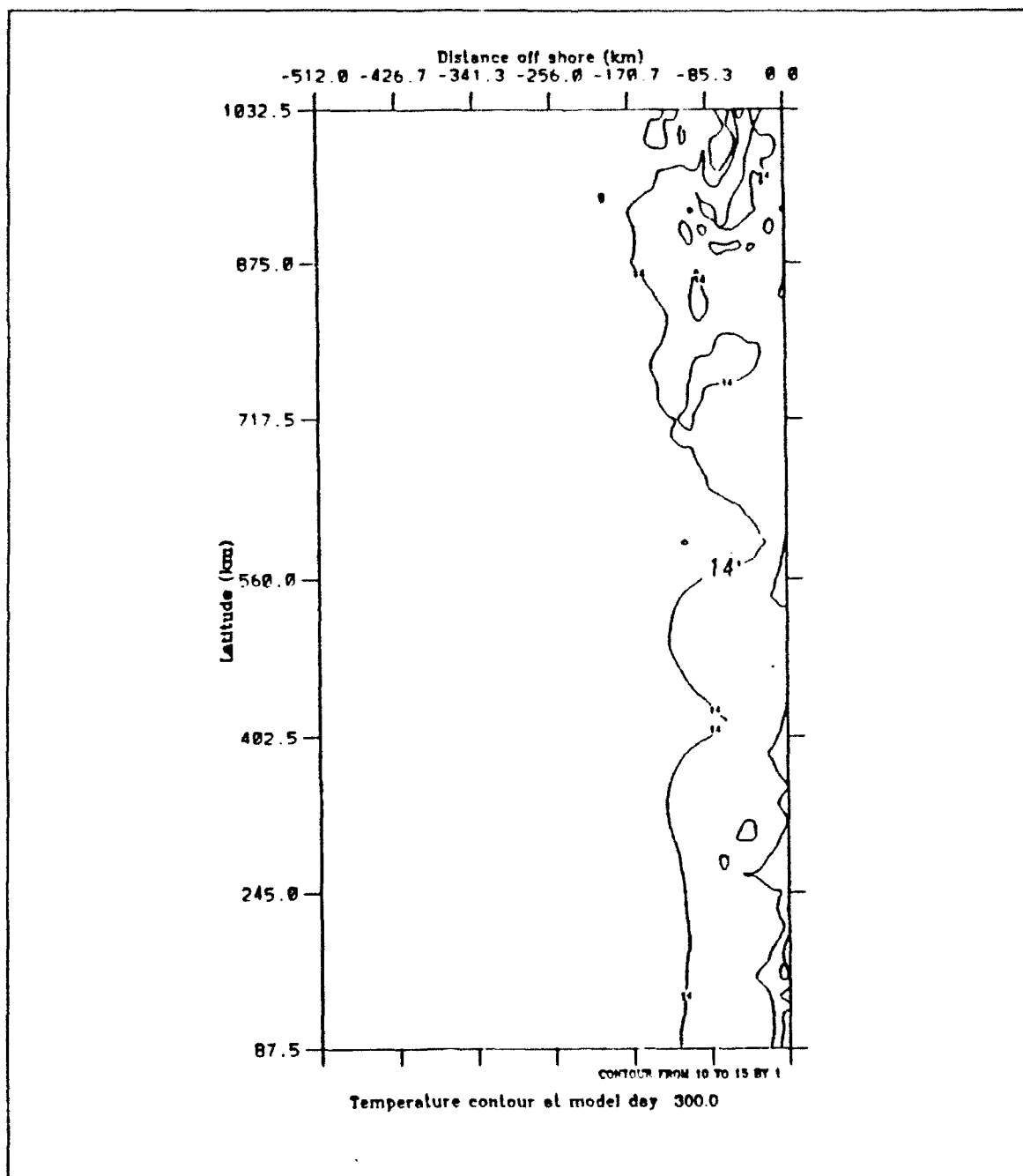
Figure 4.25 c) Experiment 4: Surface temperatures at day 300. The contour interval is 1° C. The temperature decreases toward the coast.

95
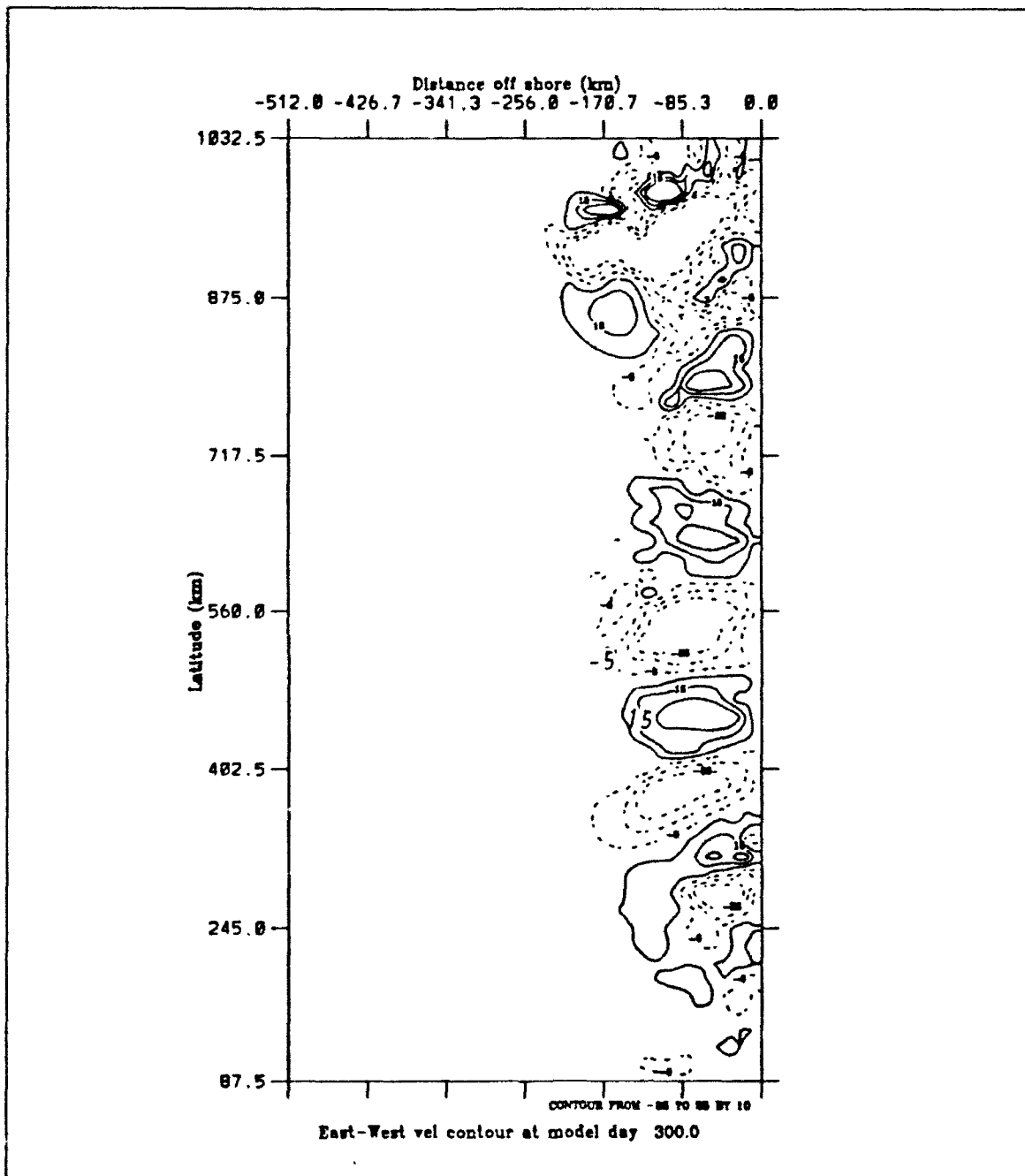
Figure 4.25 d) Experiment 4: Surface Zonal velocities at day 300. The contour interval is 10 cm s^{-1}. The dashed lines indicate westward velocities. Closed contours show the locations of eddies.
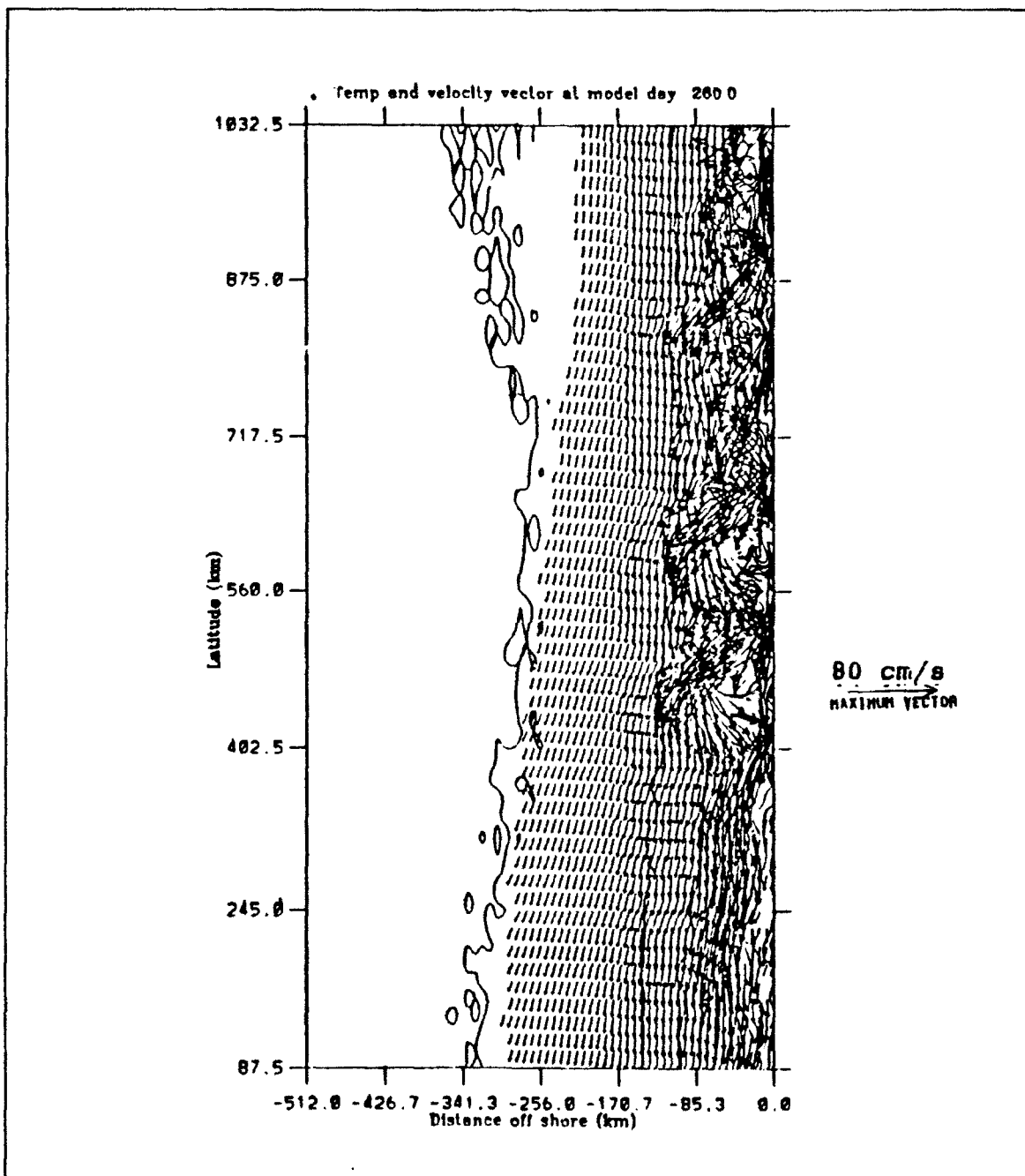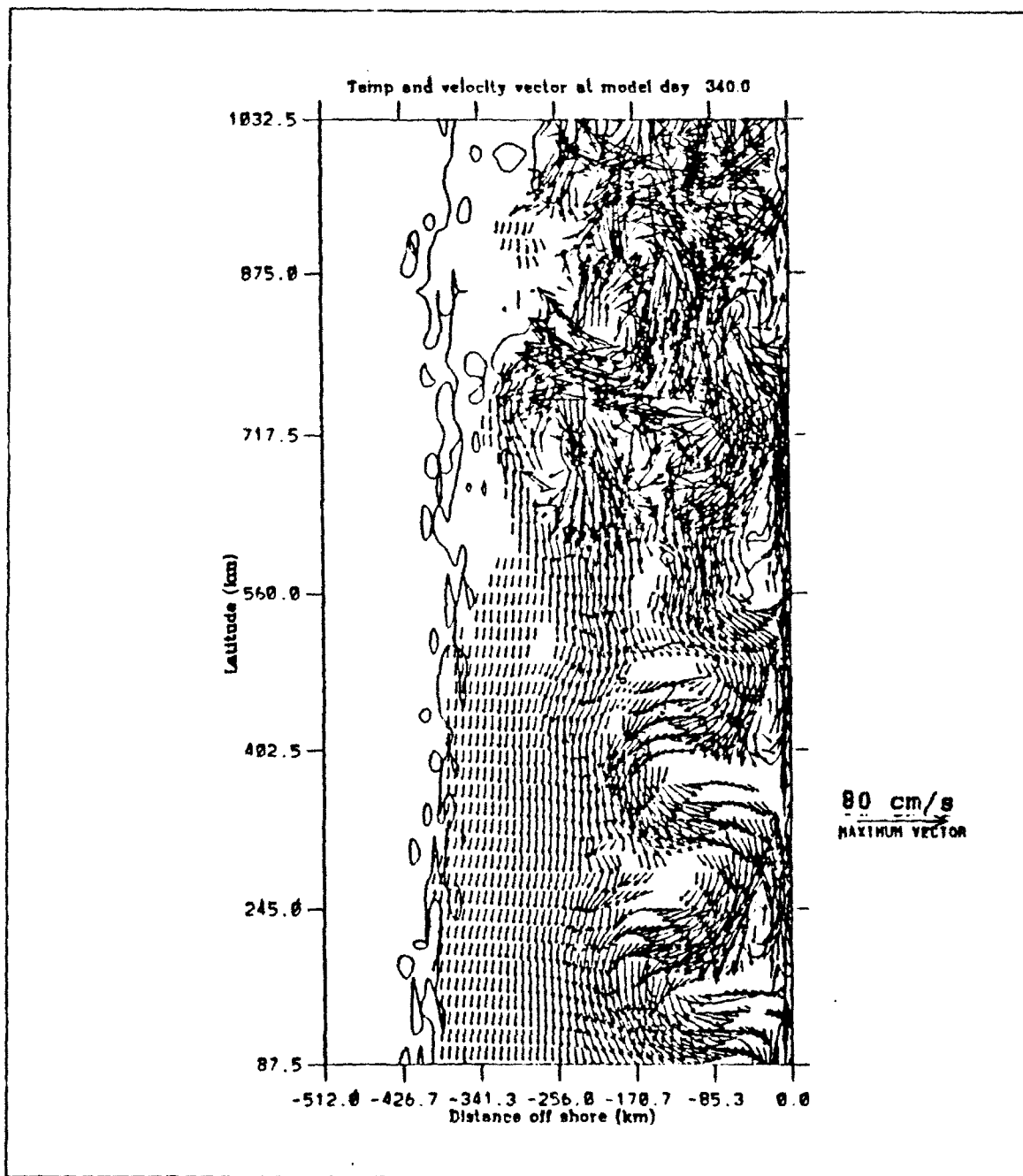
Figure 4.26 a) Experiment 4: Surface velocity vectors superimposed on temperatures at day 340. The contour interval is 0.5° C. The temperature decreases toward the coast.
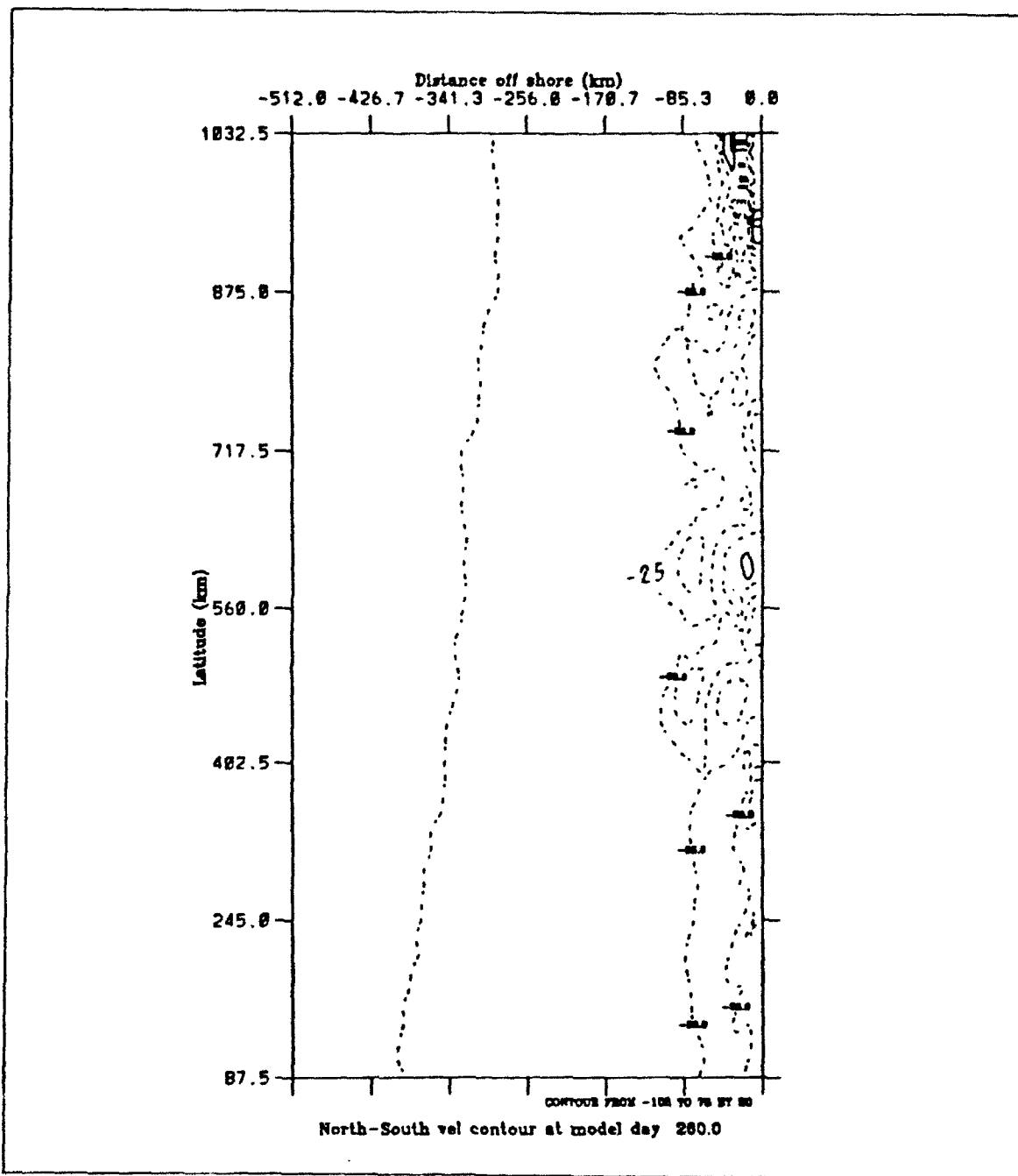
97
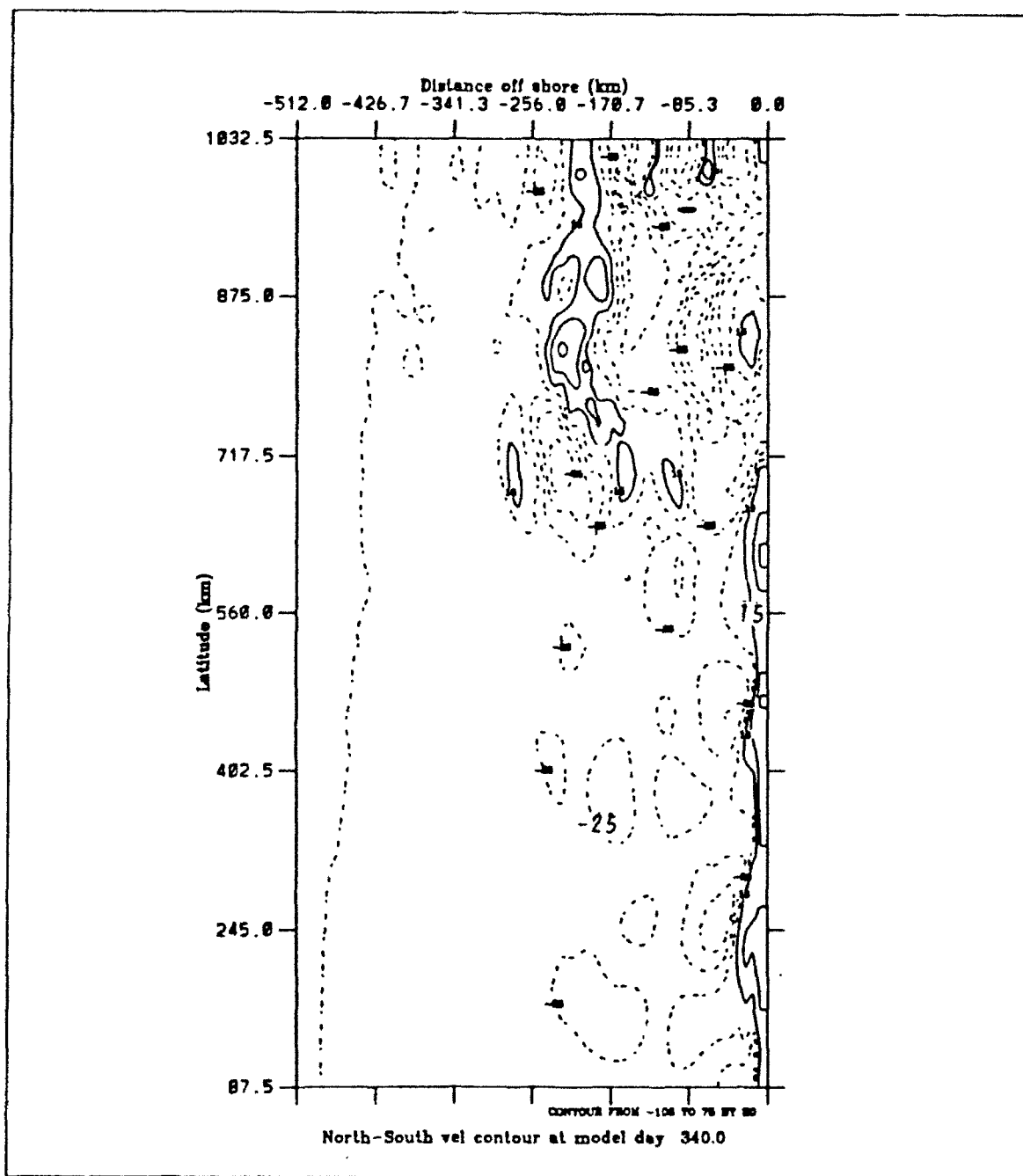
Figure 4.26 b) Experiment 4: Day 340 Meridional velocities. The contour interval is 20 cm s^{-1}. The dashed lines indicate southward velocities.
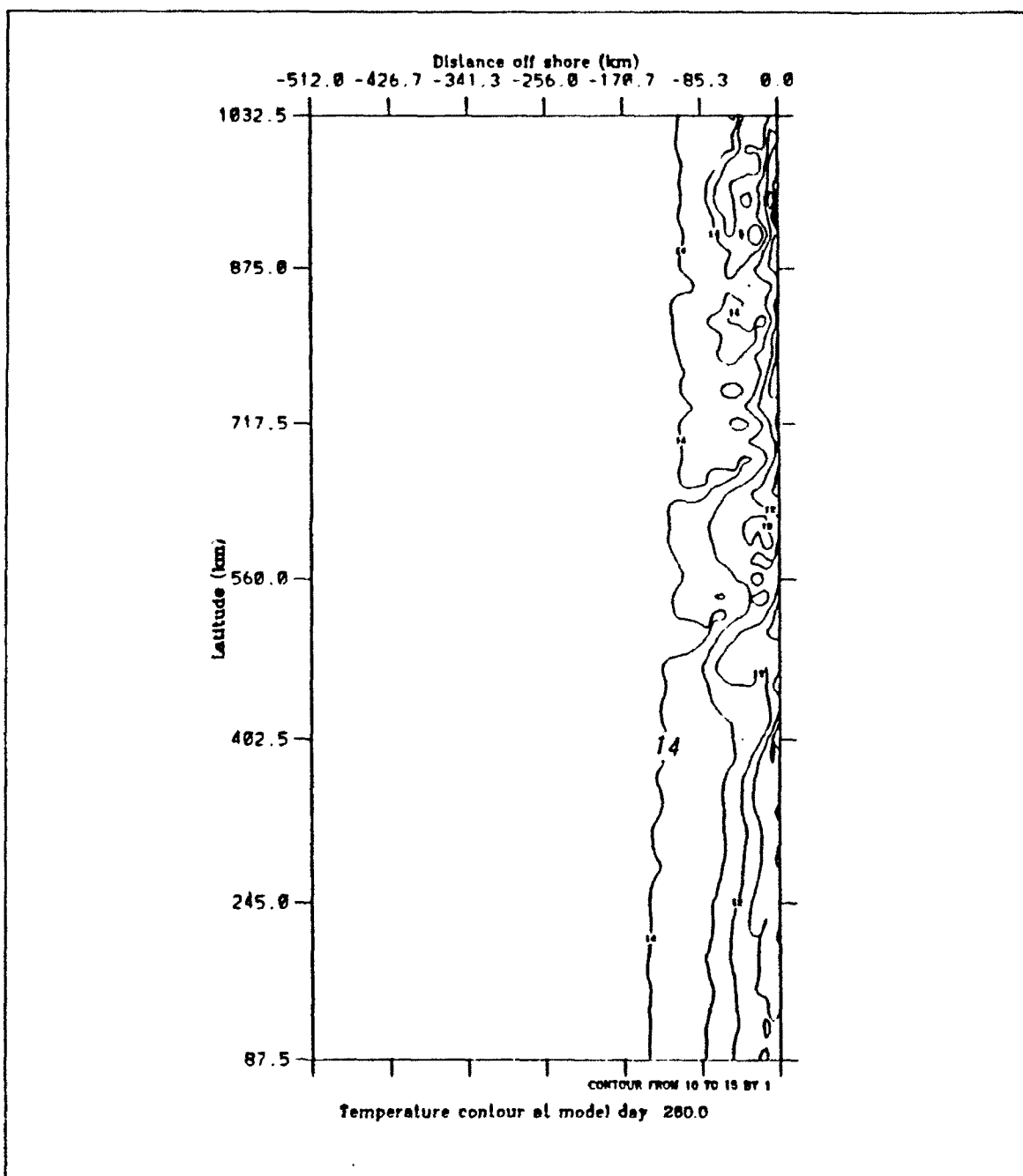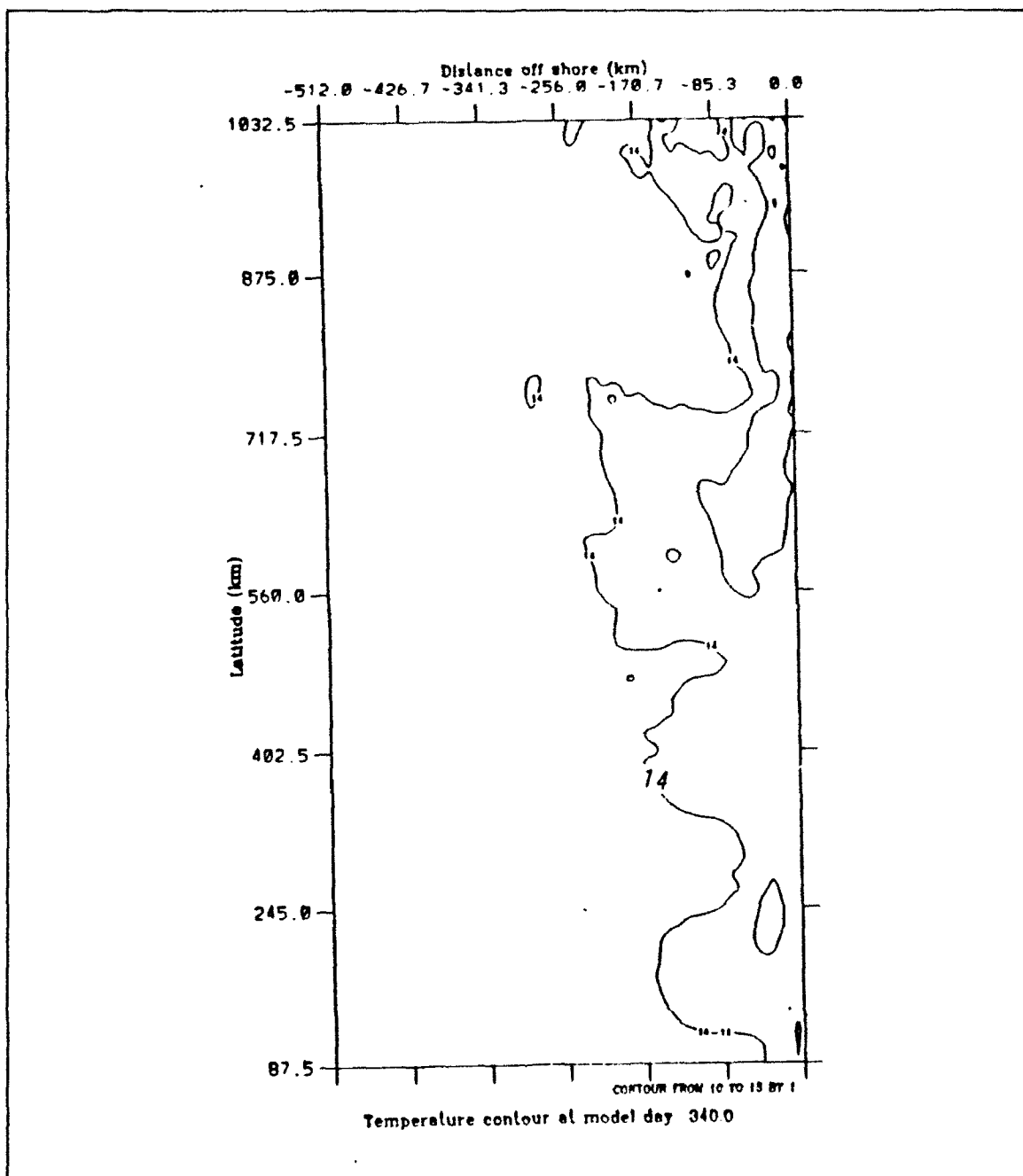
Figure 4.26 c) Experiment 4: Surface temperatures at day 340 The contour interval is 1° C. The temperature decreases toward the coast.
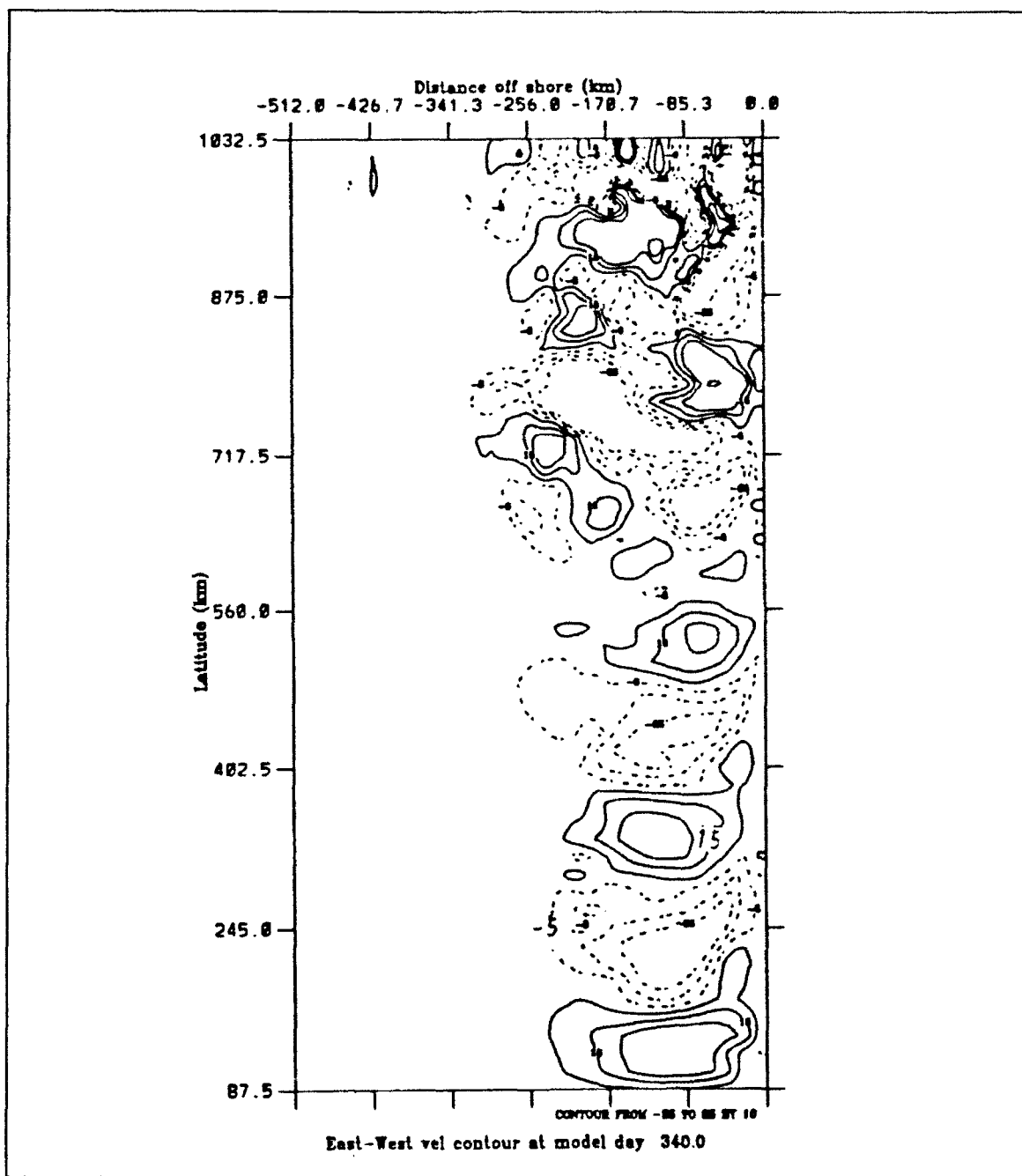
Figure 4.26 d) Experiment 4: Surface Zonal velocities at day 340. The contour interval is 10 cm s^{-1}. The dashed lines indicate westward velocities. Closed contours show the locations of eddies.
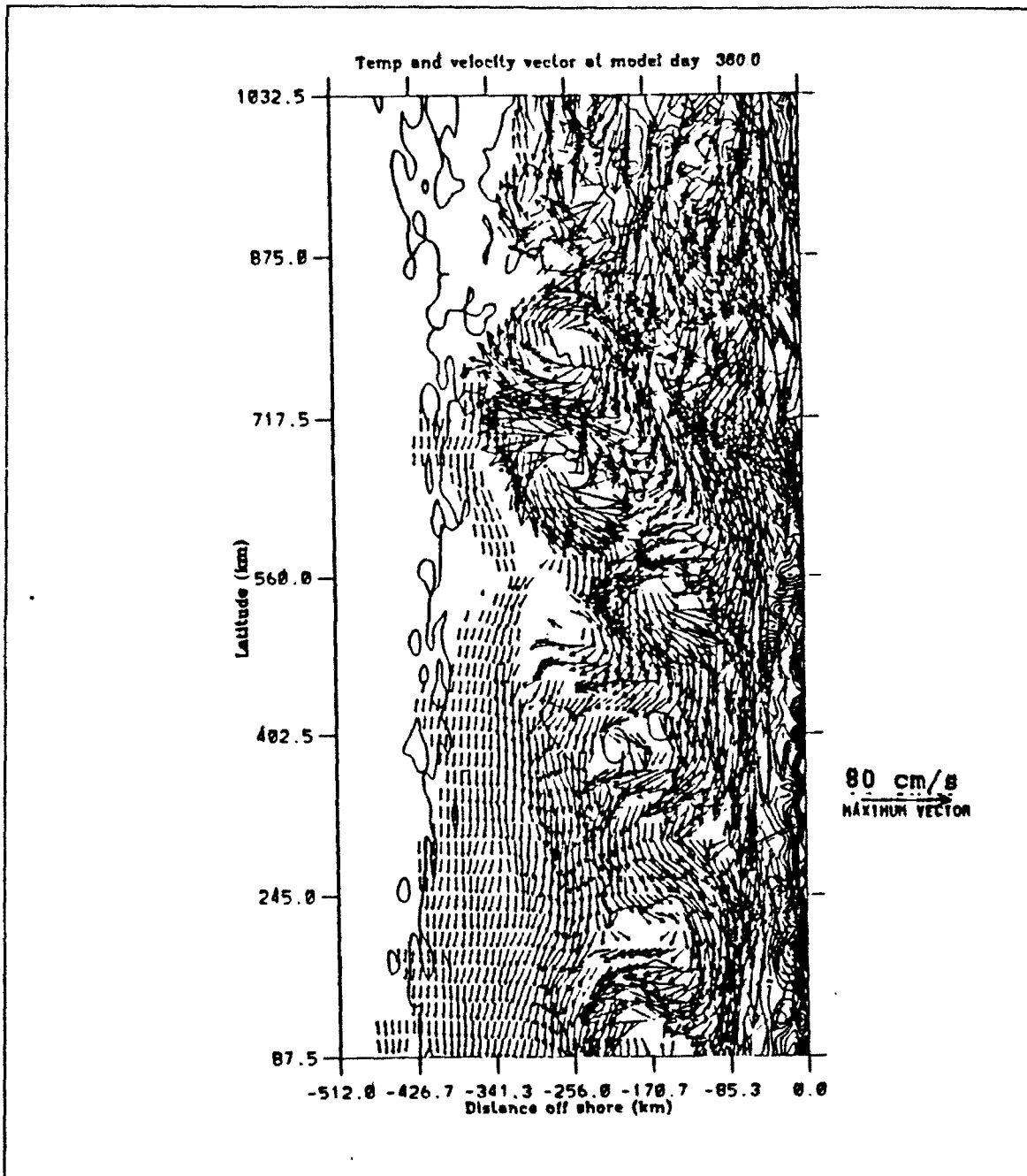
Figure 4.27 a) Experiment 4: Surface velocity vectors superimposed on temperatures at day 360. The contour interval is 0.5° C. The temperature decreses toward the coast.
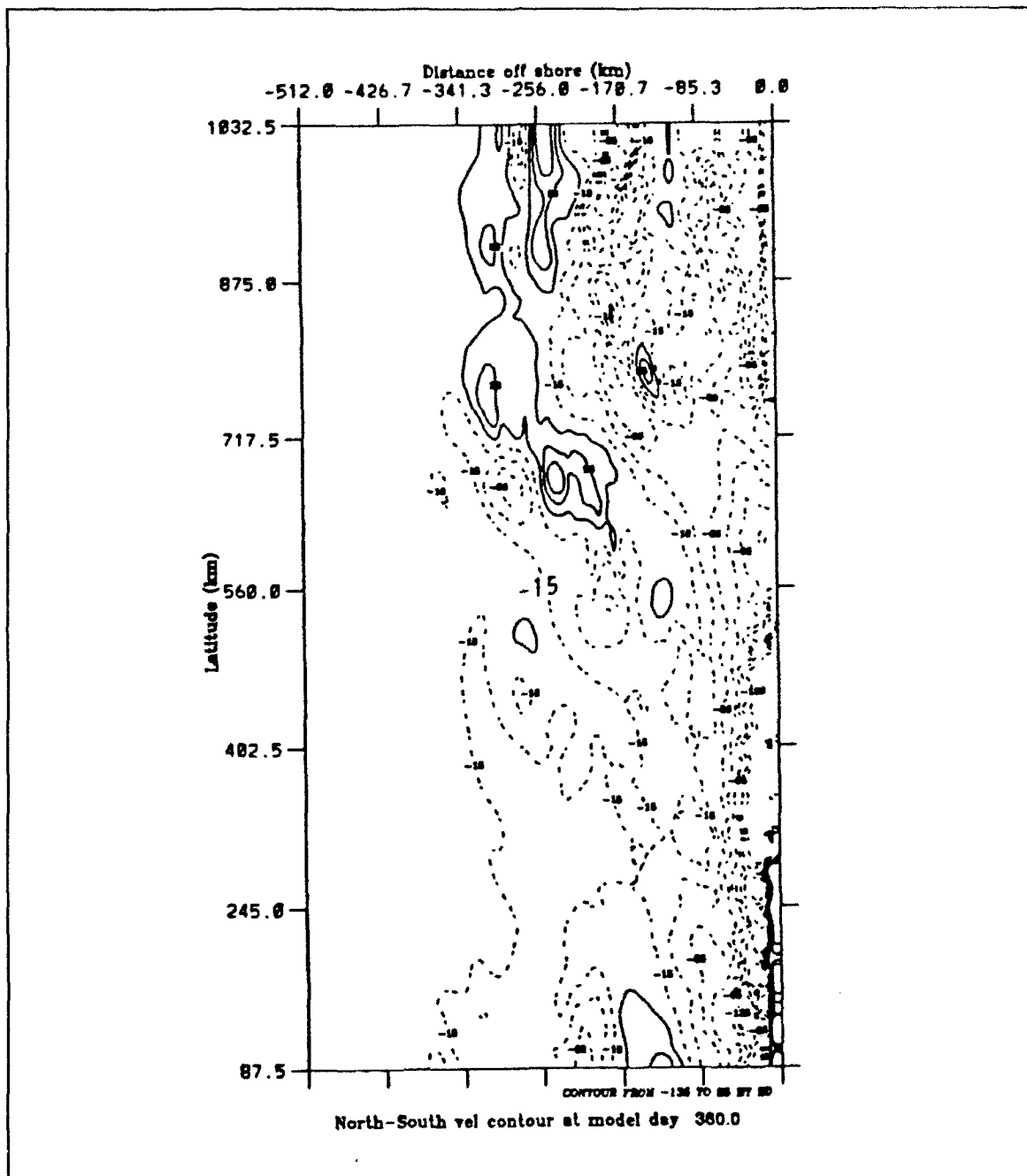
Figure 4.27 b) Experiment 4: Day 360 Meridional velocities. The contour interval is 20 cm s^{-1}. The dashed lines indicate southward velocities.
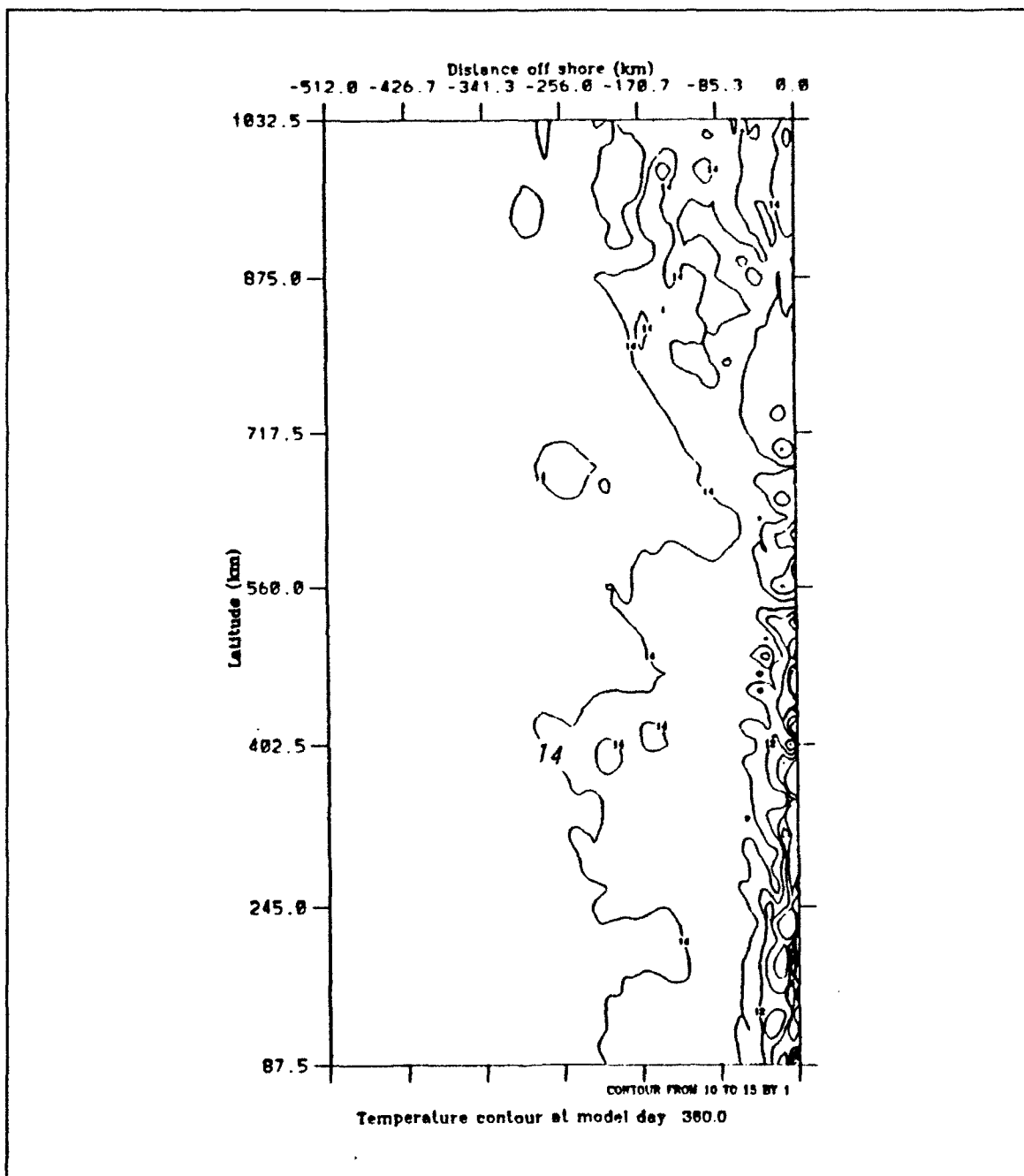
Figure 4.27 c) Experiment 4: Surface temperatures at day 360. The contour interval is 1° C. The temperature decreases toward the coast.
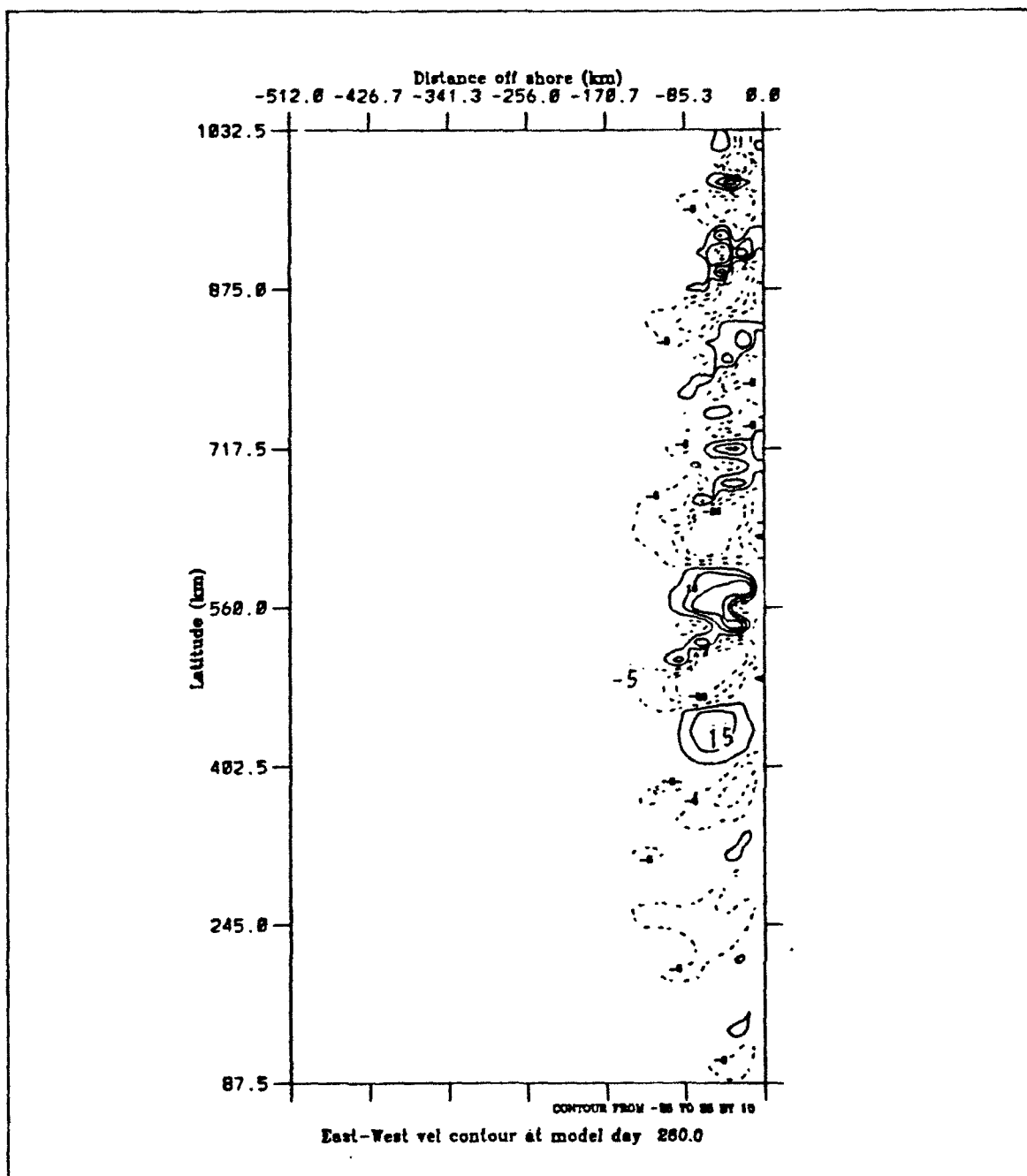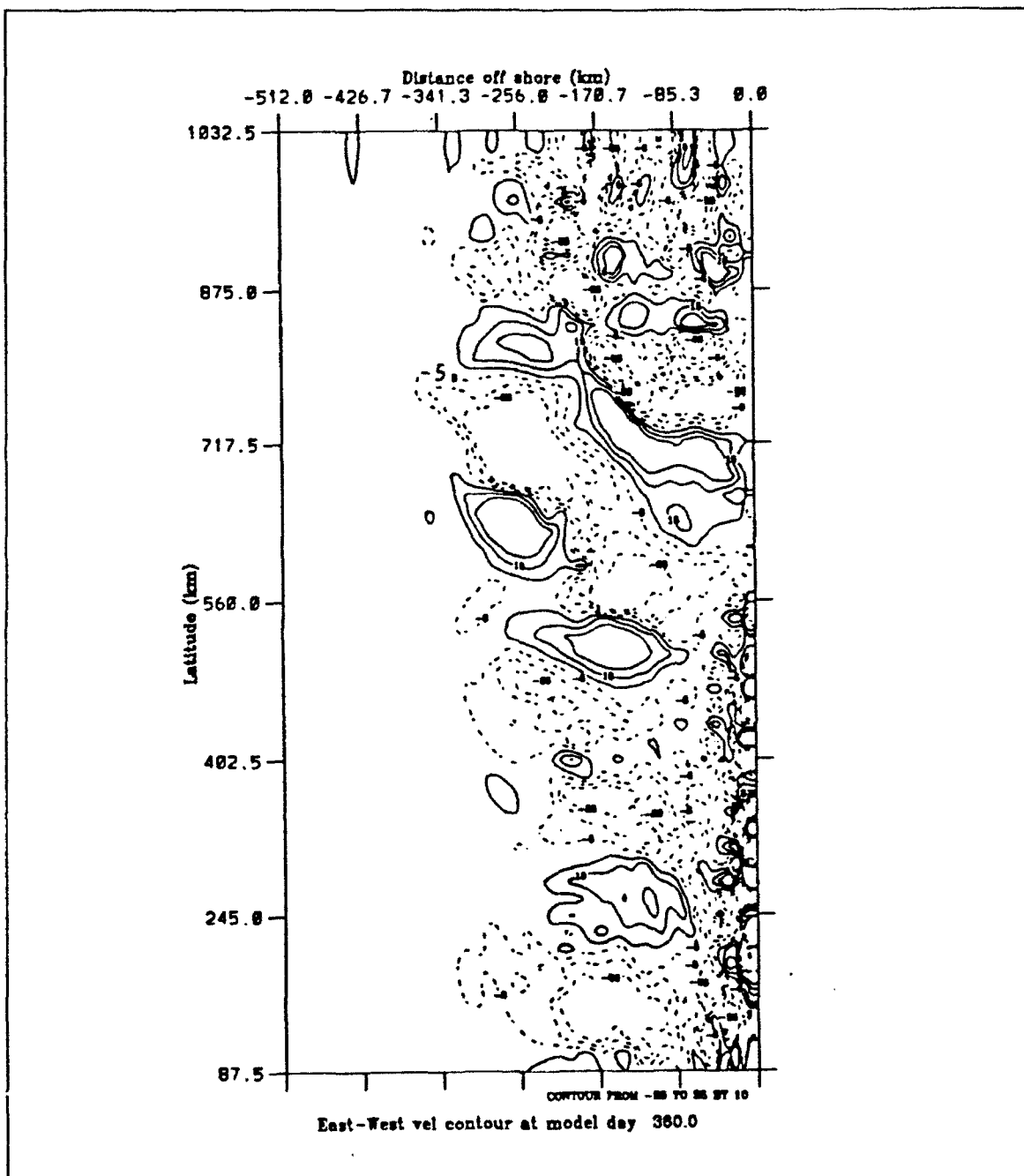
Figure 4.27 d) Experiment 4: Surface Zonal velocities at day 360. The contour interval is 10 cm s^{-1}. The dashed lines indicate westward velocities. Closed contours show the locations of eddies.

V. SUMMARY AND RECOMMENDATIONS

A. SUMMARY

In all four cases, currents and eddies were generated which shows the significant role wind forcing plays in the generation of these features. Table 5.1 shows a summary comparing the model results with available observations. The results of Experiment 1 are fair except for the weak surface current and undercurrent. Though Experiment 1 shows mostly reasonable results compared with observations, it is not likely that there would be 360 days of strong equatorward (upwelling favorable) winds. Experiment 2 showed the least reasonable results compared with observations. The coastal jet and undercurrent were much weaker and smaller than observations in Experiment 2. In all four experiments, the undercurrent was wider than seen in observations. A possible reason the undercurrent is wider than seen in observations may be due to not having topography representing the continental shelf in the model. Experiment 3 showed reasonable results with the exception of a very wide undercurrent and small eddy velocities. The results that were closest to observations were from Experiment 4. With the full climatological winds, the model was able to produce a coastal jet and eddy velocities of 85 cm s^{-1}. The conclusion obtained from the results of the four experiments is that both temporal and spatial variability in wind forcing in eastern boundary current regions are critical elements in the formation and maintenance of currents and eddies.

B. RECOMMENDATIONS

Future studies should look at the role of inter-annual variability in the wind forcing. By allowing the model to run for ten years (the 1980-1989 data set is available), it may be possible to detect what roles anomalous years such as *El Nino* have on the

currents and eddies in the CCS. Longer model simulations would also help to determine the life span of the larger eddies.

Experiments to include the topography and an irregular coastline to study the role of these features in the maintenance of currents and eddies also may make it possible to obtain a more reasonable undercurrent. Nevertheless, since both currents and eddies have been generated and maintained in these wind forcing experiments, we must conclude that wind forcing is a critical element in the formation and maintenance of these features in the CCS.

Table 5.1 INSTANTANEOUS COMPARISON OF EXPERIMENTS (EXP.) WITH OBSERVATIONS (OBS.) OF THE CCS.

	Obs.	Exp. 1	Exp. 2	Exp. 3	Exp. 4
A. Maximum coastal jet velocity (cm s^{-1})	30-100 (1,2,3,4)	25	5	35	85
B. Offshore location of coastal jet (km)	25-35 (2,3)	25-35	10-15	25-35	30-60
C. Offshore extent of coastal jet (km)	>40 (1,2,3)	100	20	40	100
D. Depth of inshore coastal jet (m)	90-150 (2,3)	80	60	80	180
E. Maximum undercurrent velocity (cm s^{-1})	5-15 (2,3)	5	1.5	5	5
F Offshore location of undercurrent axis (km)	10-40 (2,3)	25	20	40	40
G. Maximum width of undercurrent (km)	10-20 (2,3)	20	25	80	40
H. Depth of undercurrent axis (m)	200-300 (2)	280	100	350	360
I. Maximum zonal eddy diameter (km)	10->100 (2,5,6,7)	145	40	120	130
J. Maximum zonal eddy velocity (cm s^{-1})	50-100 (1,2,3,4,6,7)	25	15	35	85

References: (1) Kosro and Huyer (1986)
    (2) Huyer and Kosro (1987)
    (3) Kosro (1987)
    (4) Davis (1985)
    (5) Mooers and Robinson (1984)
    (6) Brink and Cowles (1991)
    (7) Brink et al. (1991)

LIST OF REFERENCES

Adamec, D., R.L. Elsberry, R.W. Garwood,Jr., and R.L. Haney, 1981: An embedded mixed layer-ocean circulation model. *Dyn. Atmos. Oceans, 5,* 69-96.

Allen, J.S., 1980: Models of wind-driven currents on the continental shelf. *Ann. Rev. Fluid. Mech., 12,* 389-433.

Arakawa, A., and V.R. Lamb, 1977: Computational design of the basic dynamical processes of the UCLA general circulation model. *Methods in Computational Physics,* (J. Chang, Ed.), Academic Press, 17, 173-265.

Bakun, A. and C.S. Nelson, 1991: The seasonal cycle of wind stress curl in subtropical eastern boundary current regions. Submitted to *J. Phys. Oceanogr.*

Batteen, M.L., 1989: Model simulations of a coastal jet and undercurrent in the presence of edies and jets in the California Current System. *Poleward Flows Along Eastern Ocean Boundaries,* S. J. Neshyba, C. N. Mooers, R. L. Smith and R. T. Barber, Eds., Springer-Verlag, 263-279.

Batteen, M.L., and Y.-J. Han, 1981: On the computational noise of finite-difference schemes used in ocean models. *Tellus, 33,* 387-396.

Batteen, M.L., R.L. Haney, T.A. Tielking and P.G. Renaud, 1989: A numerical study of wind forcing of eddies and jets in the California Current System. *J. Mar. Res., 47,* 493-523.

Batteen, M.L. and M.J. Rutherford, 1990: Modeling studies of eddies in the Leeuwin Current: The role of thermal forcing. *J. Phys. Oceanogr., 20,* 1484-1520.

Batteen, M.L., M.J. Rutherford and E.J. Bayler, 1991: A numerical study of wind and thermal forcing effects on the ocean circulation off Western Australia. *J. Phys. Oceanogr.,* submitted.

Bayler, E.J., 1991: Seasonal wind and ocean th...mal forcing influences on the generation of the Leeuwin Current and its eddies. M.S. thesis, Naval Postgraduate School, 193 pp.

Beardsley, R.C. and J.S. Lentz, 1987: The Coastal Ocean Dynamics Experiment Collection: An Introduction, *J. Geophys. Res., 92,* 1455-1463.

Blumberg, A.F. and G.L. Mellor, 1987: A description of a three-dimensional coastal ocean circulation model. In, *Three-dimensional Ocean Models,* N. Heaps, ed., American Geophysical Union, 4, 1-16.

Breaker, L.C., and C.N.K. Mooers, 1986: Oceanic variability off the central California coast. *Prog. in Oceanogr., 17,* 61-135.

Brink, K.H. and T.J. Cowles, 1991: The Coastal Transition Zone Program, *J. Geophys. Res., 96,* 14,637-14,647.

Brink, K.H., R.C. Beardsley, P.P. Niiler, M. Abbott, A. Huyer, S. Ramp, T. Stanton, and D. Stuart, Statistical properties of near-surface flow in the California coastal transition zone, *J. Geophys. Res., 96,* 14,693-14,706.

Camerlengo, A.L. and J.J. O'Brien, 1980: Open boundary conditions in rotating fluids. *J. Comput. Physics, 35,* 12-35.

Chelton, D.B., 1984: Seasonal Variability of alongshore geostrophic velocity off central California. *J. Geophys. Res.,* 89, 3473-3486.

Chelton, D.B., A.W. Bratkovich, R.L. Bernstein, and P.M. Kosro, 1988: Poleward flow off Central California during the spring and summer of 1981 and 1984. *J. Geophys. Res., 93,* 10,604-10,620.

Curtin, T.B. 1979: Physical dynamics of the coastal upwelling frontal zone off Oregon. Ph. D. dissertation, University of Miami, 339 pp.

Edson, R.W., 1989: The effects of climatological and transient wind forcing on eddy generation in the California Current System. M.S. thesis, Naval Postgraduate School, 139 pp.

Freitag, H.P. and D. Halpern, 1981: Hydrographic observations off Northern California during May 1977. *J. Geophys. Res. 86,* 4248-4252.

Haidvogel, D.B., A. Beckman and K.S. Hedstrom 1991: Dynamical Simulations of filament formation and evolution in the coastal transition zone. *J. Geophys. Res., 96,* 15017-15040.

Haltiner, G.J., and R.T. Williams 1980: *Numerical Prediction an Dynamical Meteorology, 2nd Ed.* John Wiley and Sons, 477 pp.

Han, Y.-J., 1975: Numerical simulation of mesoscale eddies. Ph.D. thesis, University of California, Los Angeles, 154 pp.

Haney, R.L., 1974: A numerical study of the response of an idealized ocean to large-scale surface heat and momentum flux. *J. Phys. Oceanogr., 4,* 145-167.

Haney, R.L., W.S. Shriver and K.H. Hunt, 1978: A dynamical-numerical study of the formation and evolution of large-scale ocean anomalies. *J. Phys. Oceanogr., 8,* 952-969.

Haney, R.L., 1985: Midlatitude sea surface temperature anomalies: A numerical hindcast. *J. Phys. Oceanogr., 15,* 787-799.

Hickey, B.M., 1979: The California Current System - hpothesis and facts. *Prog. in Oceanogr., 8,* 191-279.

Holland, W.R., 1978: The role of mesoscale eddies in the general circulation of the ocean-numerical experimentsusing a wind-driven quasi-geostrophic model. *J. Phys. Oceanogr., 8,* 363-392.

Holland, W.R., and M.L. Batteen, 1986: The parameterization of subgrid scale heat diffusion in eddy-resolved ocean circulation model. *J. Phys. Oceanogr., 16,* 200-206.

Huyer, A., 1983: Coastal upwelling in the California Current System. *Prog. in Oceanogr., 12,* 259-284.

Huyer, A., and P. M. Kosro, 1987: Mesoscale surveys over the shelf and slope in the upwelling region near Point Arena, California. *J. Geophys. Res., 89,* 1655-1681.

Kamenkovich, V.M., M.N. Koshlyakov and A.S. Monin, 1986: *Synoptic Eddies in the Ocean.* D. Riedel, 433 pp.

Kosro, P.M., 1987: Structure of the Coastal Current Field During the Coastal Ocean Dynamics Experiment, *J. Geophys. Res., 92,* 1637-1654.

Kosro, P.M., A. Huyer, S.R. Ramp, R.L. Smith, F.P. Chavez, T.J. Cowles, M.R. Abbott, P.T. Strub, R.T. Barber, P. Jessen, and L.F. Small, The structure of the transition zone between coastal waters and the open ocean off northern California, winter and spring 1987, *J. Geophys. Res., 96,* 14,707-14,730.

Lynn, R.J., K. Bliss and L.E. Eber, 1982. Vertical and horizontal distributions of seasonal mean temperature, salinity, sigma-*t*, stability, dynamic height, oxygen, and oxygen saturation in the California Current, 1950-1978, *CalCOFI Atlas 30, State of Calif. Mar. Res. Comm., La Jolla,* 513pp.

Lynn, R.J and J.J. Simpson, 1987: The California Current System: The seasonal variability of its physical characteristics. *J. Geophys. Res., 92,* 947-966.

McCreary, J.P., Jr., 1981: A linear stratified ocean model of the coastal undercurrent. *Phil. Trans. Roy. Soc., London, A302,* 385-413.

McCreary, J.P., Jr., P.K. Kundu and S.-Y. Chao, 1987: On the dynamics of the California Current System. *J. Mar. Res., 45,* 1-32.

McCreary, J.P., Y. Fukamachi and P.K. Kundu 1991: A numerical investigation of jets and eddies near and eastern ocean boundary. *J. Geophys. Res., 96,* 2515-2534.

Mooers, C.N.K. and A.R. Robinson, 1984: Turbulent jets and eddies in the California Current and inferred cross-shore transports. *Science, 223,* 51-53.

Nelson, C.S., 1977: Wind stress and wind stress curl over the California Current. *NOAA Tech. Rep. NMFS SSFR-714,* U.S. Dept. Commerce, 155 pp.

Nelson, C.S. and D.M. Husby, 1983: Climatology of surface heat fluxes over the California Current Region. *NOAA Tech. Rep. NMFS SSFR-714,* U.S. Dept. Commerce, 155 pp.

Olivier, D.A., 1987: Numerical simulations of the California Current: Filament formation as related to baroclinic instability. M.S. thesis, Naval Postgraduate School, 69 pp.

Paulson, C.A. and J.J. Simpson, 1977: Irradiance measurements in the upper ocean. *J. Phys. Oceanogr., 7,* 952-956.

Reid, J.L., 1962: Measurements of the California Countercurrent at a depth of 250 meters. *J. Mar. Res., 20,* 134-137.

Reid, J.L. and R.A. Schwartzlose, 1962: Direct measurements of the Davidson Current off Central California. *J. Geophys. Res., 67,* 2591-2597.

Reid, J.L., G.I. Roden and J.G. Wyllie 1958: Studies of the California current system. *CalCOFI Progress Report 7-1-56 to 1-1-58, State of Calif. Mar. Res. Comm., Sacramento, CA,* 27-56.

Reid, J.L., 1960: Oceanography of the northeastern Pacific during the last ten years. *CalCOFI Report 7,* 77-90.

Semtner, A.J., and Y. Mintz, 1977: Numerical simulation of the Gulf Stream and mid-ocean eddies. *J. Phys. Oceanogr.*, 7, 208-230.

Smith, R.L., 1968: Upwelling. *Oceanography and Marine Biology reviews*, 6, 11-46.

Suginohara, N. 1977: Upwelling front and two-cell circulation. *Journal of the Oceanographical Society of Japan*, 33, 115-130.

Sverdrup, H.U., M.W. Johnson, and R.H. Fleming, 1942: *The Oceans: Their Physics, Chemistry and General Biology.* Prentice Hall, Englewood Cliffs, New Jersey, 1087 pp.

Trenberth, K.E., W.G. Large and J.G. Olson, 1989a: The effective drag coefficient for evaluating wind stress over the oceans. *J. Climate.*, 1507-1516.

Trenberth, K.E., J.G. Olson, and W.G. Large, 1989b: A global ocean wind stress climatology based on ECMWF analyses. *NCAR Tech. Note NCAR TN-338+STR*, 93 pp.

Trenberth, K.E., W.G. Large and J.G. Olson, 1990: The mean annual cycle in global ocean wind stress. *J. Phys. Oceanogr.*, 20, 1742-1760.

Weatherly, G.L., 1972: A study of the bottom boundary layer of the Florida Current. *J. Phys. Oceanogr.*, 2, 54-72.

Wooster, W.S., and J.L. Reid, 1963: Eastern Boundary Currents, In: *The Sea, volume 2*, M.N. Hill, editor, Wiley intrscience, New York, pp. 253-280.

INITIAL DISTRIBUTION LIST

No. Copies

1. Defense Technical Information Center   2
   Cameron Station
   Alexandria, VA 22304-6145

2. Library, Code 52   2
   Naval Postgraduate School
   Monterey, CA 93943-5002

3. Chairman (Code OC/Co)   1
   Department of Oceanography
   Naval Postgraduate School
   Monterey, CA 93943-5000

4. Chairman (Code MR/Hy)   1
   Department of Meteorology
   Naval Postgraduate School
   Monterey, CA 93943-5000

5. Dr. Mary L. Batteen, (Code OC/Bv)   2
   Department of Oceanography
   Naval Postgraduate School
   Monterey, CA 93943-5000

6. Commander   1
   Naval Oceanography Command
   Stennis Space Center
   MS 39529-5000

7. Technical Director   1
   NRL
   Stennis Space Center
   MS 39529-5004

8. Office of Naval Research (Code 420)   1
   800 N. Quincy Street
   Arlington, VA 22217

9. Director of Research Administration (Code 012)   1
   Naval Postgraduate School
   Monterey, CA 93943-5000

10. Commanding Officer   1
    Fleet Numerical Oceanography Center
    Monterey, CA 93943-5005

11. Lt. Ross Mitchell   2
    Department Head Class 128
    Surface Warfare Officers School Command
    446 Cushing Road
    Newport, RI 02841-1209

12. Library   1
    Marine Biological Laboratory
    Woods Hole, MA 02543

13. Library   1
    Moss Landing Marine Lab
    P.O. Box 450
    Moss Landing, CA 95039-450

14. Library   1
    Scripps Institute of Oceanography
    UCSD
    La Jolla, CA 92037

15. Library   1
    Monterey Bay Aquarium Research Institute
    160 Central Avenue
    Pacific Grove, CA 93950